(19) Europäisches Patentamt
European Patent Office
Office européen des brevets

(11) EP 1 168 464 A1

(12) **EUROPEAN PATENT APPLICATION**
published in accordance with Art. 158(3) EPC

(43) Date of publication:
02.01.2002 Bulletin 2002/01

(21) Application number: **00909748.6**

(22) Date of filing: **17.03.2000**

(51) Int Cl.[7]: **H01L 41/08**, H01L 41/22, H03H 9/19

(86) International application number:
PCT/JP00/01691

(87) International publication number:
WO 00/57494 (28.09.2000 Gazette 2000/39)

(84) Designated Contracting States:
AT BE CH CY DE DK ES FI FR GB GR IE IT LI LU MC NL PT SE

(30) Priority: **19.03.1999 JP 11695799**
12.04.1999 JP 14055799
09.10.1999 JP 32449299
09.10.1999 JP 32449399

(71) Applicant: **Nagaura, Yoshiaki**
Chikushino-shi, Fukuoka 818-0053 (JP)

(72) Inventor: **Nagaura, Yoshiaki**
Chikushino-shi, Fukuoka 818-0053 (JP)

(74) Representative: **Goddar, Heinz J., Dr.**
FORRESTER & BOEHMERT Pettenkoferstrasse 20-22
80336 München (DE)

(54) PIEZOELECTRIC ELEMENT AND PRODUCTION METHOD THEREFOR

(57) The objective of present invention Is introduce machining tools and to manufacturing method to make extremely thin electronic material such as a piezoelectric element as a quartz oscillator, silicone or Gallium Arsenic and so on as well as a optical lens, which were difficult to be machined by conventional techniques.

The manufacturing process of piezoelectric element and silicone and so forth is featuring to make plural concave parts on the surface of the piezoelectric blank (80 μm thick and 2 inch diameter for example), which is machined by lapping tools as dual faced, one faced or others, is lapped by using the conventional chemical etching method as the first step, and to make thinner typically 12 μm (to 62 μm for example) on another surface of the blank by the reactive ion etching (RIE) as the second step. Finally both surfaces are lapped by the dual-face mechanical lapping machine, one face machine or float polishing machine in order not only to eliminate the rough ion-damaged layer in a few μm thickness (for example convex and concave surface exists in thickness from 0.2 μm to 3 μm due to RIE) after the chemical RIE process, dry etching as ion milling and plasma etching or wet etching, but also to form the oscillating part in a convex lens shape at the opposite surface of concave part.

Fig.100

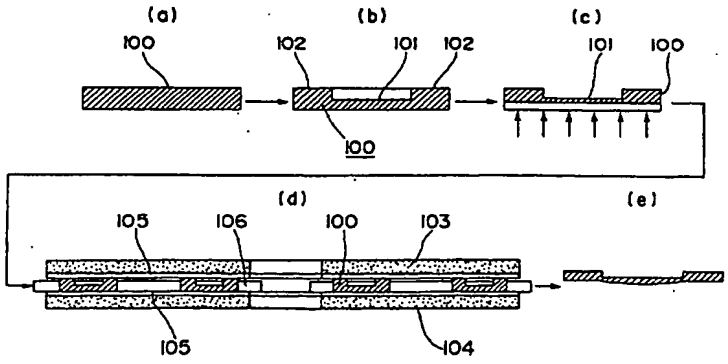

EP 1 168 464 A1

Printed by Jouve, 75001 PARIS (FR)

BEST AVAILABLE COPY

Description

Technical Field

[0001] The present invention is related to a piezoelectric element and a manufacturing method, which is greatly capable to enhance the fundamental oscillation frequency.

Related Art

[0002] A quartz oscillator, which is one of piezoelectric element, can apply to a wide variety of devices such as standard frequency sources of communication equipment and detection instrumentation, general purpose computers, OA information apparatus, micro computer clock pulses of home electric appliances and so forth. Therefore, the fundamental oscillation frequency is required to be enhanced by making the thickness thinner in order to get the higher performance of the information processing and the transmitting capability.

[0003] Also, the novel shape is proposed to shape the element in lens configuration in order to manufacture the high quality oscillator, and the element has achieved the high performance relatively in lower frequency zone.

[0004] However, there exists a problem to thinner the oscillator, and the dual-face lapping machine could make it only down to 24.0 μm (approximately 70 MHz resonance). Also when the lens shape piece could not be made up, since the curve face was extremely difficult to manufacture.

[0005] Furthermore, although conventional detection and prediction methods of earthquake were the underground structure probe techniques for ocean observation, oil, methane gas, gold, silver and diamond, otherwise earth magnetic field detection, GPS survey or laser scan between tow distances, the air vibration detection of the earthquake and Tsunami may be one of promising candidates. The sound collection microphone was used to change the air vibration to the electric signal to record and analyze it easily, however it is too difficult for this microphone to detect the specific frequency, since this can frequently pick up noises.

[0006] Quartz oscillators are essential electronic devices for digital equipment for communications and computers. The oscillator is required to increase the fundamental frequency by thinner the element for the higher performance of the information processing and the transmitting speed. Furthermore for mobile communication equipment, the primary frequency should be higher to make them smaller and to save the electric power.

[0007] The manufacturing methods of Quartz oscillator were generally the mechanical polishing and chemical wet etching. The former could make oscillator in various surface shape, however the minimum thickness was 30 μm. The latter could made thinner in principle without the surface processing damage, but this process also had the limitation to be thinner with the etch channel and so on. On the other hand, a reactive ion etching (RIE) or plasma etching (these are called as the chemical dry etching) would introduce the ion-damaged surface, however the dry etching will be capable to make the oscillator thinner without the surface roughness.

[0008] The mass production process is developed to employ these advantageous methods for high frequency quartz oscillators. However as the thinner oscillator, the conventional manufacturing method with dual-face lapping machine had the limitation at 30 μm (frequency 55.6 MHz). Furthermore in case of finishing the surface in a lens shape, the manufacturing was extremely difficult to make the surface in curved shape on the thinner element, and there existed no means to mass-produce thinner oscillators at a reasonable cost.

Disclosure of Invention

[0009] Therefore, the first object of the present invention is both to introduce the piezoelectric element, which thickness is thinner than any other one, and to disclose the manufacturing process. The second object is to introduce a sound to electric transducer, accurately to detect the sound wave of the specific frequency with the minimum noise. The manufacturing process of piezoelectric element in the present invention to solve the above problems is featuring to make a concave part on one surface of plate by using the chemical etching method, and to make thinner on the other surface by the reactive ion etching, and to polish the both surfaces of the element by the mechanical lapping in order not only to eliminate the rough layer due to RIE but also to form the oscillating part in a convex lens shape at the concave part.

[0010] Figure 100 shows the manufacturing process of the present invention. First of all, a quartz blank plate 100 which thickness is 50 μm for example is cut from an artificial quartz blank 100 (Figure 100 (a)), and a concave part 101 in the cross section is formed by resolving the one surface (the central part of upper side) of said plate by a chemical etching method with fluorine hydride (Figure 100 (b)). The thinner part from the base surface of the concave part 101 to the lower surface of the quartz blank 100 is the oscillating part, which generates high frequency, and remaining part is a frame part 102. This is in the same way of the conventional manufacturing process.

[0011] As the next stage, the lower whole surface of the quartz blank 100 was etched by ion etching process with fluorine gas, and the plate becomes thinner (Figure 100(c)). The ion etching is a manufacturing method, where atoms of fluorine ionized gas in the plasma state, are accelerated by electric voltage and collided to the blank 100, and silicone atoms in SiO_2 are etched from the surface.

[0012] The chemical etching alone cannot machine the plate thinner than 20 μm as mentioned above. Afterward the plate will become thinner down to 10.3 μm

approximately with ion etching process. However even ion etching cannot attain the 10 μm target. Although the ion etching makes the Plate thinner, this process is found to make "ion-damaged layer", which is non-crystalline part and unknown defect formed by atom collisions at the single crystalline surface. The thickness of this layer is from 0.2 μm to 0.3 μm.

[0013] The mechanical lapping is to be consequently employed. The final dual-face surface polishing (Figure 100 (d)) will be executed at the lapping layer of approximately 0.3 μm. This dual lapping machine is a similar construction of gear mechanism like a planet. First of all the quartz plate 100 is set in a steel-made carrier 106 (planet gear) which rotates round its axis and revolves around a fixed point, and the plate is set between an upper ground table 103 and the lower table 104. Two polyurethane lapping pads 105 are pasted on the two ground tables.

[0014] While cerium oxide powders in water are filled, the quartz plate 100, which is fixed by the carrier 106, rotates and also revolves between the ground tables 101, 104, and both surfaces of the plate 100 are to be polished.

[0015] As shown in Figure 100 (e), the shape of quartz plate 100 after the dual-face lapping process is similar to a convex lens which lower surface is in a convex curve. An oscillator in this shape of lens like cross section is known to eliminate higher order oscillations (spurious frequency), which are harmful to electronics, and also to show a stable performance.

[0016] Figure 101 shows the reason why the plate becomes the convex lens shape. The lapped mass is proportional to the lapping pressure. Although the frame part 102 of the concave quartz plate 100 after the ion etching receives extremely high lapping pressure between the upper and lower ground tables 103 and 104, the concave part 101 which becomes the oscillating part receives small lapping pressure only by the lower ground table 104. Furthermore the lapping pressure becomes lower at the central part of the concave plate 101 since the shape is concave (Figure 101 (a)). Therefore the lapped mass becomes minimum at the center of the concave part 101, it is maximum near the frame part 102, and the lapping quantity between the center and frame changes as a spherical part with a certain curvature. As the consequence the quartz oscillator becomes the convex lens shape (Figure 101 (b)). The central part of the lens is most thick as 10 μm.

[0017] As understand well, only 0.3 μm layer is lapped by the dual-face lapping process. The small lapping process eliminates the damaged layer and forms the convex lens. Actually the chemical and ion etchings are the coarse lapping, and the dual-face lapping is the fine finishing process.

[0018] The present invention with these technology combinations enables piezoelectric element to be the thinnest among conventional processes, and more stable oscillation without spurious frequency is achieved by the oscillation part in the convex lens shape.

[0019] In order to achieve the second object, the sound to electric transducer has the pressure detection surface of piezoelectric effect material in the center of the cylinder. The pressure detector has a pair of electrode.

[0020] Also the manufacturing method of the sound to electric transducer in the present invention is to machine two cylindrical holes from both ends of the piezoelectric material by using the specific drilling means, and to make the pressure detection surface of the required thickness at the center of the circular rod, and to transfer the signal of the exterior sound vibration by a pair of electrode at the pressure sensor. The machining means are to make grooves at the surface of barrel whetstone, and to rotate the whetstone either by injecting compressed air and liquid, or by using other techniques. Also the barrel stone can be made by steel sphere which cross section is near circle.

Brief Description of Drawings

[0021] Figure 1 is the flow chart of the manufacturing process in the present invention.

[0022] Figure 2 is the first manufacturing example of Quartz oscillator, and (a), (b) and (c) shows the cross section of the Quartz oscillator, the microgram of the resonator and the reactance-frequency diagram, respectively. The blank material is AT cut, the thickness is 103 μm, the diameter is 5 mm, the machined dimension is 25 μm, the curvature radius is 30 mm.

[0023] Figure 3 is the second manufacturing example of quartz oscillator, and (a) and (b) shows the cross section of the quartz oscillator and the reactance-frequency diagram, respectively. The blank material is AT cut, the thickness is 103 μm, the diameter is 5 μm, the machined dimension is 9 μm, the curvature radius is 200 mm.

[0024] Figure 4 is the third manufacturing example of Quartz oscillator, and (a) and (b) shows the cross section of the quartz oscillator and the reactance-frequency diagram, respectively. The blank material is AT cut, the thickness is 77 μm, the diameter is 5 mm, the machined dimension is 27 μm.

[0025] Figure 5 is the reactance-frequency diagram of AT cut blank and thick quartz oscillator.

[0026] Figure 6 is the reactance-frequency diagram of AT cut blank and thick quartz oscillator.

[0027] Figure 7 is the reactance-frequency diagram of AT cut blank and thin quartz oscillator.

[0028] Figure 8 is the reactance-frequency diagram of AT cut blank and thin quartz oscillator.

[0029] Figure 9 is the reactance-frequency diagram of AT cut blank and more thin quartz oscillator.

[0030] Figure 10 is the reactance-frequency diagram of AT cut blank and thinner quartz oscillator.

[0031] Figure 11 is a cross section of the first machining supporter in the present invention of the manufacturing method.

[0032] Figure 12 is a cross section of the second machining supporter in the present invention of the manufacturing method.

[0033] Figure 13 is the set cross section of the first machining supporter, the second supporter and quartz plate.

[0034] Figure 14 is a cross section of another example for the present invention of the manufacturing method.

[0035] Figure 15 is the cross section and the plan of one manufacturing method for the present invention.

[0036] Figure 16 is the cross section of the present manufacturing setup between the lapping plate.

[0037] Figure 17 is the plan diagram of another machining supporter for the present invention of the manufacturing setup.

[0038] Figure 18 is the cross section of the quartz plate, which is manufactured by the machining supporter in Figure 13.

[0039] Figure 19 is the cross section of the quartz plate, which is manufactured by the machining supporter in Figure 13.

[0040] Figure 20 is the plan diagram of the lapping plate motion.

[0041] Figure 21 is the plan diagram of the lapping plate motion.

[0042] Figure 22 is the cross section diagram of an executed example in the present invention.

[0043] Figure 23 is the cross section diagram of an executed example in the present invention.

[0044] Figure 24 is the cross section diagram of an executed example in the present invention.

[0045] Figure 25 is the cross section diagram of the machining setup example in the present invention.

[0046] Figure 26 is the cross section of quartz plate manufactured by the setup in Figure 25 and others.

[0047] Figure 27 is the cross section of another example of the machining setup.

[0048] Figure 28 is the cross section of another example of the machining setup.

[0049] Figure 29 is the cross section of another example of the machining setup.

[0050] Figure 30 is the cross section of the executed example in the present invention.

[0051] Figure 31 is the cross section of the executed example in the present invention.

[0052] Figure 32 is the cross section diagram of the machining method in the present manufacturing invention.

[0053] Figure 33 is the side view diagram of the machining tool in the present manufacturing invention.

[0054] Figure 34 is the side view and A-A cross section diagram of the machining stone in the present manufacturing invention.

[0055] Figure 35 is the cross section diagram of one example executed for the present manufacturing invention.

[0056] Figure 36 is the side view and cross section diagram of another machining stone in the present manufacturing invention.

[0057] Figure 37 is the cross section diagram of another machining tool in the present manufacturing invention.

[0058] Figure 38 is the cross section diagram of another machining tool in the present manufacturing invention.

[0059] Figure 39 is the cross section diagram of another machining tool in the present manufacturing invention.

[0060] Figure 40 is the side view and plan diagram of the machining tool for the actual manufacturing diagram in the present invention.

[0061] Figure 41 is the enlarged cross section and plan diagram of the machining tool for the actual manufacturing diagram in the present invention.

[0062] Figure 42 is the cross section of the manufactured sample the present invention.

[0063] Figure 43 is the cross section of the manufactured sample the present invention.

[0064] Figure 44 is the cross section of the quartz plate manufactured by the machining supporter in Figure 13.

[0065] Figure 45 is the cross section of the quartz plate manufactured by the machining supporter in Figure 13.

[0066] Figure 46 is the cross section of the quartz plate manufactured by the machining supporter in Figure 14.

[0067] Figure 47 is the cross section of the sample manufactured by the present invention.

[0068] Figure 48 is the cross section of the sample manufactured by the present invention.

[0069] Figure 49 is the cross section of the sample manufactured by the present invention.

[0070] Figure 50 is the cross section of the sample manufactured by the present invention.

[0071] Figure 51 is the cross section of the sample manufactured by the present invention.

[0072] Figure 52 is the cross section of the sample manufactured by the present invention.

[0073] Figure 53 is the cross section of the sample manufactured by the present invention.

[0074] Figure 54 is the cross section of the sample manufactured by the present invention.

[0075] Figure 55 is the cross section of the sample manufactured by the present invention.

[0076] Figure 56 is the cross section of the sample manufactured by the present invention.

[0077] Figure 57 is the reactance-frequency diagram of the thin quartz oscillator of AT cut material.

[0078] Figure 58 is the reactance-frequency diagram of the thinner quartz oscillator of AT cut material.

[0079] Figure 59 is the reactance-frequency diagram of the thinner quartz oscillator of AT cut material.

[0080] Figure 60 is the reactance-frequency diagram of the thinnest quartz oscillator of AT cut material.

[0081] Figure 61 is the cross section and plan diagram

to show the machining method of the present invention.

[0082] Figure 62 is the cross section diagram to show the machining method of the present invention.

[0083] Figure 63 is the cross section diagram to show the machining method of the present invention.

[0084] Figure 64 is the cross section diagram to show the machining method of the present invention.

[0085] Figure 65 is the cross section and plan diagram to show the machining method of the present invention.

[0086] Figure 66 is the cross section and plan diagram to show the machining method of the present invention.

[0087] Figure 67 is the cross section and plan diagram to show the machining method of the present invention.

[0088] Figure 68 is the cross section and plan diagram to show the machining method of the present invention.

[0089] Figure 69 is the cross section and plan diagram to show the machining method of the present invention.

[0090] Figure 70 is the cross section and plan diagram to show the machining method of the present invention.

[0091] Figure 71 is the cross section diagram to show the machining method of the present invention.

[0092] Figure 72 is the cross section diagram to show the machining method of the present invention.

[0093] Figure 73 is the cross section diagram to show the machining method of the present invention.

[0094] Figure 74 is the cross section diagram to show the machining method of the present invention.

[0095] Figure 75 is the measured upper surface shape diagram of the AT cut quartz oscillator in the concave lens shape.

[0096] Figure 76 is the measured rear surface shape diagram of the AT cut quartz oscillator in the concave lens shape.

[0097] Figure 77 is the reactance-frequency diagram of the AT cut quartz plate in the concave lens shape, which is made by wet etching process.

[0098] Figure 78 is the reactance-frequency diagram of the AT cut quartz plate in the concave lens shape, which is made by the mechanical lapping means after the wet etching process.

[0099] Figure 79 is the cross section diagram to show the manufacturing method of the present invention.

[0100] Figure 80 is the cross section diagram to show the manufacturing method of the present invention.

[0101] Figure 81 is the cross section diagram to show the manufacturing method of the present invention.

[0102] Figure 82 is the cross section diagram to show the manufacturing method of the present invention.

[0103] Figure 83 is the cross section diagram to show the manufacturing method of the present invention.

[0104] Figure 84 is the reactance-frequency diagram of the AT cut quartz plate in the concave lens shape which is made by the mechanical lapping means after the wet etching process.

[0105] Figure 85 is the reactance-frequency diagram of the AT cut quartz plate in the concave lens shape which is made by the mechanical lapping means after the wet etching process.

[0106] Figure 86 is the reactance-frequency diagram of the AT cut quartz plate in the concave lens shape which is made by the mechanical lapping means after the wet etching process.

[0107] Figure 87 is the measured upper surface shape diagram of the AT cut quartz oscillator in the concave lens shape

[0108] Figure 88 is the measured upper surface shape diagram of the AT cut quartz oscillator in the concave lens shape

[0109] Figure 89 is the cross section diagram to show the manufacturing method of the present invention.

[0110] Figure 90 is the cross section diagram to show the manufacturing method of the present invention.

[0111] Figure 91 is the cross section diagram to show the manufacturing method of the present invention.

[0112] Figure 92 is the cross section diagram to show the manufacturing method of the present invention

[0113] Figure 93 is the reactance-frequency characteristics of thick quartz oscillator which material is AT cut, and the plan the cross section of the resonator of the single inverted mesa type.

[0114] Figure 94 is the reactance-frequency characteristics of thin quartz oscillator.

[0115] Figure 95 is the shape diagram of thin quartz oscillator, which is measured by the interference microscope.

[0116] Figure 96 is the reactance-frequency characteristics of thin quartz oscillator which material is AT cut.

[0117] Figure 97 is a peak to valley (P-V) diagram.

[0118] Figure 98 is a graph of inverted curvature radius in the convex lens shape of single inverted mesa type.

[0119] Figure 99 is a graph of the surface roughness change at the concave center of single inverted mesa type.

[0120] Figure 100 is the flow diagram of the manufacturing process for the present invention.

[0121] Figure 101 describes the formation mechanism of the piezoelectric convex lens for the present invention.

EMBODIMENT OF Invention

[0122] This chapter presents the embodiments carrying out our invention.

The present inventors succeeded to develop novel machining method in a field of lapping machine and to make quartz oscillators which thickness is 9 μm and shape is plano-convex. Furthermore, relations between the thickness and the electric characteristics of oscillators, which were thinner than 500 μm, were surveyed in order to develop the higher performance quartz oscillators.

As quartz is fragile, the matched machining method was thought to be limited to the mechanical lapping or chemical wet etching. Therefore, the lapping machining method was seldom used to make quartz oscillators for high frequency use.

[0123] The lapping method invented by the present authors uses a ball whetstone 1, which steel sphere is gilt by diamond grinding grains 57 as shown in Figure 1. In other words, the quartz plate 4 is set on a cylindrical magnet 3, which is set on the primary axis of ultra high precision lathe, and the tool supporter 6 with a sphere stand is mounted at the end of the grinding spindle 5. When this is accessed to the cylindrical magnet 3, the steel sphere is attracted to the tool supporter 6 by the magnetic induction. Since the tool supporter 6 is smaller than the diameter of cylindrical magnet 3, the magnetic flux between the ball whetstone 1 and the tool supporter 6 is stronger than that between the ball whetstone 1 and the cylindrical magnet 3. Therefore the ball whetstone 1 is strongly attracted to the tool supporter 6, and they are one-body without the separation even if during the high frequency rotation.

[0124] The present lapping method employs a ball whetstone 1 which is gilt electrically by diamond grains 57 on the steel sphere. Also the centering of the whetstone 1 becomes unnecessary during the exchange, since the tool holder 6 is cylindrical and the steel sphere is accurately made. Therefore the exchange of the whetstone 1 becomes speedy from the rough machining to the final lapping. This motion of the ball whetstone 1 is controlled by NC machine, and the curved surface can be also made.

[0125] The diameter of diamond whetstone grain 57, which is electrically gilt on the ball whetstone 1 of steel sphere for ball bearing and so on, is various and is for example 30 μm for the rough machining, 16 μm for the middle one and 4 mm for the fine one, respectively. Since the diameter of diamond whetstone grain 57 depends on the machining stage, the central point of the ball whetstone 1 moves perpendicularly along the diameter of the whetstone grain 57, when the ball whetstone 1 is absorbingly hold to the cylindrical holder 6 by the magnetic induction of the cylindrical magnet 3 at the primary axis 2.

[0126] As shown in Figure 1 (b) the solution to this problem is only for the area of the cylindrical holder 56 at the ball whetstone 1, which is set by the tool holder 6, not to be contacted to the diamond grain 57. Then the ball whetstone 1, which is either for the rough lapping, for the middle one or for the final one, can be easily changed for any diameter of diamond whetstone grain 57, since the central line of the x and y axes for the ball whetstone 1 are fixed especially as for the perpendicular axis x as shown in Fig. 1 (c).

[0127] The present inventors succeeded to make the plano-convex shape oscillator which holder 51 is combined to the groove 52 as shown in Figure 2 (a). It is called as the smooth line 53 to combine the holder 51 and the groove 52. The lens shape is 25 μm thick, 3 mm curvature radius and the shaping error less than 0.1 μm as shown in Figure 2 (b) where the central part of quartz disk is machined. Conventionally the quartz resonator in this shape was thought to be spuriously vibrated and in poor performance. However as seen in Figure 2 (c), the reactance-frequency characteristics is steeply resonated without any spurious signal, and this is understood as an ideal quartz oscillator.

[0128] Further trial to make thinner quartz resonators brought a success to manufacture 9 μm thick and 200 mm curvature radius oscillators. After this was lapped by cerium oxide and eliminated the surface of approximately 0.5 μm thickness, we got the product as shown in Figure 3 (a). Figure 3 (b) shows the reactance-frequency property, which curve is no so steep and the Q value is slightly smaller than that in Figure 2, however there is utterly no spurious oscillation. The reason why the curve is no so sharp is that there exists a damaged layer inside the surface of the resonator, and that the relative ratio of the layer becomes larger in thinner quartz. However, this damaged layer can be improved by the additional etching process.

[0129] The next stage was tried to increase the thickness of quartz lens for a condition of the constant curvature radius as 30 mm. When the thickness was less than 125 μm, there was a sharp resonance without the spurious oscillation as seen in Figure 2. However, new phenomena appeared to be spurious or to be not resonated, when the thickness is over 125 μm.

[0130] On the other hand we made quartz oscillators which were 27 μm thick and in the planar or concave lens shape called as the inverted mesa type as shown in Figure 4 (a). Figure 4 (b) shows the electric characteristics, which is slightly poor than that of the plano-convex type, however there was no spurious signal. Also as the thickness of the inverted mesa type resonator was increased, there was no oscillation over 30 μm thickness. Since the inverted mesa type is thought to be the plano-convex lens with the infinite diameter, this quartz oscillator with the ring support has the good resonance or non-resonance region, which depends on the thickness of the oscillating part.

[0131] This invented method introduced the following conclusions. Although the quartz oscillator with no spurious signal was thought to be conventionally bi-convex, the plano-convex type quartz can also show the ideal resonance without the spurious oscillation when the thickness is less than approximately 30 μm. Also the manufacturing technique of plano-convex type in Figure 1 can be applied to the concavo-convex or bi-convex type.

[0132] The present inventors devoted their efforts the research of quartz resonator as thin as possible. Figure 5 and Figure 6 show the reactance-frequency characteristics of respectively 76. 7 μm and 100 μm thickness with 5 mm diameter.

[0133] In this Figure there are spurious signals near the fundamental oscillation.

[0134] Figure 7 shows the reactance-frequency curve of 33μm quartz oscillator, and there is no spurious peak within 5 MHz of the fundamental frequency.

[0135] Figure 8 shows many spurious signals in 6

MHz intervals approximately. Figure 9 is the reactance-frequency property of 31 μm thick quartz oscillator, and no spurious peak is seen within 5 MHz of the fundamental frequency, but the spurious signal is approximately 8 MHz apart from the fundamental one as shown in Figure 10. Then the thinner the quartz oscillator is, the farther the spurious signal from the primary oscillation.

[0136] From Figure 11 to Figure 19, the manufacturing system of the quartz oscillator is presented. This system has the groove or step 12 in ring, rectangular or other shapes as shown in Figure 11. This groove or ring 12 is inserted by the second machining auxiliary tool 19, which is in ring, other ring shapes or cylindrical shape deeper than the ring or groove 12. The lapping object as quartz oscillator 13 in this case is set inside the second machining auxiliary tool 19. This quartz oscillator is as high as the protruding height (for example 40 μm) of the second tool 19 from the first tool 11, and the shape of the oscillator 13 is disk or others.

[0137] As other lapping procedures the following methods are convenient to correct the distortion during machining the quartz oscillator 13.

(1) Before the oscillator 13 is set on the first auxiliary tool 11, the one surface is evaporated by metals as gold, silver or aluminum etc as the preprocessing.
(2) After one side of oscillator 13 has the metal membrane or other processes are used, the surface of one side is processed so as to discriminate the front from the rear surface.
(3) Then for instance when the very thin metal membrane is made, the oscillator 13 is set on the first tool 11, and the plate 13 is lapped to 20 μm thick for example after this is lapped to be 40 μm by the dual face lapping machine.
(4) Even during the lapping process, the lapped surface of the plate 13 has substantial distortion. In order to eliminate the distortion, the washing is required for the first tool 11, the second tool 19 and the plate 13 after these are took off from the dual face lapping machine.
(5) Then the surface of metal membrane on the plate 13 is set upwards again, the plate 13 during the lapping is set on the first tool 11, this plate 13 is lapped from the surface of the metal membrane, and the final plate 13 is made to be 10 μm thick approximately. At the same time since the plate 13 is lapped from both sides, the distortion is limited to be minimum when the plate 13 is lapped from one side.

[0138] Another example in Figure 15 shows the lapping process of the Quartz plate 13 only with the second auxiliary tool 19 without the first tool 11. Also as seen as an another case in Figure 7 (a) (b), plural holes 16 are made in the first tool 11. The number of holes 16 is 2 or 3, and the quartz plate 13 is connected to the first tool 11 only at the area of holes 16 after the holes 16 are filled with the viscous material as honey, a bond or grease of adhesive 59 or other adhesives. The plate 13 can also sucked by the vacuum force through the holes 16. The hole 16 locate at the circumferential region as shown in Figure 17(a), or they are set coaxially as Figure 17 (b), but these are not all cases. When the quartz plate 13 is connected by the holes 16 of the first tool 11 only at the small area of holes 16, the second tool 19 is not always used.

[0139] When the quartz plate 13 is used to be absorbed to the upper surface of the first auxiliary tool 11, the one face lapping machine is employed, since the dual faced lapping machine is not used. However it is omitted to show the structure diagram of the upper tool surface 11 to be connected.

[0140] Figure 18 and Figure 19 show the shape of the quartz plate 13, which is lapped by the first lapping tool 11 and the second tool 19 as seen in Figure 13. It is the reason why the shape of the plate 13 in Figure 18 is different from that in Figure 19 that the material of the second tool 19 is different between Figure 18 and Figure 19. This is applicable only to the case of the lapping plate 17 and 18, which is made of the suede (pad or buff), and the shape in Figure 18 becomes identical to that in Figure 19 when the lapping plates 17 and 18 are made from iron, tin and so forth. However the lapping agent 65 for the lapping plate of tin should be made from cerium oxide, diamond or GC etc.

[0141] The second tool 19 in Figure 18 is made from hard glass of quartzite which hardness is same as the quartz plate 13, and the tool 19 in Figure 19 is made from hard metal as super steel or iron or fro plastic which is more difficult to be machined than the quartz plate 13. The lapping agent 65 must be cerium oxide, since the quartz plate 13 can be well lapped by the agent 65 due to the quartz similarity of quartzite as hard glass, however the second tool 19 made from hard metal as super steel or iron is too hard to be lapped by the agent 65.

[0142] As shown in Figure 20 and Figure 21, the upper and lower lapping plate 17 and 18 revolves with the supply of slurry (moving whetstone grains), the quite thin quartz plate 13 can be lapped easily. When the carrier 37 of the first lapping auxiliary tool 11 is set between the sun gear 39 and the internal gear 38 and the first tool 11 revolve around the sun gear 39 and also rotate itself, which is known as the planet motion, the extremely thin quartz oscillator is easily lapped, while the upper surface of quartz plate 13, which is held by one surface of the first tool 11 machined by the upper lapping plate 18, and another surface of the quartz plate 13 is machined by the lower lapping plate 17 as shown in Figure 16 (b). In case of one side lapping method, the same technique is used to lap the quartz plate 13.

[0143] After the Quartz plate 13 is machined to be extremely thin as 10 μm for example by the above techniques, it becomes very difficult for the thin plate 13 to be handled and also to set the electrode of the plate 13. Then as shown in Figure 22, the quartz plate 13 is set

at the center of the holding frame 48, which is made from an isolator or a non-isolator, the plate 13 is held to the frame 48 by a fine gold wire 49 (for example 18 μm) with the bonding machine. After the quartz plate 13 is set to the frame 48, it is still better for the whole surface of the plate 13 to be pushed upwards, otherwise for the gold wire 49 to be tightened by other means as seen Figure 23 (b), since the wire 48 is loose as shown in Figure 23 (a). As shown in Figure 23 when the quartz plate 13 is fixed to the frame 48 by the wire 49 from three directions at least as shown in Figure 22, the vibration of the plate 13 is absorbed by the wire 49 and the quartz property is enhanced to the uttermost degree, since the plate 13 becomes the state of floating as if in the air.

[0144] After the quartz plate 13 is set to the frame 48 by the wire 49 as seen Figure 23, the electrode 50 is deposited to the small central part of the plate 13 by gold and so on, and electrodes at both surfaces are connected to the gold wire 49 by the bonding machine as shown in Figure 24. Then electrodes 50 are set only at the center of the plate 13 by the fine gold wire 49 (approximately 18 μm), and the quartz property does not deteriorated as the conventional electrodes (for example the evaporated ones at the whole quartz plate).

[0145] Figure 25 shows the manufacturing system of concave quartz oscillator 13 at one side. In Figure 25, the number 11 is the first lapping auxiliary tool, 19 is the second lapping auxiliary tool, 41 is a motor to rotate these tools 11 and 19 at a low speed (foe example from 100 to 300 rpm), 43 is a motor to rotate a lapping tool 44 at a high speed (for example 5000 rpm). The lapping tool 44 is made from soft material as felt, cotton stick, buff etc., this tool laps approximately at 1 mm/min by cerium oxide, GC or diamond grains and so forth. As seen in Figure 26, the quartz plate 13 of approximately 40 μm thickness is finished to the plate 13 of the central 2 ~10 μm thickness. Also Figure 25 shows the manufacturing system of quartz plate 13 in a concave lens shape. In this case, when the lapping tool 44 is electrically gild by diamond whetstone grains, the quartz plate 13 can be easily lapped to the concave shape. Afterward, when the concave quartz plate 13 is lapped by the dual face lapping machine or one face machine, the concave quartz oscillator 13 is finished up in the concave shape as seen in Figure 43 (b).

[0146] The lapping auxiliary tool 11a or 11b in a plane shape is made from Quartz, super steel, plastics, quartzite, glass or metal plate as shown in Figure 27, Figure 28 and Figure 29 in addition to those structures in Figure 11 and Figure 12. An adhesive layer 59 is made from pine resin and paraffin and so forth as shown in the hatched zone, the quartz plate 13 in the plane or convex shape is fixed and connected to the auxiliary tool. This plate 13 and tool 11a or 11b are lapped by the dual-face lapping machine (lapping table). After the one face lapping machine 17 is laps the auxiliary tool and another one 18 does the quartz plate 13, the Quartz plate is detached from the tool. This procedure enables the quartz plate 13 to be lapped accurately down to very thin shape regardless of thickness of the carrier 37 of the lapping table. When the material of the tool 11c in Figure 29 is quartz or super steel, the following merits are got compared to the tool 11b in Figure 28.

(1) The quartz plate 13 can be fixed to the auxiliary tool 11c by the side wall of the plate 13, since the adhesive layer 59 is thicker than that in Figure 28.
(2) Even if the thickness of the plate 13 becomes extremely thin, the plate 13 can be connected the tool 11c, since the thickness of the layer 59 can be thicker.

[0147] (From Figure 30 to Figure 41, the examples of sound to electric converter are given in the last part of this section.)

[0148] Figure 42 (a) shows a piezoelectric plate 57 for an angular velocity sensor, this is made by pasting two piezoelectric plates 57 of lithium niobate or potassium niobium and so on to an adhesive layer 59 of isolator. One side of the piezoelectric layer 57 is thick as 350 μm, and another side of the layer 57 is thin as 25 μm.

[0149] Figure 42 (b) shows a piezoelectric plate of static electric capacity type, which is developed by the manufacturing method in Figure 1. In this case the central thick part of the piezoelectric plate 57 is machined to be in a circular concave lens shape (inverted mesa) of 3 mm diameter, the thickness of the lens is 25 μm, and the adhesive layer is also 25 μm.

[0150] Figure 43 (a) shows the shape of quartz plate 13, which is made by the following process.

(1) The plate 13 is masked by the resist pasting, the membrane is made from metal film or other materials.
(2) When the plate 13 is lapped by the chemical wet etching or by RIE process of fluorine gases, the concave inverted mesa type is made at the diameter of 1.5 mm for example.

[0151] The following merits are listed for the lapping method as shown in Figure 44, Figure 45 and Figure 46.

1. The dual face lapping machine can make quartz oscillators in extremely thin plane or concave shape.
2. When the dual face lapping machine is used to make oscillators, the machining accuracy of the plane and concave part is unchanged, since the rear surface can only be lapped without machining the plane or concave surface.
3. When the dual face lapping machine is used to make oscillators from the rough lapping to the fine polishing, the machining accuracy of the plane and concave part is unchanged, since the one side lapping can be done with the first lapping auxiliary tool 11.

4. The one side lapping method with the first lapping auxiliary tool 11 can maintain the parallel accuracy and plane accuracy for the dual face lapping machine.
5. The first lapping auxiliary tool 11 can accomplish the merit for the RIE or chemical etching, one side lapping machine and for the dual face lapping machine.
6. The first lapping auxiliary tool 11 can cancel the disadvantage of one side lapping machine.

[0152] Figure 47 shows the shape of the quartz oscillator which electric property is enhanced by motioning the dual face lapping machine like a planet on the quartz plate 13, which both sides are made to be concave by RIE, plasma or other wet etching process, and by eliminating the reaction changed layer (fluorine combination or oxide layer) due to the wet chemical etching and so forth, without using the first auxiliary lapping tool 11 shown in Figure 13.

[0153] Figure 48 shows the ground plans of masking on the quartz plate 13 of 2 inch wafer, when the quartz plate 13 is actually made, of the etched quartz plate 13 in hundreds and thousands of planer, one-side concave or both-side concave shape by the chemical etching process, and of a rectangular or circular blank after the Quartz plate 13 is cut. By the way the rectangular shape is usually employed, though the circular shape is seen in Figure 48 (a) and (b).

[0154] Although only one blank is made in Figure 44, 45, and 46, many blanks are actually etched at the same time as shown in Figure 48 where the quartz plate 13 of 2 inch wafer is etched by the wet chemical process and so forth after it is masked by the resist powder.

[0155] The quartz plate 13 which has many holes of single-side concave, double side concave or planer shape after substantial etching processes is lapped by the lapping auxiliary tool 11, the tool 11' or the third auxiliary lapping tool 61 in Figure 49. Otherwise, the dual face lapping can be directly done by the planet motion of the carrier 37 in Figure 20, or the plate can be machined by the single side lapping machine. By these processes the precise costless plate 13 can be mass-produced in a short time by individually cutting the quartz plate 13 after the wet chemical etching again to adjust the resonance frequency.

[0156] When the quartz plate 13 of 2 inch wafer in Figure 48 (a), (b), (c) and (d) is lapped to be concave in one by one, hundreds, thousands pieces, the quartz plate 13 can also be directly lapped dual facedly by the planet motion with the carrier 37 in Figure 20, after the plate 13 is inserted into the space 13 of the third auxiliary machining tool 61 which is made from plastic, super steel, steel or other metal and material.

[0157] Although Figure 49 shows one manufacturing process of lapping in addition to the machining of quartz plate 13, the lapping and machining processes of one by one, hundreds, thousands concaves are exactly identical to those of the plate 13 in Figure 49.

[0158] The manufacturing conditions of the quartz plate 13 in Figure 49 are that the rear surface of the concave shape is lapped by the lapping plate 18 pasted by the pad or suede 15 and that the concave surface is lapped by the lapping plate 17 of steel or metal plate as tin plate. When the lapping is done by the lapping agent 65 of tiny diamond, GC or cerium oxide and so forth, the quartz plate 13 is put into the space 62 of the third auxiliary tool 61, and the plate 13 combines the third tool 61. If the combined plate 13 and the tool 61 move always like a planet with the carrier 37 in Figure 20, the quartz plate 13 can be effectively manufactured up to the ultimate accuracy, since the third tool 61 which is made from super steel etc and located around the plate 13 improves the parallelism and surface accuracy of the lower lapping plate 17 of tin and so forth.

[0159] When the cerium oxide is used to lap due to the good fitting of the quartz plate 13 as a lapping agent 65 by using the lower lapping plate 17 of metal as steel and tin and the upper lapping plate 18 pasted by the pad or suede 15, over 90 percent of the lapped thickness is machined by the upper lapping plate 18. Therefore the oscillating plate of the Quartz plate 13 is only lapped to be very thin step, since the rear flat surface of the concave plate 13 can solely be machined as shown in Figure 49 (b).

[0160] Furthermore even if the height of the third tool 61 is same as that of the concave quartz platel3, the plate 13 inside the tool 61 can be lapped approximately into 15 μm, when the lapping plate 18 of urethane or fabrics is used, since the third tool 61 is made from super steel. For instance when the plate 13 is 80 μm thick, the quartz plate 18 can be lapped to 80μm-15μm=65μm, even if the height of the third tool 61 is same as that of the plate 13.

[0161] There are some cases where the rectangular pate quartz plate 13 inside the rectangular space 62 with the third tool 62 and the direct carrier 37 in Figure 49 (c) is lapped more effectively than that in the circular space 62 in Figure 49 (e).

[0162] Figure 50 shows the lapped states of quartz plate 13 which is 15 μm deep concave, when the plate 13 is etched by RIE from the upper side of the plate 13 after masking the plate 13 by a mask plate 63 which is made from the ultrasonically machined quartz with 5 mm holes, Tungsten or other materials.

[0163] It is the reason why the masking plate 63 is used instead of the masking metal membrane that the membrane on the quartz plate 13 is utterly consumed to zero during the lapping process to the concave 15 μm which shape, since the thickness of the optically made membrane is only 1 μm. Then it is impossible for the quartz plate 13 to be shaped more deeply down to 15 μm by RIE process without employing the masking plate 63 with 0.5 mm holes for example. The material of the masking plate 63 for RIE is quartz or similar one as quartzite, since the surface of the quartz plate 13 is dis-

solved by fluorine gases for RIE, deposited by other material in the plasma state and becomes rough. Then the precise making of the quartz plate 13 becomes impossible, and quartz and similar quartzite is utilized for the masking plate 63 on the quartz plate 13. If Pyrex is used for the masking membrane 63 as a poor case, various impurities as aluminum in Pyrex is dissolved by fluorine gas, the combined alumina deposits on the surface of quartz plate 13, and we can use Pyrex etc.

[0164] Instead of the above methods, it is possible for the masking easily to paste the resist on the surface of the quartz plate 13 by Dry Film (trademark of Dupon MRC Dry Film Inc.). Another method of the masking can be to paint the resist on the surface of the quartz plate 13.

[0165] Figure 51 and Figure 52 show a mechanical lapping method, after the quartz plate 13 is etched in the double-sided concave or convex shape by means of RIE, the plasma etching or other chemical wet etching processes. It is for the etching changed layer of the chemical wet etching process in the concave shape to be eliminated by the dual face lapping machine or the one face lapping machine as the secondary lapping method, and to make the accurate parallel surface without the undulation. The quartz plate can be lapped to be ultimately thin by the mechanical lapping method, by smoothing the rough surface due to the etching.

[0166] In these Figures the hatched area is eliminated by using the mechanical lapping or the chemical etching process.

[0167] Figure 52 and Figure 53 show the second manufacturing method of the quartz plate 13 which central part of 0.5 mm diameter was previously lapped by RIE or other wet etching processes, while the first method is the finishing mechanical lapping process in Figure 1 (a). Since the second method requires small gripping area to lap the quartz, it becomes possible for the plate to be machined to be convex in the single or double sided shape in a short time, and also to be made to combine the holder 51 to the convex or concave lens part by the smooth line 53 as seen in the Figure.

[0168] After the quartz plate is machined to the bi-convex shape both by the machining and lapping processes in Figure 54 c, and the both faces are similarly lapped as 9. 25 μm by RIE etching, ultra thin quartz oscillators are easily manufactured very accurately as seen in Figure 54 (d) or Figure 54 (d').

[0169] Figure 55 (a) and Figure 56 (a) shows one inch rectangular quartz plate 13, which is lapped to be 80 μm thick in the mirror surfaces by the dual face lapping machine.

[0170] Figure 55 (b) and Figure 56 (b) shows 12 μm thick quartz plate 13 which one side is lapped 68 μm by RIE process. Figure 55 (c) shows the 10.5 μm thick plate 13 which rough layer (non crystalline state due to RIE) as 1. 5 μm is lapped by the wet etching process. Figure 56 (c) shows 9 μm thick quartz plate 13 which is lapped as 1.5 μm from the both sides of 12 μm plate.

[0171] Figure 57 shows the electric frequency property (56.595 MHz), which is measured for the 29.5 μm thick plate similar to Figure 57. Figure 58 shows the property (96. 1599 MHz) of 17. 36 μm quartz plate. Figure 59 shows the frequency as 96. 8547 MHz of 17.2 μm plate. Figure 60 shows the frequency as 136.1149 MHz of 12.26 μm plate. These frequency-reactance characteristics are measured to be very excellent.

[0172] Figure 61 and Figure 62 shows the lapping process of the quartz plate 13, which has little distortion since the lapping plates 17 and 18 are made from same material as quartz as the plate 13. Figure 62 and Figure 63 have the hatched black region which is made from resin and used to reinforce the concave part of the plate 13.

[0173] As shown in Figure 64, after the quartz plate 13 is pasted by the adhesive as pine resin on the forth lapping auxiliary tool 66 which is made from quartz, hard glass, metal or other material in a planar shape with holes 64, the rear surface of the plate 13 and one face of the tool 66 are lapped by the upper and lower lapping plate 17 and 18 of the dual face machine. The shadow region in Figure 64 is the balanced state of the lapping pressure to the concave internal force as seen in the arrow of Figure 64 (b), however there exists no concave shape. The stronger the lapping pressure is compared to the internal force, the better concave the quartz plate is seen Figure 64 (d).

[0174] Figures 65, 66, 67, 68, 69 and 70 show the quartz plate 13, which is 80 μm thick and 60 μm deep concave as shown in Figure 61 and the diameter is 2 mm or 1 inch. Figure 71 and Figure 72 show the quartz plate 13, which is 80 μm thick and 6 mm diameter and the handling area is different.

[0175] From Figure 71 to Figure 78, the quartz plate 13 is shown for 8 cases of the diameter 2, 3, 4, 5, 6 mm and 1 inch. Figure 75 is a measured diagram of the quartz plate 13, which one surface is machined to be in an inverted mesa type shape by the chemical wet etching process and another surface is in a plane shape. Figure 76 shows interference stripes of the resonating part, which is perpendicular to the rear concave surface of the quartz plate 13 in Figure 75, after the plate 13 is lapped b the dual face lapping machine in Figure 74 (d).

[0176] Figure 79 and Figure 80 show the lapping state of the quartz plate 13, which is double inverted mesa type after the plate is machined by the upper and lower lapping plate 17 and 18 of the dual face lapping machine in Figure 71. Figures 81, 82 and 83 show the lapping process of the quartz plate 13, which is double inverted mesa type after the rough surface (approximately from 0.1 μm to 0.5 μm thick) due to the etching is machined by the upper and lower lapping plate 17 and 18 of the dual face lapping machine in Figure 71. Figure 83 shows another lapping state of the quartz plate 13, which is machined by the upper and lower lapping plate 17 and 18 with the pad or suede 15.

[0177] Figure 85 shows the reactance-frequency

property of the quartz resonator 13, which is machined to be an inverted mesa shape by the lapping machine in Figure 84 and both rough surfaces (0.02 μm thick) are eliminated. The resonance frequency is 91.5 MHz, and the thickness of the plate in Figure 85 is 18.25 μm. Figure 86 shows the reactance-frequency property of the quartz resonator 13, which is machined to be an inverted mesa shape by the lapping machine in Figure 84 and both rough surfaces of 0.217 μm are eliminated and thickness of the plate in Figure 86 is 18.034 μm. Figure 87 shows the surface shape of the Quartz resonator 13, which resonating surface is enlarged and the convex height is 0.8 μm.

[0178] Figure 88 and Figure 89 show the lapping state of the quartz plate 13, which double inverted mesa type plate is machined by the dual face lapping machine, after the plate is shaped to be concave by the wet etching or other RIE processes.

[0179] As shown in Figures 88, 89, 90 and 91, when the quartz plate 13 is etched chemically and machined by the dual face lapping machine, the plate becomes naturally convex or concave as seen in Figures 88 (e), 89 (e) and 91 (e), since the force to the lower lapping plate over the upper one is 55/45.

[0180] Figure 92 (a) shows an example of reactance-frequency characteristics for the quartz resonator, which is made by so-called dry etching process as RIE, ion milling or plasma etching. Near the peak fundamental frequency there is a spurious peak possibly due to RIE ion damage. After the surface is lapped manually, the spurious peak disappears as shown in Figure 92 (b), and the property improves.

[0181] Figure 93 shows the quartz oscillator of single inverted mesa type, which quartz wafer is masked and etched chemically for the mass production of quartz blank. As seen in Figure 93 (b), the reactance-frequency property is similar to RIE in Figure 1 (a).

[0182] Figure 94 shows the reactance-frequency property of thin high frequency quartz oscillator in the single mesa shape, which is made by RIE and mechanical polishing with the dual face lapping machine. Figure 95 shows the property of the single mesa type quartz oscillator, which is made by the dual face lapping machine of two different upper lapping plate. The ratio of the load for the upper lapping plate of iron is 1.8 times of aluminum. Figure 96 shows the reactance-frequency property of quartz resonator, which has four lapping materials and two lapping pressures. The stronger the pressure is, the sharper the resonance is, however the spurious resonance is observed. There is the optimum pressure and aperture/thickness ratio.

[0183] Figure 97 shows the peak to valley (P-V) at 1.44x1.31 mm central part in order to study the effect of the resonating thickness to the form and surface thickness.

[0184] Figure 98 shows the inverse of curvature radius for the convex lens. Figure 99 shows the surface roughness of the concave central part.

[0185] These tests result in the conclusion that the optimum diameter to thickness ratio is between 10 and 350 and approximately 80, and that the high frequency quartz resonator over 334 MHz is found to be made to show excellent electric property, as follows.

(1) When quartz blanks of single inverted mesa type is used as the lapped material, quartz oscillators for ultra high frequency applications became feasible to be excellent electrically, after these blanks were machined by the conventional dual face lapping machine, float polishing system or other lapping machines.

(2) These developed machines could make plano-convex type oscillators from single inverted mesa types. Electric characteristics of double inverted mesa types were improved as well as the single types.

(3) The optimum diameter to thickness ratio (d/t) was found to be between 10 and 350, and the typical value of d/t was approximately 80.

[0186] In the following section a sound-electric converter is introduced as an application of the piezoelectric element. The conventional prediction of earthquake uses sea observation, underground structure search, global magnetic detection, GPS and ground displacement search of laser distance measurement, however another method may be air vibration sensing. A sound gathering microphone was employed to convert the air vibration to electric signal, which is easy to record and analyze, but it was difficult to detect the sound of the specific frequency due to the noise pickup.

[0187] Figure 30 (a)-(e) show five examples of sound-electric converter, which are executed by the piezoelectric element of the present invention. In these Figures piezoelectric cylinders 21 and 54 are made from monocrystal as quartz or lithium niobate etc. or ceramics as barium titanate and so forth. The central part of the cylinder 21 and 54 has a pressure surface 22, which has a pair of electrodes 23 and 24 connected to an amplifier 25 to measure the induced voltage between the electrodes. Figure 30 (a) (b) (c) (d) and (e) shows the bi-convex, dual concave, plane, round circumferential plane and plano-convex type, respectively. As seen in Figure 30 (a), A room is made by sealing the inside of cylinder 21 with two plugs, and B room is made by sealing the inside of cylinder 54.

[0188] Figure 31 is the upper view diagram of the sound-electric converter in Figure 30 (a) (e), where a hole or space 47 is formed by the pressure sensing surface 22. Then the vibration, which is induced from cylinders 21 and 54, moves freely from A to B or from B to A in Figure 30 (a) (e), the vibrations at A and B resonate at the central part, and the pressure sensor 22 is vibrated more strongly than the case without the hole or space 47.

[0189] The pressure sensor 22 is made as follows.

Basically as shown in Figure 32, it hold a circle stick 30 with the zipper 31 of the processing machine such as a lathe, and hold the processing tool 33 that rotation set up the whetstone 32 which made a diamond whetstone grain stick to the surface of the metal ball again in the tip freely with the tool holder 34. The whetstone 32 is the sphere body that a confrontation side was cut as shown in Figure 33, and it is gaining rotation freely with it through the shaft carrier 36 at the tip of the support arm 35. As seen in Figure 34, it has the direction that a V letter-shaped groove 32a is contained in the form groove 32a wall one side whetstone 32 center pass side. Another application of the above lapping process is shown in Figures 2, 3 and 4 by using a whetstone 32 in Figure 36 (e).

[0190] The whetstone 32 of the much smaller diameter from the hole diameter is used as shown in Figure 37, and it turns a whetstone 32 with going along the tune side of the pressure side 22 with the NC device and so on and moving it. The tool to turn around the usual shaft can be used for processing of the hole of the circle form, and the whetstone of the circular board surface form shown in the whetstone of the spherical surface form shown in Figure 38 and 39 can be also used.

[0191] And it is the production figure of the grinding device to show it in the figure 40 and 41, which has structure to show in Figure 33. When the diameter of the whetstone 32 is 20 mm and the depth of the groove 32 (a) is 1 mm, it faces on one side of the whetstone 32, and the number of the actual measurement value that the number of the rotation of the whetstone 32 was measured with the air pressure when it was jetted in the tangent direction is shown to grinding and a grinding device in the following from the air nozzle 40.

1. The rotation of the whetstone 32 is approximately 12,200 rpm, when the air pressure is 0.5 atmosphere.
2. The rotation of the whetstone 32 is approximately 22,000 rpm, when the air pressure is 1.0 atmosphere.
3. The rotation of the whetstone 32 is approximately 37,500 rpm, when the air pressure is 2.0 atmosphere.
4. The rotation of the whetstone 32 is approximately 47,800 rpm, when the air pressure is 3.0 atmosphere.
5. The rotation of the whetstone 32 is approximately 50,000 rpm which is the limiting case of the bearing, when the air pressure is 4.0 atmosphere.

Effect of Invention

[0192] The present invention of the piezoelectric element has the following effects.

1. High frequency quartz oscillators for example, which have an excellent electrical characteristics, become possible to be manufactured from the quartz blank by the conventional dual-face lapping machine, single-face lapping machine or float polishing machine.
2. The present invention enables the single inverted mesa type shape to be the plano-convex type. Also the electrical performance of the double inverted mesa type shows same improvement as the single inverted mesa type.
3. The Quartz oscillator over 334 MHz becomes available when the aperture ratio of the diameter to the depth is approximately 80.

[0193] As mentioned above, the present invention makes the piezoelectric element to be extremely thin as less than 10 μm and to show practically no spurious signals.

Industrial Applicability

[0194] The present invention can be applied to a wide variety of fundamental oscillation sources for communication instruments and detection instruments, and micro clock generators for general computers, OA information technology and other instrumentations.

Claims

1. An arbitrary shape piezoelectric element comprising a planer concave part at one central oscillating surface and a convex-lens-shape convex part at another central surface.

2. An arbitrary shape piezoelectric element comprising a concave-lens-shape concave part at one central oscillating surface and a convex-lens-shape convex part at another central surface.

3. An arbitrary shape piezoelectric element comprising a convex-lens-shape concave part at one central oscillating surface and a convex-lens-shape convex part at another central surface.

4. An arbitrary shape piezoelectric element comprising a concave-lens-shape concave part at one central oscillating surface and a convex-lens-shape concave part at another central surface.

5. An arbitrary shape piezoelectric element comprising a convex-lens-shape concave part at one central oscillating surface and a plane-lens-shape concave part at another central surface.

6. An arbitrary shape piezoelectric element comprising a convex-lens-shape concave part at one central oscillating surface and a convex-lens-shape concave part at another central surface.

7. Manufacturing method for a piezoelectric element featuring the mechanical dual-face lapping of said piezoelectric blank and the polishing of said surface small roughness due to the chemical etching, after one surface or both surfaces of said piezoelectric element which are machined by the mechanical lapping process are chemically etched and become thinner.

8. Manufacturing method for said extremely thin piezoelectric element featuring the manufacturing process of said element by forming grooves and steps on the upper surface of the first auxiliary lapping tool, by connecting the second auxiliary lapping tool which is slightly higher than the depth of said grooves or steps into the grooves or steps of said first auxiliary lapping tool, by setting said piezoelectric blank on the upper surface of said first auxiliary lapping too] inside said second auxiliary lapping tool, and by lapping said blank with the upper lapping plate on said piezoelectric blank and with the lower lapping plate under said auxiliary lapping tool.

9. Manufacturing method for said piezoelectric element as in claim 8 featuring the process of filling liquid in said grooves or steps on said first auxiliary lapping tool surface, setting said piezoelectric blank so as to contact the lower surface of said piezoelectric blank to said liquid, and fixing said blank to said first auxiliary lapping tool by said liquid surface tension or by freezing.

10. Manufacturing method for said piezoelectric element as in claim 9 featuring to set said piezoelectric blank on a thin wet plate with water, and fixing said blank to said first auxiliary lapping tool by using said water surface tension of said thin wet plate.

11. Manufacturing method for said piezoelectric element as in claim 8 featuring making plural holes on said first auxiliary lapping tool, filling viscous material as adhesive into said holes, and fixing said blank to said first auxiliary lapping tool by connecting the lower surface of said piezoelectric blank to said viscous material or by vacuum force.

12. Manufacturing method for said piezoelectric element as in claim 8 featuring to fix said blank to said first auxiliary lapping tool by using pine resin, paraffin, starch paste or other adhesives.

13. Manufacturing method for said piezoelectric element as in any of claim 8 to 12 featuring to use hard glass or metal as super steel as material of said first auxiliary lapping tool, and to use super steel, iron, hard glass or other glasses as material of said second auxiliary lapping tool.

14. Manufacturing method for said piezoelectric element featuring to make a concave part by chemical etching on one surface of said piezoelectric blank, to make thin the base surface of said concave side by ion etching of the opposite surface of said concave side, to lap mechanically both surfaces of said piezoelectric blank, to eliminate the roughness due to said ion etching process, and to form convex-lens shape oscillating part in said concave part.

15. Manufacturing method for said piezoelectric element of the previous claim 14 featuring to make a concave part by RIE process, ion milling plasma etching or other wet etching means only on the central part, after masking said piezoelectric blank one surface by the mask.

16. Manufacturing method for said piezoelectric element featuring to hold said piezoelectric blank on said auxiliary tool, to lap one surface of said piezoelectric blank by one lapping surface of said dual-face lapping machine, to lap at the same time one surface of said auxiliary tool by another lapping surface, and to use said dual-face machine as a single face lapping tool.

17. Manufacturing method for said piezoelectric element featuring to hold the front surface or the rear surface of said piezoelectric blank by said auxiliary lapping tool, and to lap the concave surface of said piezoelectric blank by one lapping surface, and at the same time one surface of said auxiliary lapping tool by another lapping surface of dual-face lapping machine

18. Manufacturing method for said extremely thin piezoelectric element featuring to make the concave part on said piezoelectric blank, to hold said concave part by said auxiliary lapping tool, and to lap the opposite surface of said concave part by one lapping surface and at the same time one surface of said auxiliary lapping tool by another lapping surface by using said dual-face lapping machine.

19. Manufacturing method for said extremely thin piezoelectric element featuring to lap said piezoelectric blank, which surface is concave, concavo-convex or bi-convex, at the same time from the upper side and lower side by using said dual-face lapping machine.

20. Manufacturing method for said piezoelectric element as in claim 19 featuring to fill pine resin, paraffin or other adhesives into the concave pit of said concave piezoelectric blank, and to lap said reinforced concave blank.

21. Manufacturing method for said piezoelectric ele-

ment as in any of claim 16 to 18 featuring to make said auxiliary lapping from hard glass, plastics or metal as super steel or iron, which is hardly lapped by said lapping material as selenium oxide etc, and not easy to lap the one surface of said auxiliary lapping tool.

22. Manufacturing method for said piezoelectric element, as in claim 14, featuring to make the concave part on said piezoelectric blank, after setting the masking plate of holed quartzite on the piezoelectric blank and making the ion etching machining by using the masking technique.

23. Manufacturing method for said piezoelectric element, as in claim 14, featuring to higher the surface lapping accuracy of quartz and so on by using Argon mixed with fluorine gas as CF4, CHF3 or C2H8 etc, when the piezoelectric material as quartz and so forth is ion-etched.

24. Manufacturing method for said piezoelectric element, featuring to make electrodes to impress the electric voltage on the piezoelectric element after connecting fine gold wires to the central part of said piezoelectric plate.

25. Manufacturing method for very thin piezoelectric element, featuring to make the concave part on said piezoelectric blank, after lapping at the same time both surfaces of said piezoelectric blank, which one surface is flat and another side is concave, by using said dual-face lapping machine.

26. Manufacturing method for said piezoelectric element featuring to lap at the same time both surfaces of said piezoelectric blank, which one surface is stil flat and another side is concave, by using said dual-face lapping machine, and to make outer a convex lens shape of plano-convex, concavo-convex or bi-convex at the front side.

27. Manufacturing method for said piezoelectric element featuring to only to lap one surface of said piezoelectric blank by one surface of said dual-face lapping machine after putting said blank naturally on said auxiliary lapping tool made from metal or other material or pasting said blank by adhesives as pine resin, paraffin or others; and also to lap the rear surface of said auxiliary lapping tool by anther surface, and to make plano-convex type, concavo-convex type or bi-convex type by lapping the rear surface of said blank.

28. Manufacturing method for said piezoelectric element featuring to only to put said concave piezoelectric blank on said auxiliary lapping tool with vertical holes, or to paste by adhesives as pine resin or paraffin etc., and to lap one surface of said dual-face lapping machine after putting said blank naturally on said auxiliary lapping tool made from metal or other material, and also to lap the rear surface of said auxiliary lapping tool by anther surface, and to make plano-convex type, concavo-convex type or bi-convex type by lapping the rear surface of said blank.

29. Manufacturing method for said piezoelectric element featuring to lap the damaged layer, which is produced during the conventional wet etching and RIE processes, by mechanical lapping process, after said mechanically lapped piezoelectric blank is made to be extremely thin by said chemical and ion etchings.

30. Manufacturing method for said piezoelectric element, featuring to lap said blank so that one surface is in concave lens shape and another side is protruding as convex lens.

31. Manufacturing method for said piezoelectric element featuring that one surface is in concave lens shape and another side is protruding as convex lens which convex part is only made to be imminent from the flat plate.

32. Manufacturing method for said piezoelectric element featuring that the ratio of the diameter to the depth is from 10 to 350, or preferentially from 30 to 150 for said element.

33. Manufacturing method for said piezoelectric element, featuring to make the perpendicular and horizontal central lines unchanged to the tool holder for any diameters of diamond whetstone grains, by using the ball whetstone which diamond grains are not solely electrically gilt to the touching part of the tool holder, when the ball whetstone is set to the cylindrical tool holder by the magnetic induction of magnet in cylindrical shape etc of the primary axis.

34. Sound to electric converter, featuring to make pressure sensing surface of piezoelectric effect material at the central part and to set a pair of electrodes at said surface.

35. Sound to electric converter, as in claim 34, featuring to make pressure sensing surface of piezoelectric effect material together to the cylinder.

36. Sound to electric converter, as in claim 34 or 35, featuring to make the central pressure sensing surface vibrate intensively, after forming holes or space at the circumferential part of the pressuring surface in order to resonate the air oscillation when the sound comes into both sides of the cylinder towards

said pressuring surface.

37. Manufacturing method of sound to electric converter, featuring to make cylindrical hole into both sides of circular piezoelectric rod by milling method, to make the pressure sensing surface of required thickness at the center of said rod, and to set a pair of electrodes at the pressure outer surface in order to get the electric signal amplified from the environmental air oscillation.

38. Machining method of piezoelectric effect material, as in claim 37, featuring to make grains on the barrel surface of whetstone, to inject air or liquid to the grains, and rotate said whetstone, as the machining means, or to use other mechanical techniques.

39. Manufacturing method for said sound to electric converter, as in claims37 and 38, featuring to make barrel whetstone by using steel sphere in a genuine circular cross section.

40. Manufacturing system for said sound to electric converter, featuring no only to include the machine to fix one end of piezoelectric circular rod and to rotate around the rod axis line, but also to use the machining tool, of which end has the driving mechanism to rotate said whetstone in barrel shape in high speed.

Fig.1

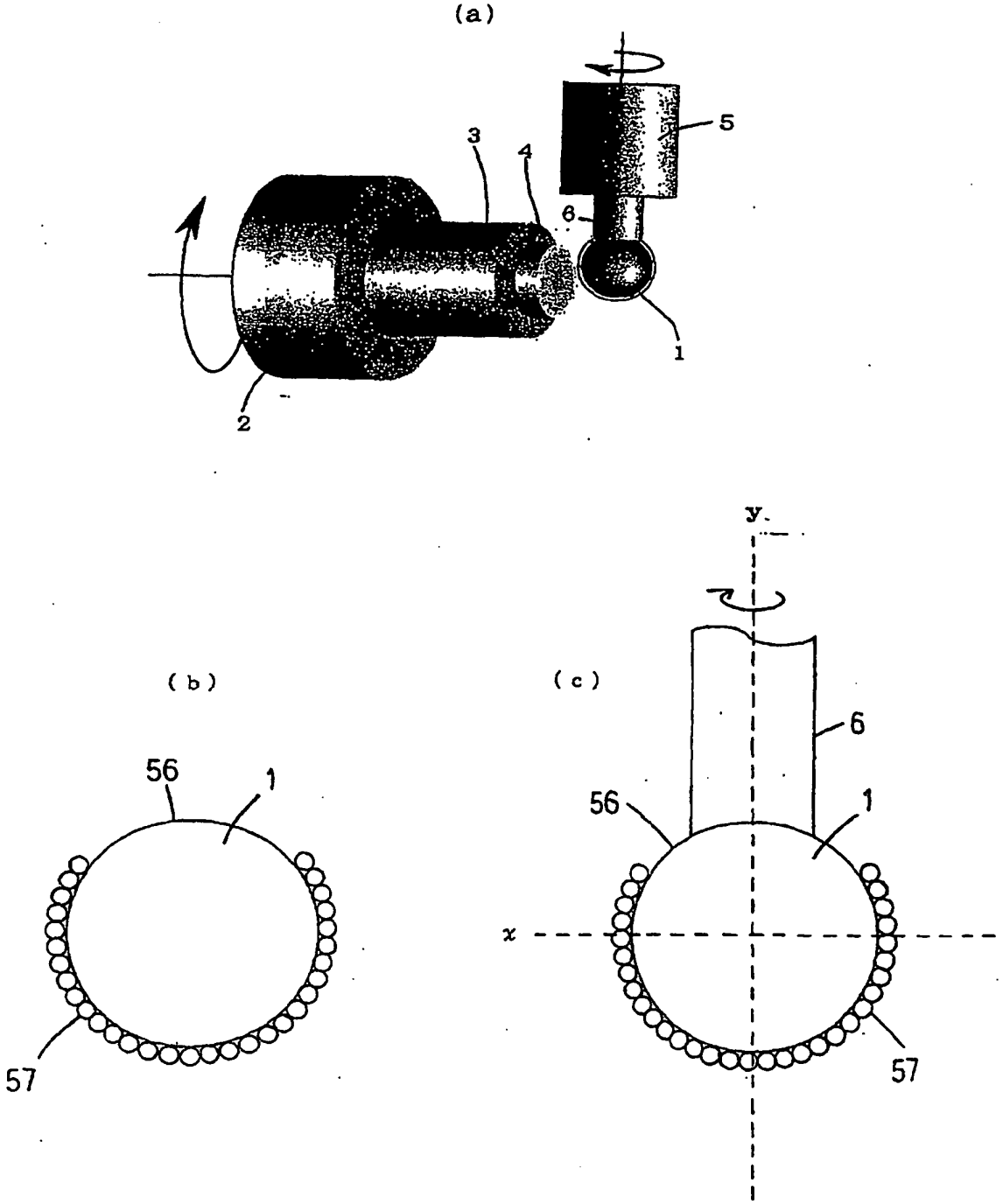

Fig.2

(a)

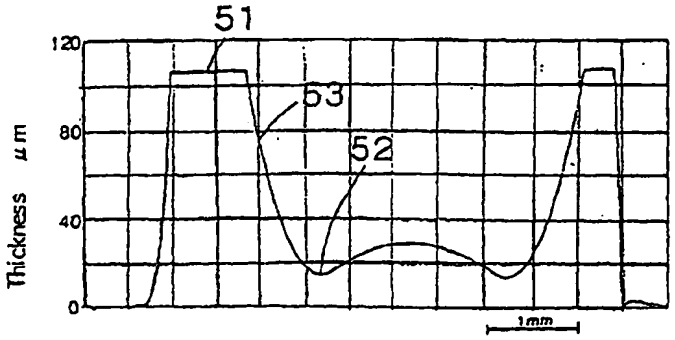
51
53
52
120
80
40
0
Thickness μm
1mm

(b)

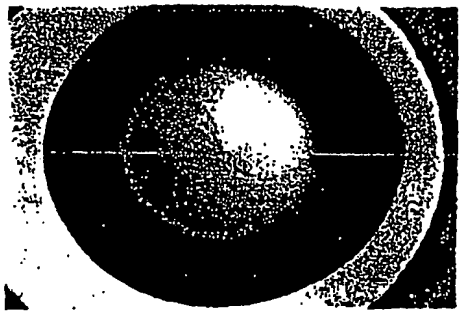

(c)

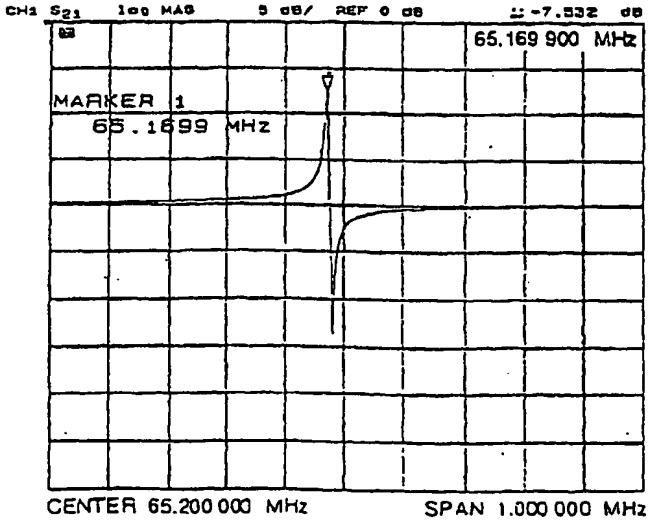
CH1 S21 log MAG 5 dB/ REF 0 dB -7.532 dB
65.169 900 MHz
MARKER 1
65.1699 MHz
CENTER 65.200 000 MHz
SPAN 1.000 000 MHz

Fig.3

(a)

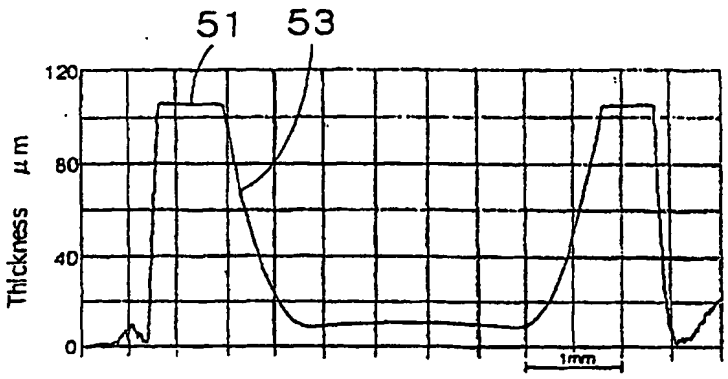
51
53
120
80
40
0
Thickness μm
1mm

(b)

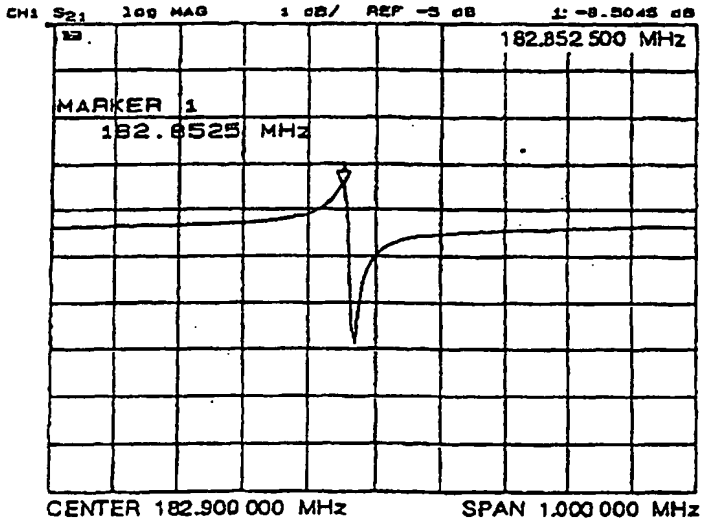
CH1 S21 log MAG 1 dB/ REF -3 dB 1: -8.5045 dB
182.852 500 MHz
MARKER 1
182.8525 MHz
CENTER 182.900 000 MHz
SPAN 1.000 000 MHz

Fig.4

(a)

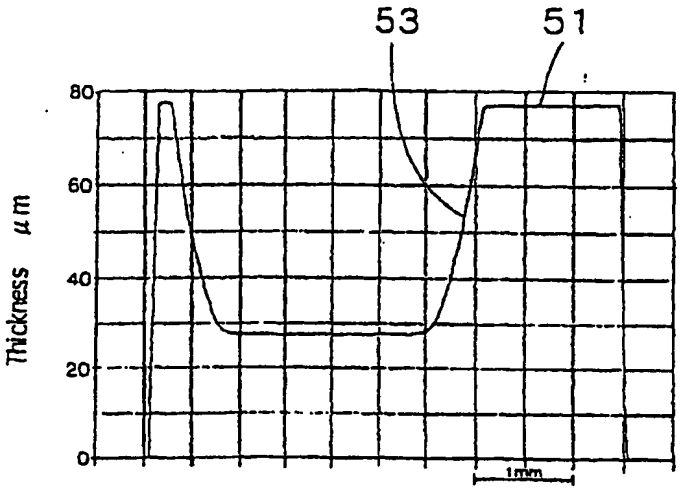
53
51
80
60
40
20
0
Thickness μm
1mm

(b)

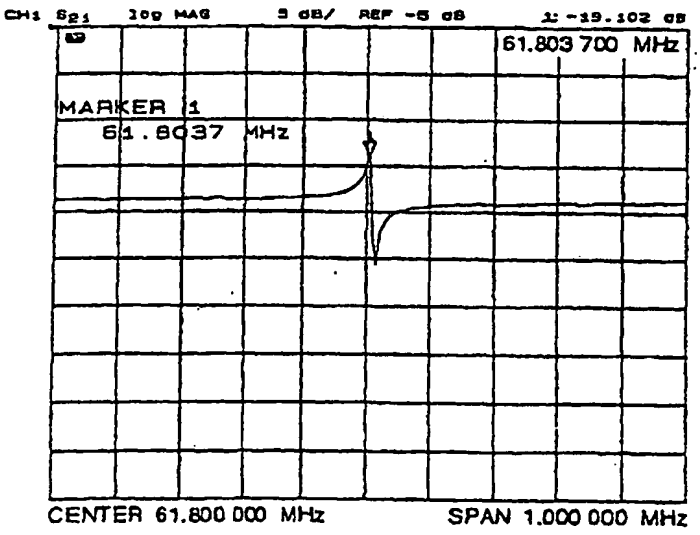
CH1 S21 log MAG 5 dB/ REF -5 dB
61.803 700 MHz
MARKER 1
61.8037 MHz
CENTER 61.800 000 MHz
SPAN 1.000 000 MHz

Fig.5

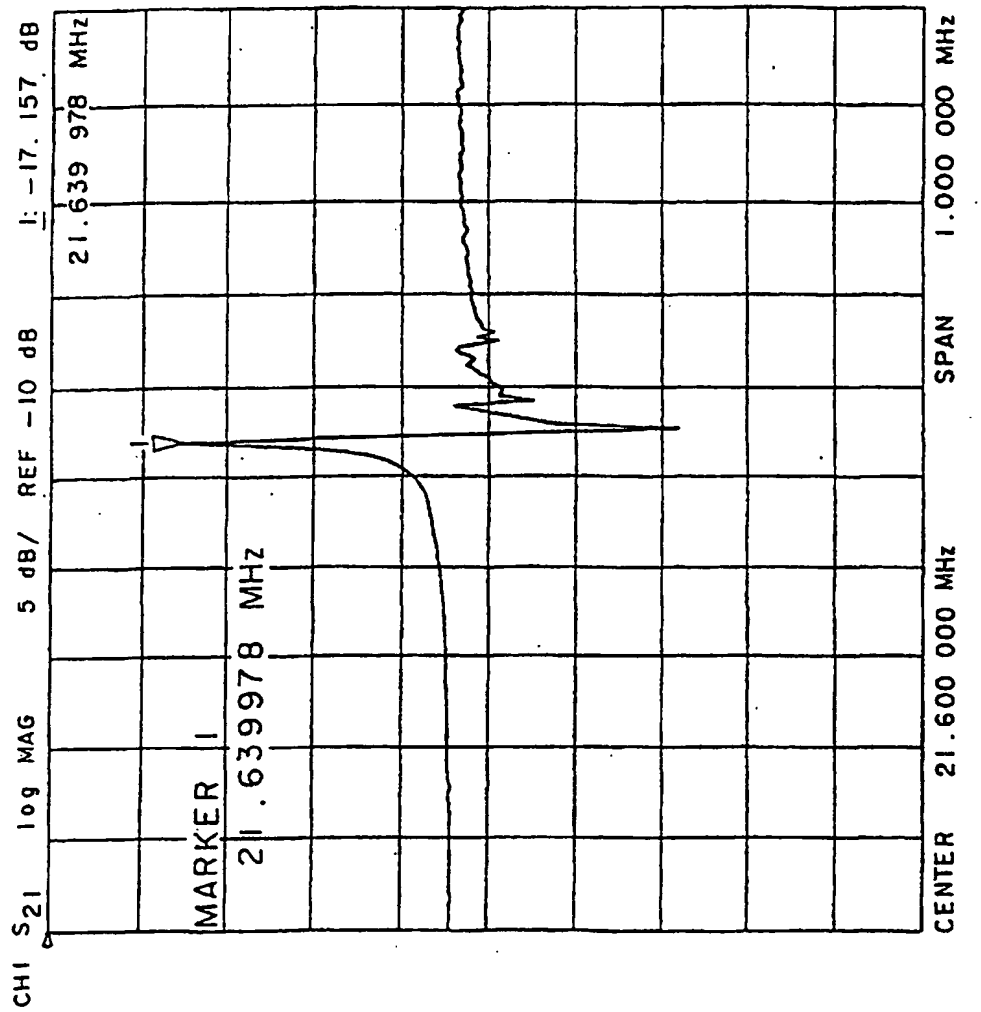
CH1 S21 log MAG 5 dB/ REF -10 dB
1: -17.157 dB
21.639 978 MHz
MARKER 1
21.639978 MHz
CENTER 21.600 000 MHz
SPAN 1.000 000 MHz

Fig.6

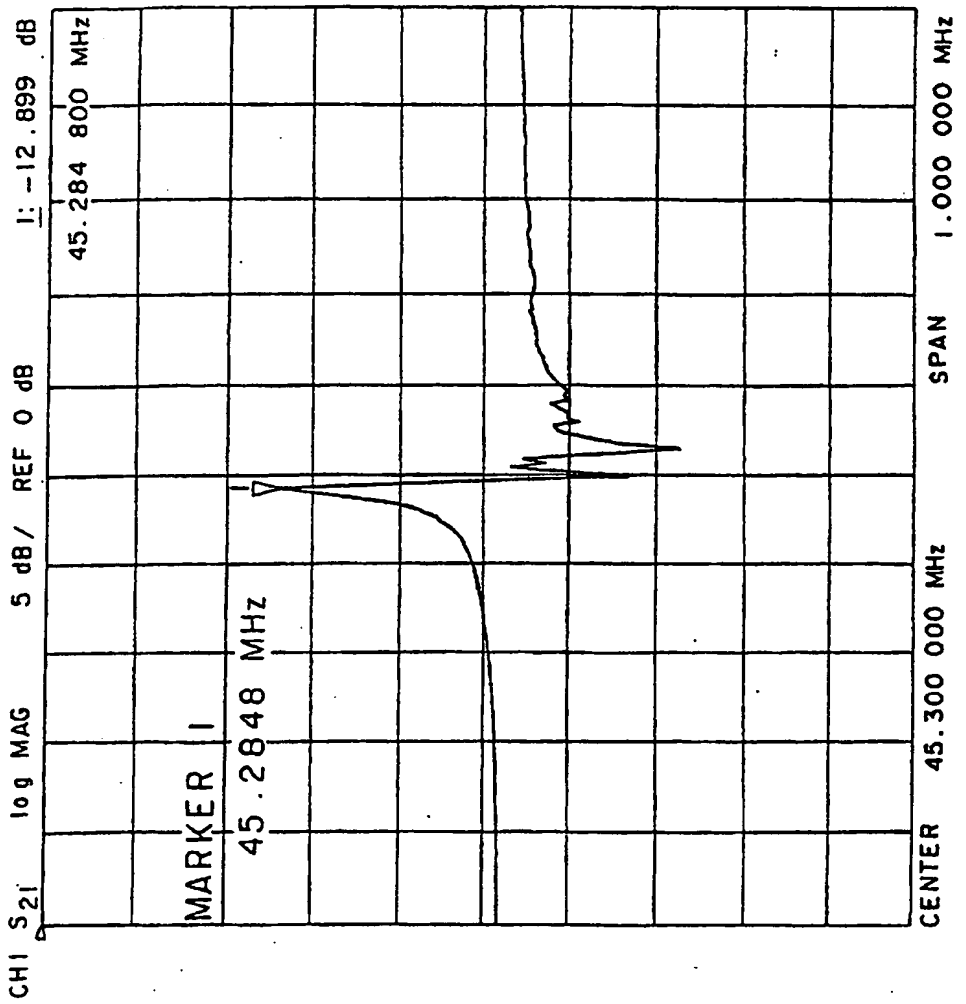
CH1 S21
log MAG
5 dB/
REF 0 dB
1: -12.899 dB
45.284 800 MHz
MARKER 1
45.2848 MHz
CENTER 45.300 000 MHz
SPAN 1.000 000 MHz

Fig.7

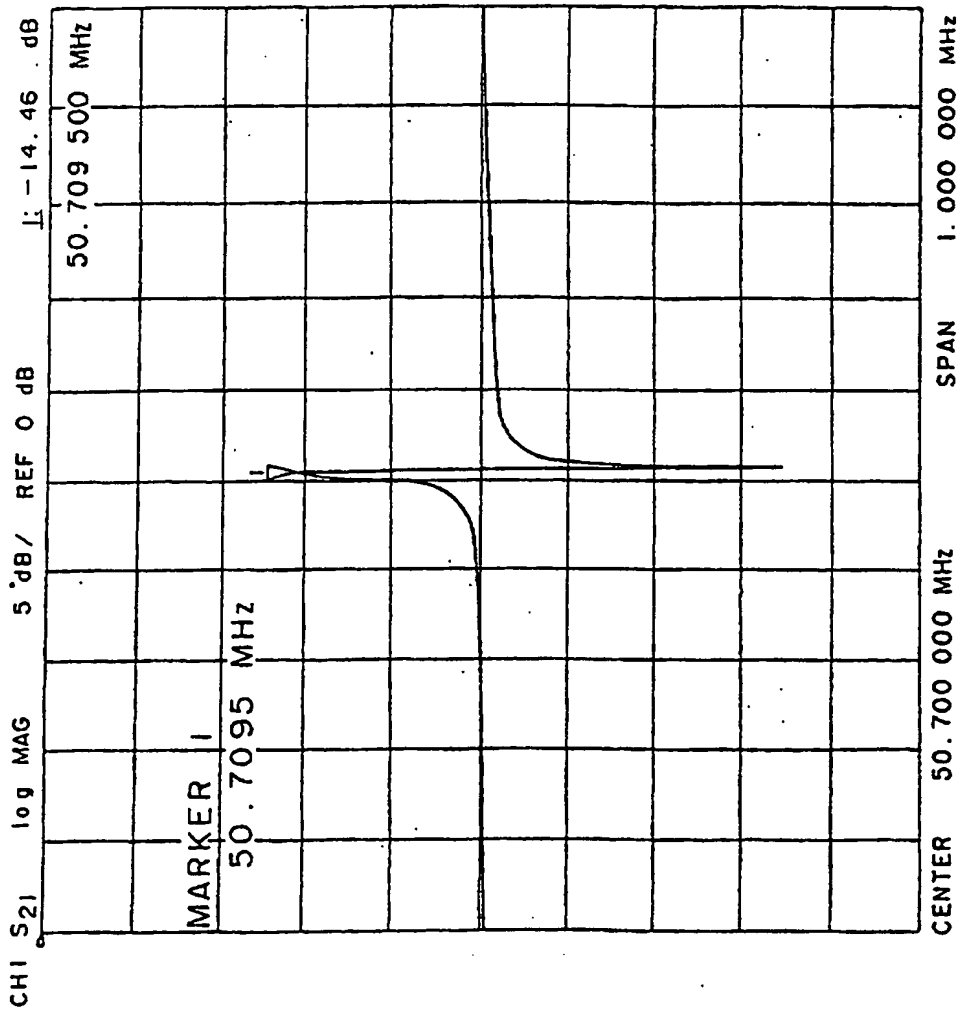
CH1 S21
log MAG
5 dB/
REF 0 dB
1: -14.46 dB
50.709 500 MHz
MARKER 1
50.7095 MHz
CENTER 50.700 000 MHz
SPAN 1.000 000 MHz

Fig.8

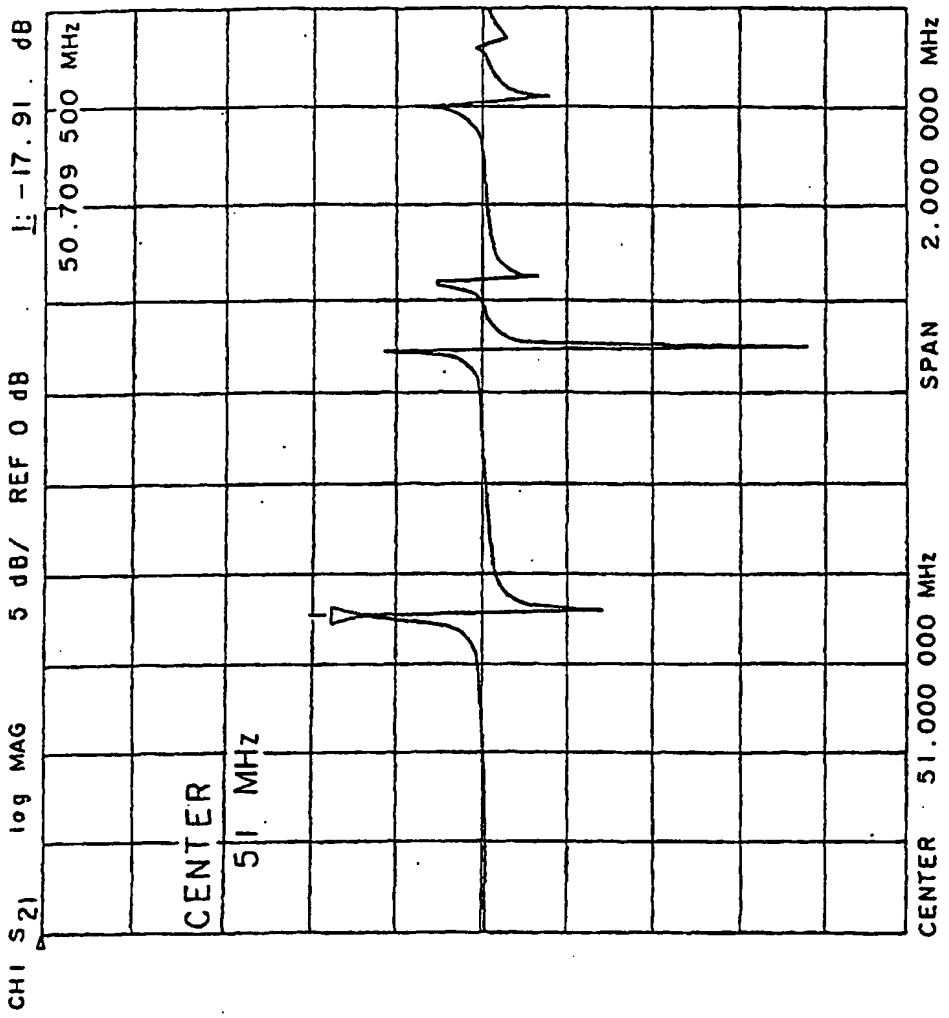
CH1 S21
log MAG
5 dB/
REF 0 dB
1: -17.91 dB
50.709 500 MHz
CENTER
51 MHz
CENTER 51.000 000 MHz
SPAN 2.000 000 MHz

Fig.9

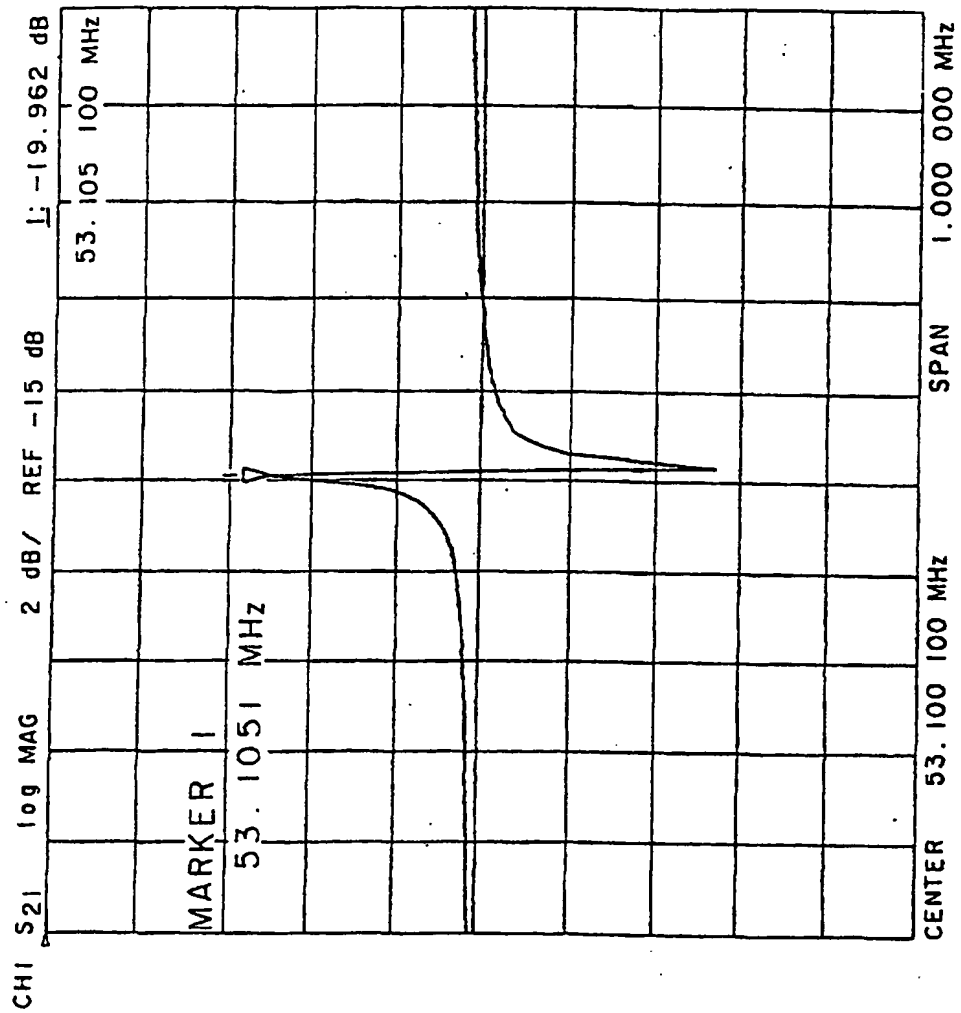
CH1 S21 log MAG 2 dB/ REF -15 dB
1: -19.962 dB
53.105 100 MHz
MARKER 1
53.1051 MHz
CENTER 53.100 100 MHz
SPAN 1.000 000 MHz

Fig.10

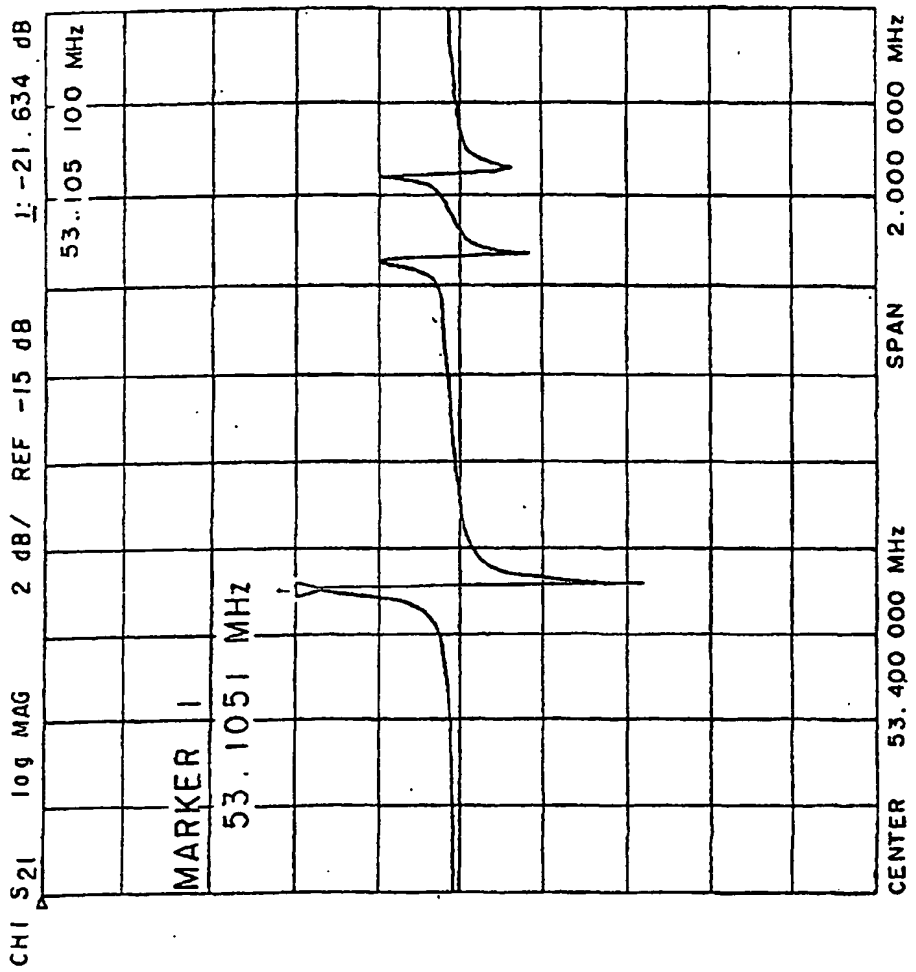

Fig.11

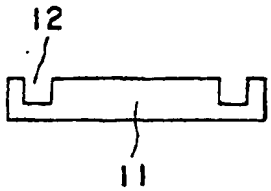

Fig.12

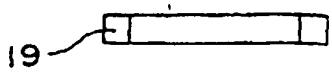

Fig. 13

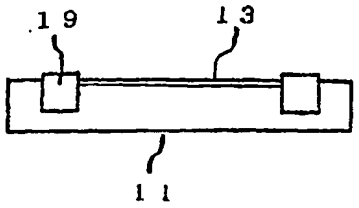

Fig. 14

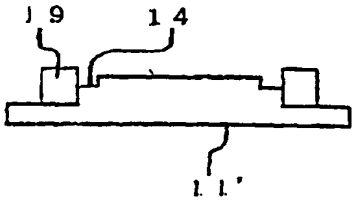

Fig. 15

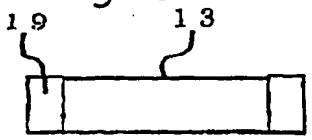

Fig. 16

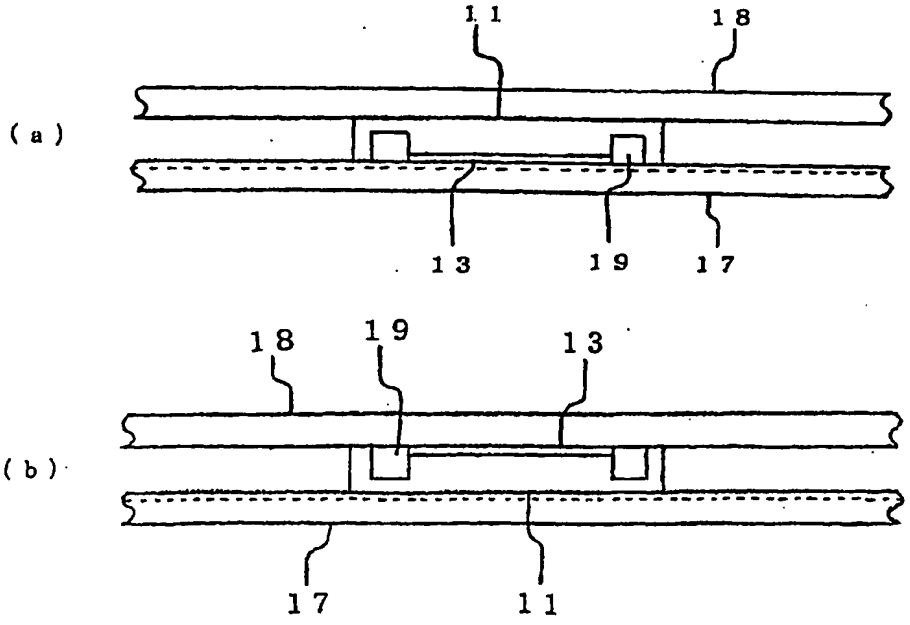

Fig.17

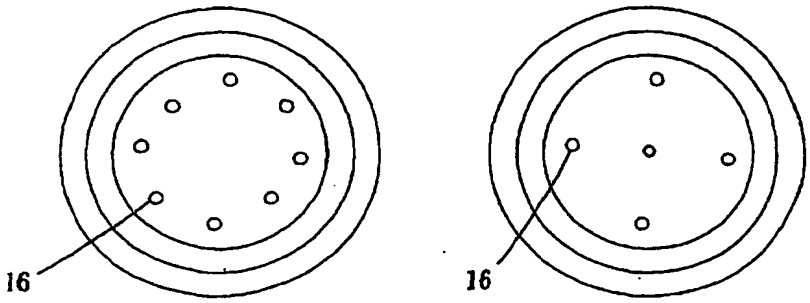

Fig.18

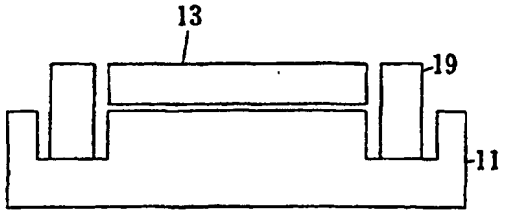

Fig.19

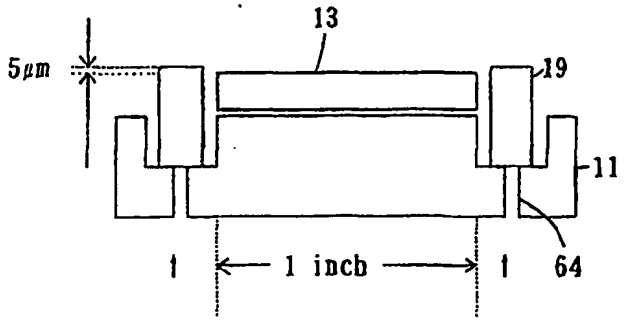

Fig.20

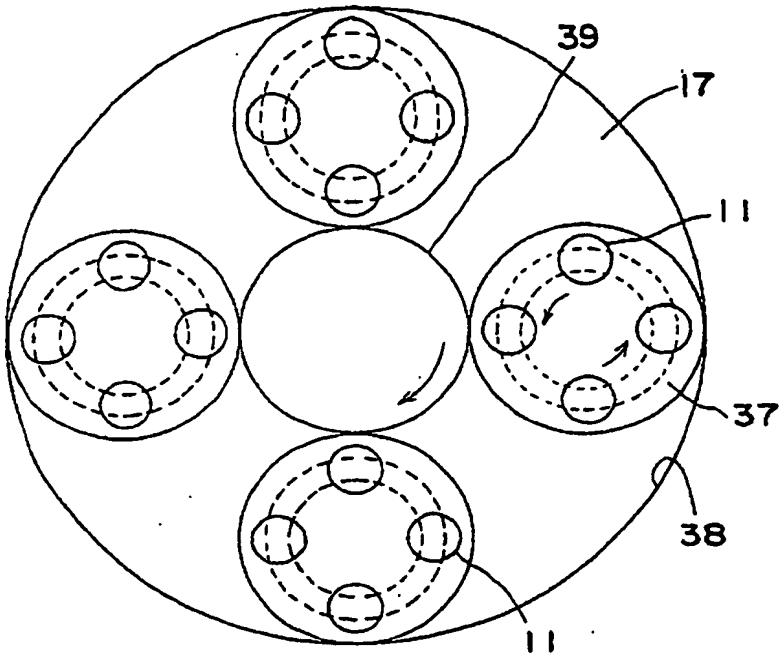

Fig.21

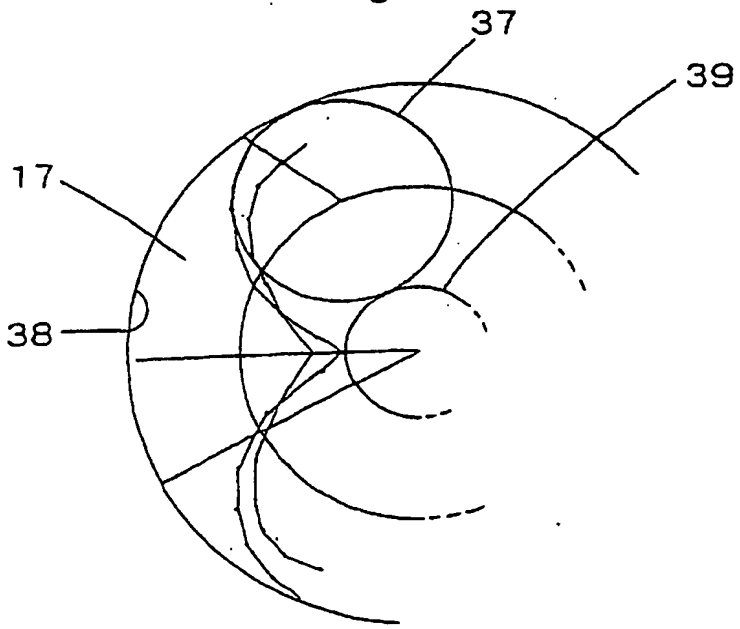

Fig.22

(a)

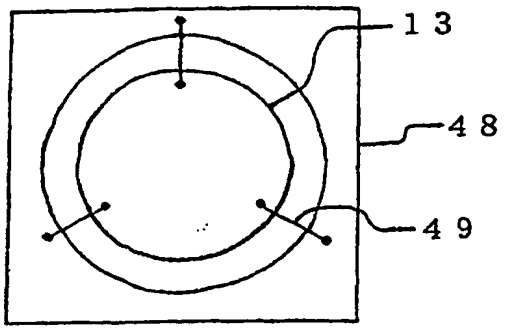

(b)

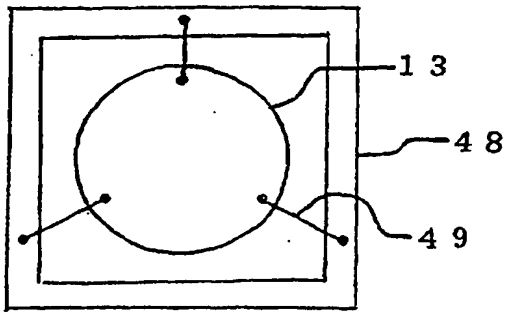

(c)

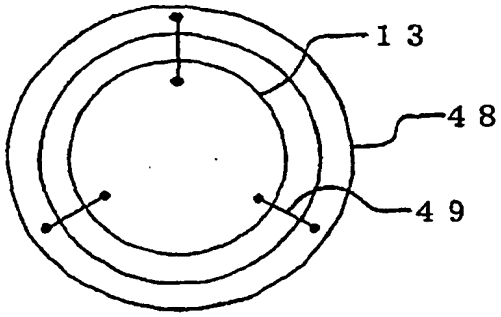

Fig. 23

(a)

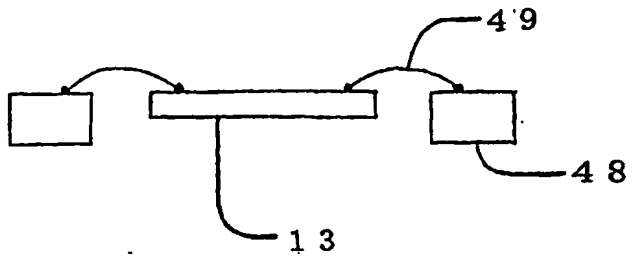

(b)

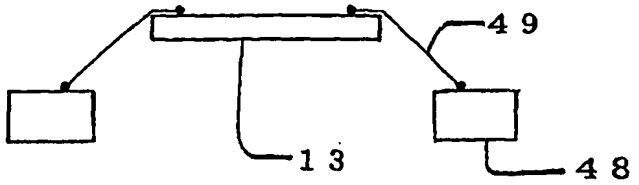

Fig. 24

(a)

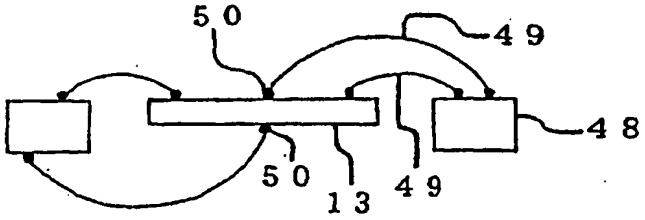

(b)

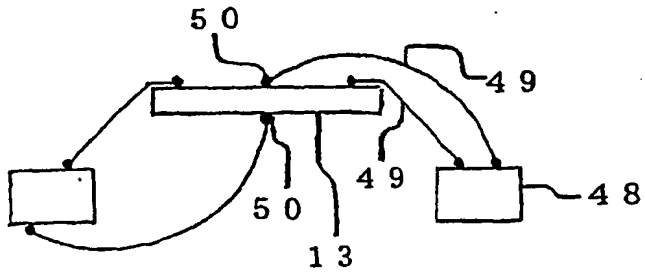

Fig.25

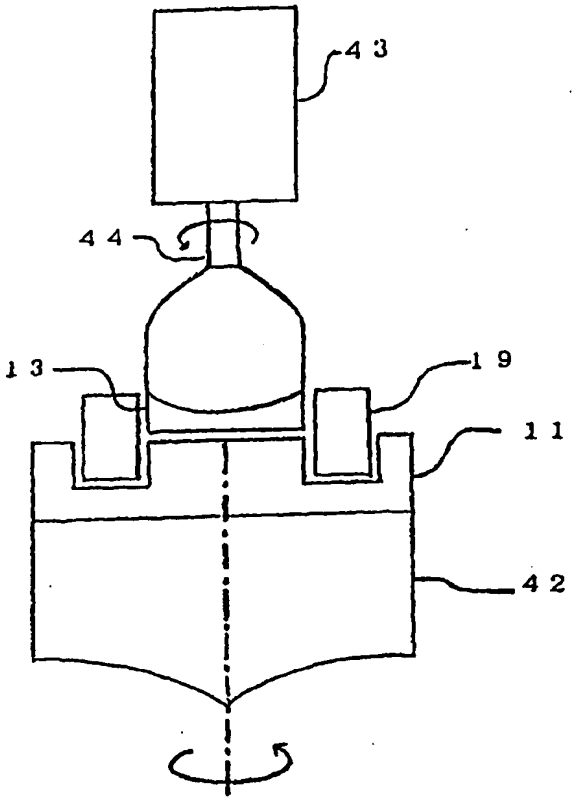

Fig.26

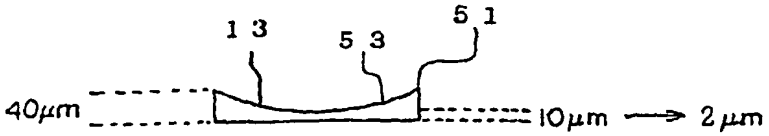

Fig.27

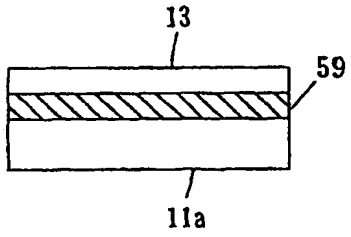

Fig.28

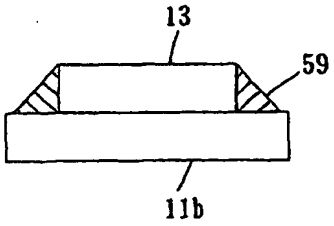

Fig.29

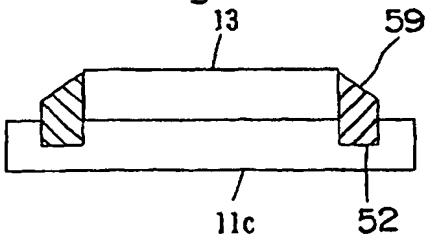

Fig.30

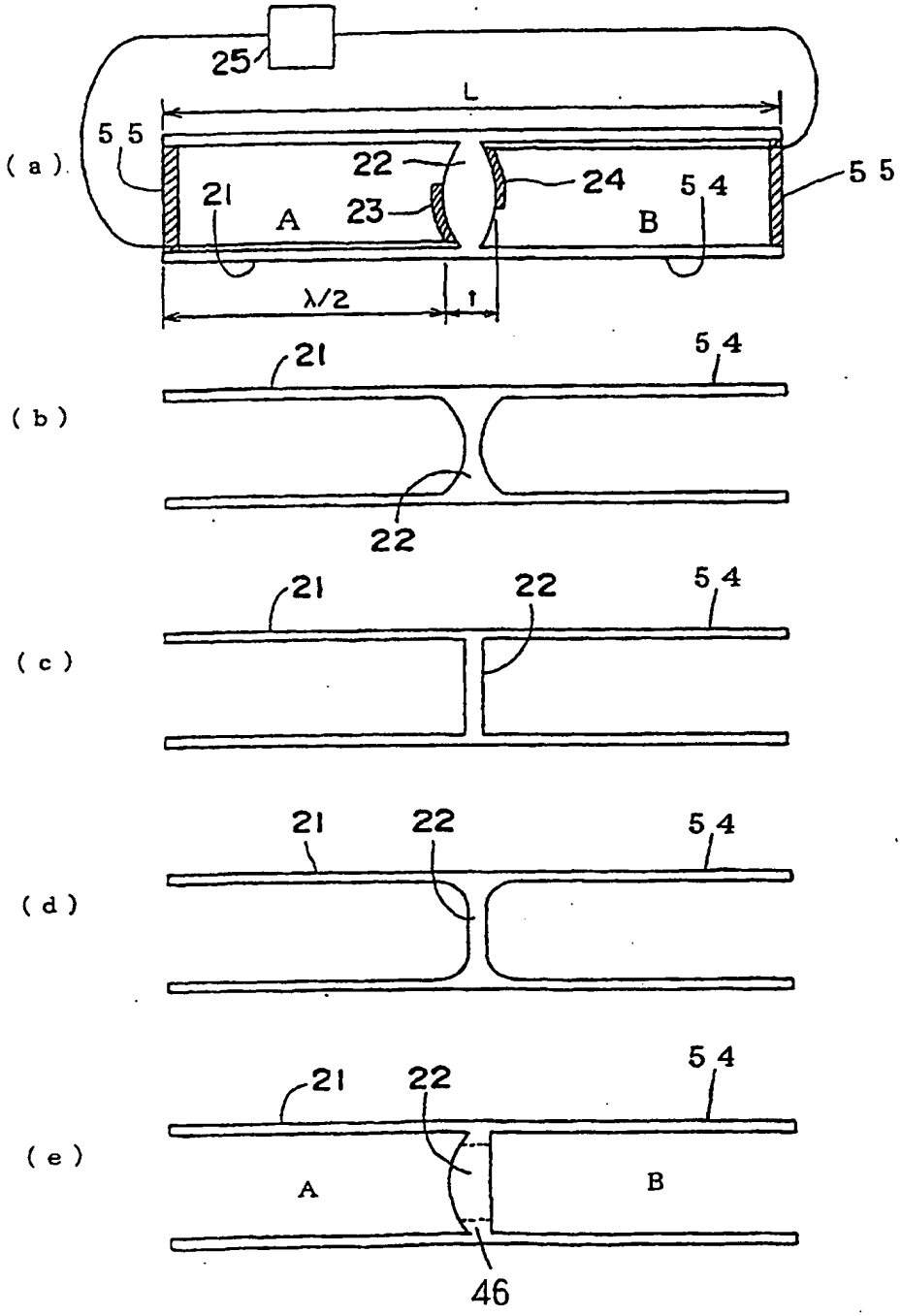
25
L
(a)
55
22
24
54
55
21
A
23
B
λ/2
t
(b)
21
54
22
(c)
21
22
54
(d)
21
22
54
(e)
21
22
54
A
B
46

Fig.31

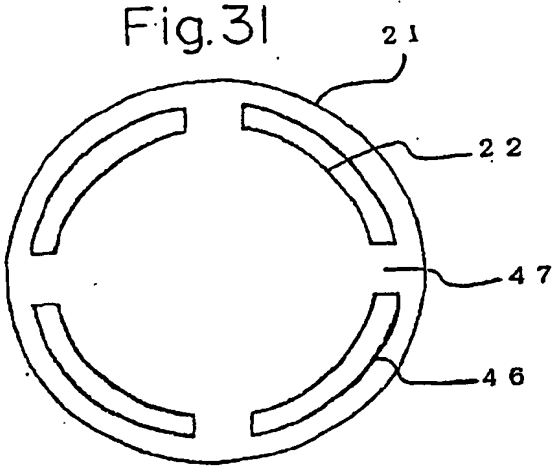

Fig.32

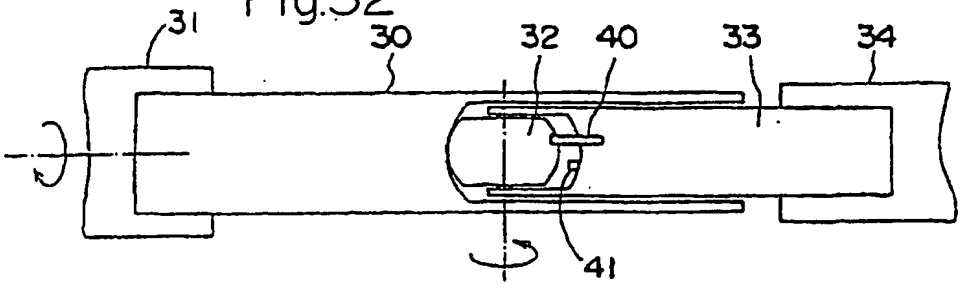

Fig.33

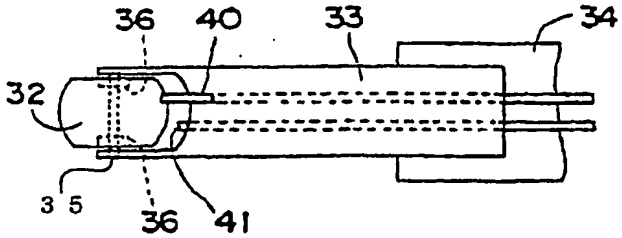

Fig.34

(a) (b)

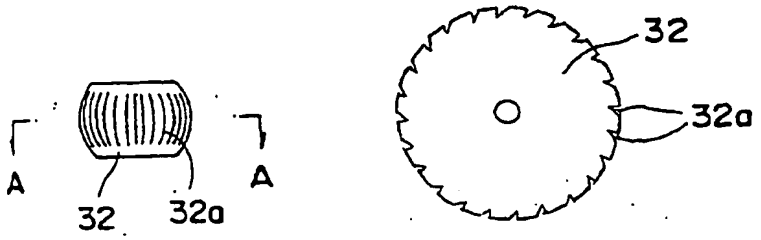

Fig.35

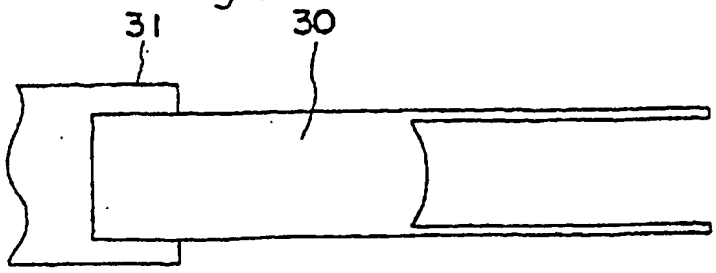

Fig.36

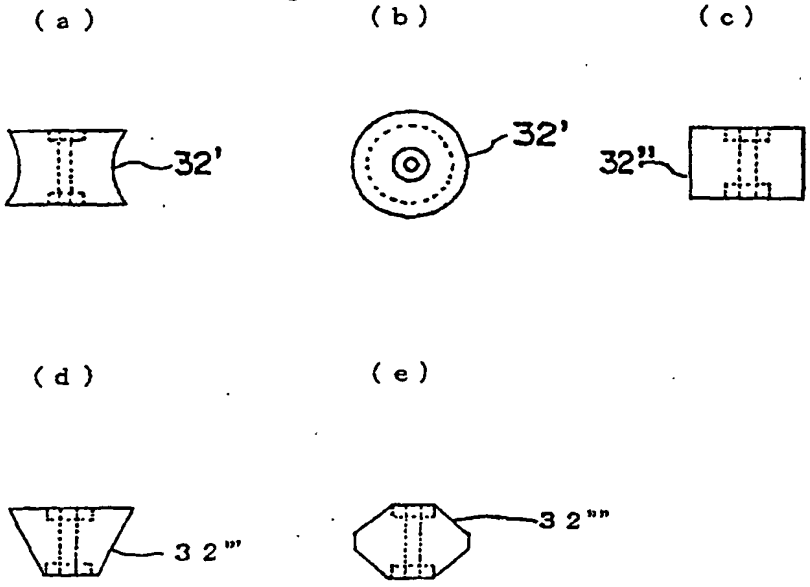

Fig.37

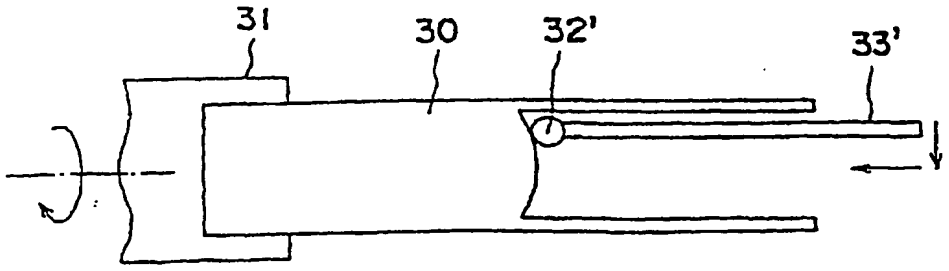

Fig.38

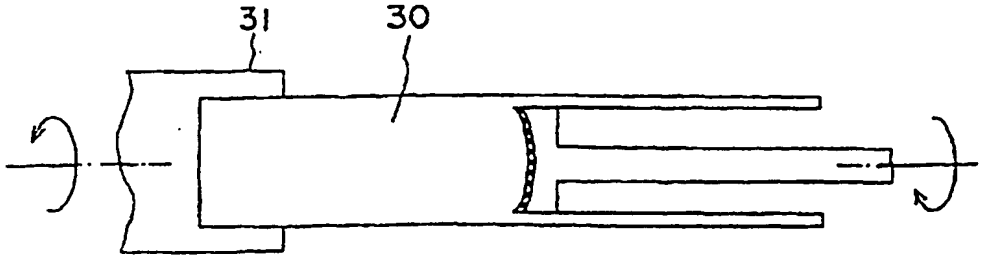

Fig.39

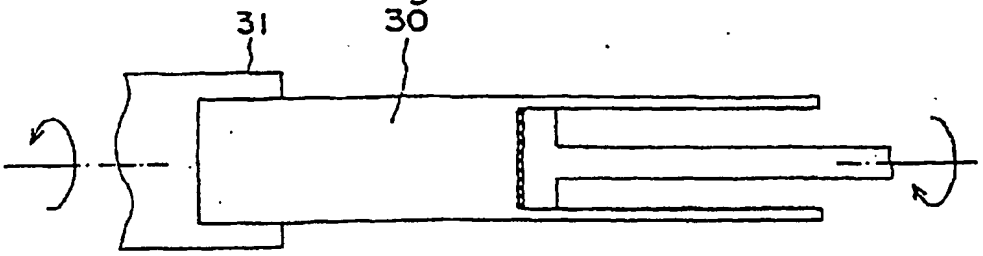

Fig.40

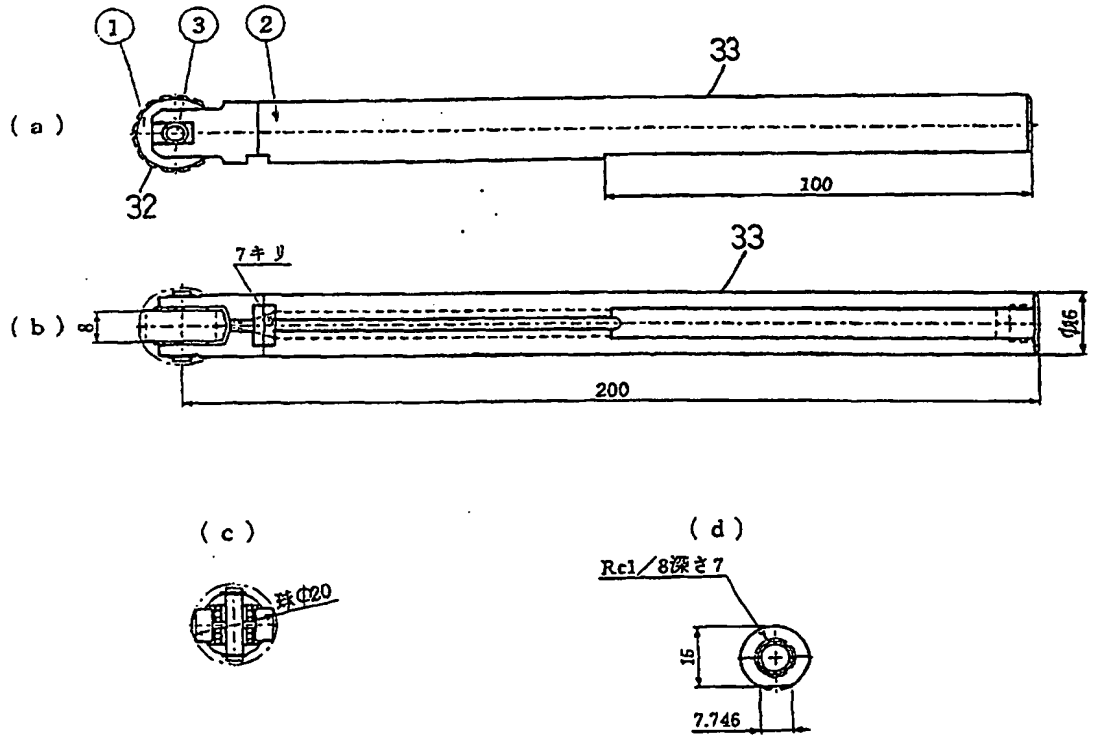

Fig.41

(a)

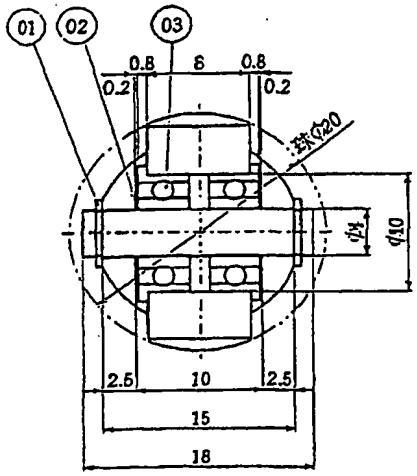
01
02
03
0.8
8
0.8
0.2
0.2
φ20
φ10
2.5
10
2.5
15
18

(b)

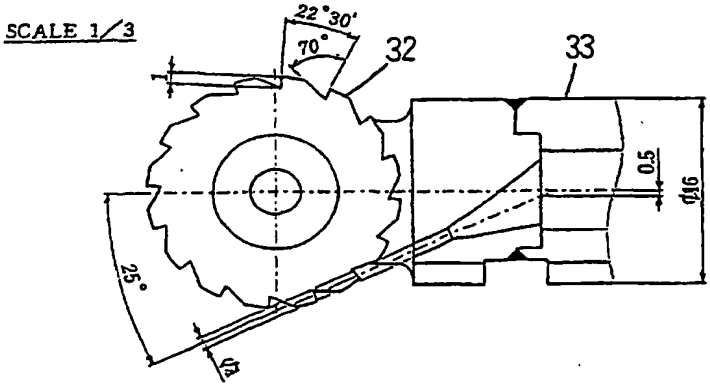
SCALE 1/3
22°30'
70°
32
33
0.5
φ16
25°

Fig.42

(a)

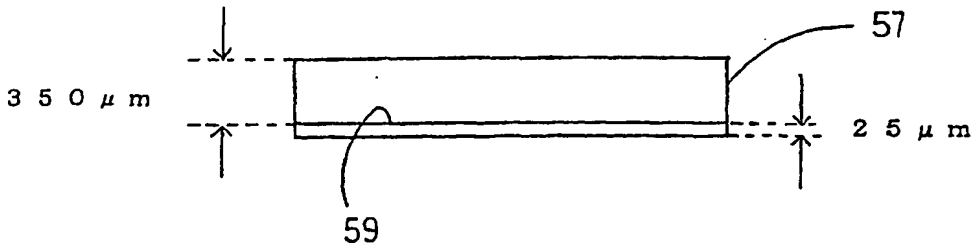

(b)

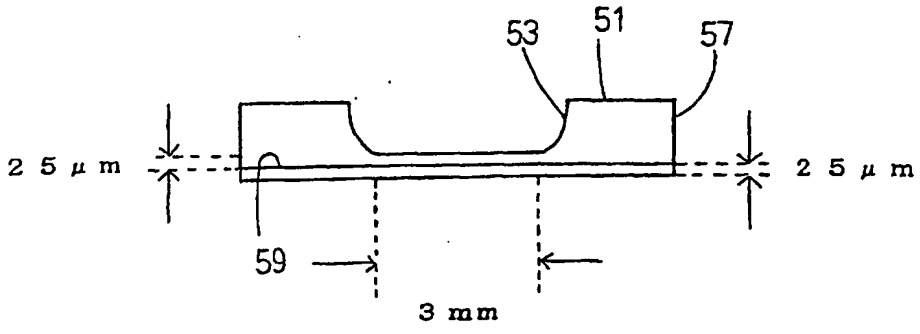

Fig.43

(a)

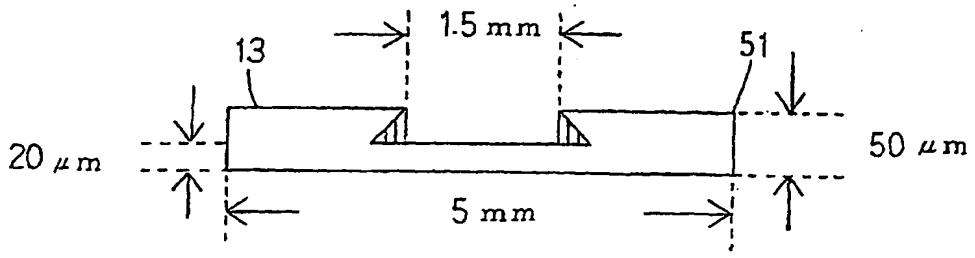

(b)

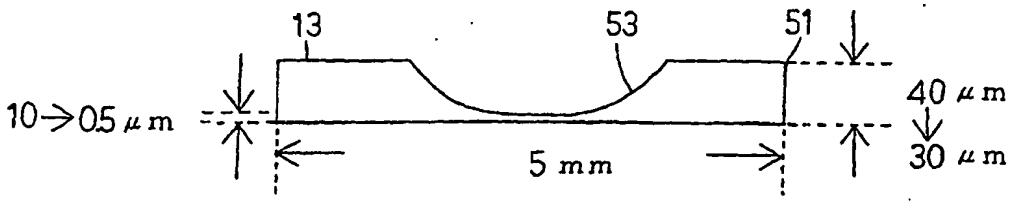

Fig.44

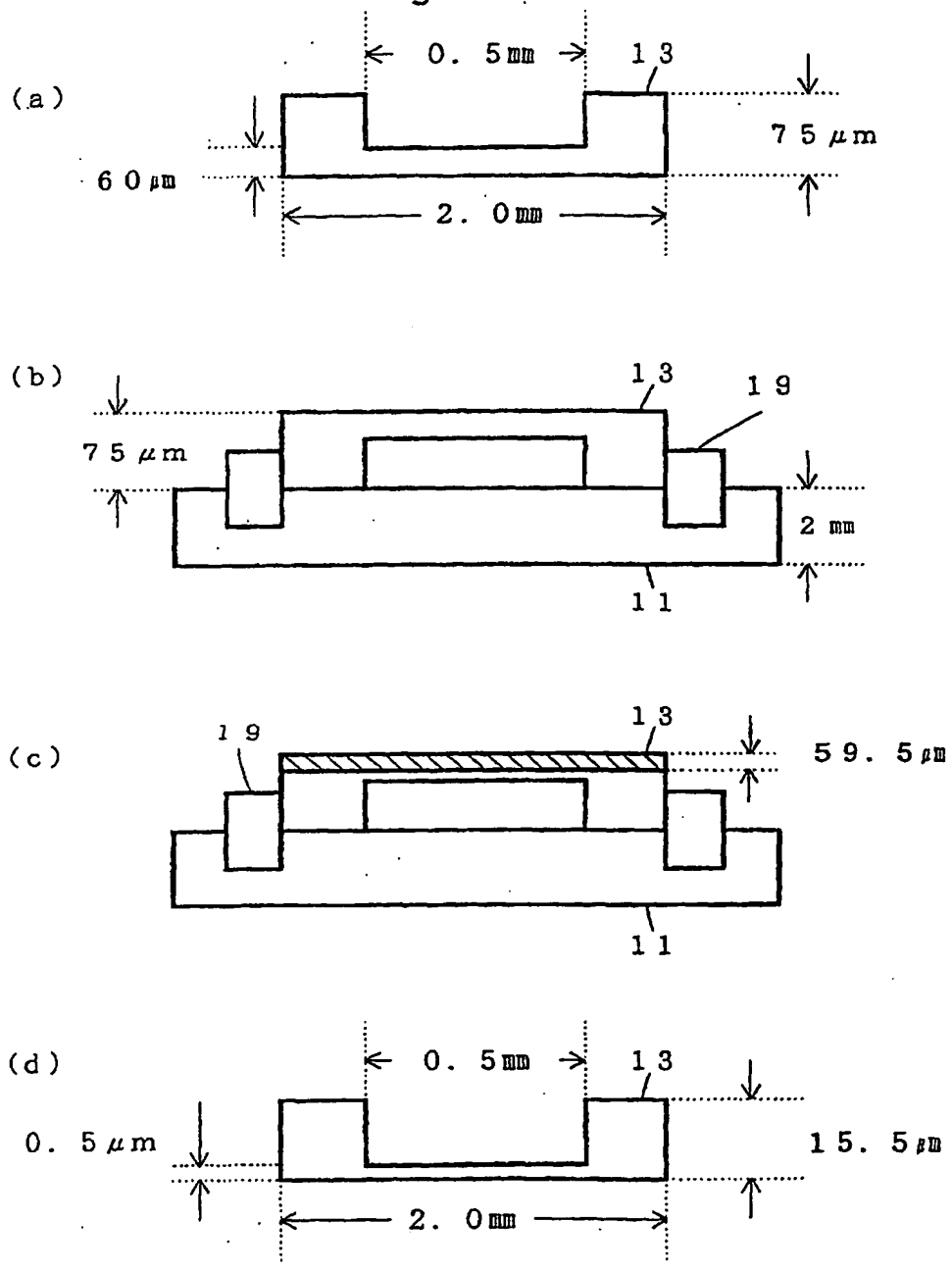
(a)
0.5mm
13
75μm
60μm
2.0mm
(b)
13
19
75μm
2mm
11
(c)
19
13
59.5μm
11
(d)
0.5mm
13
0.5μm
15.5μm
2.0mm

Fig. 45

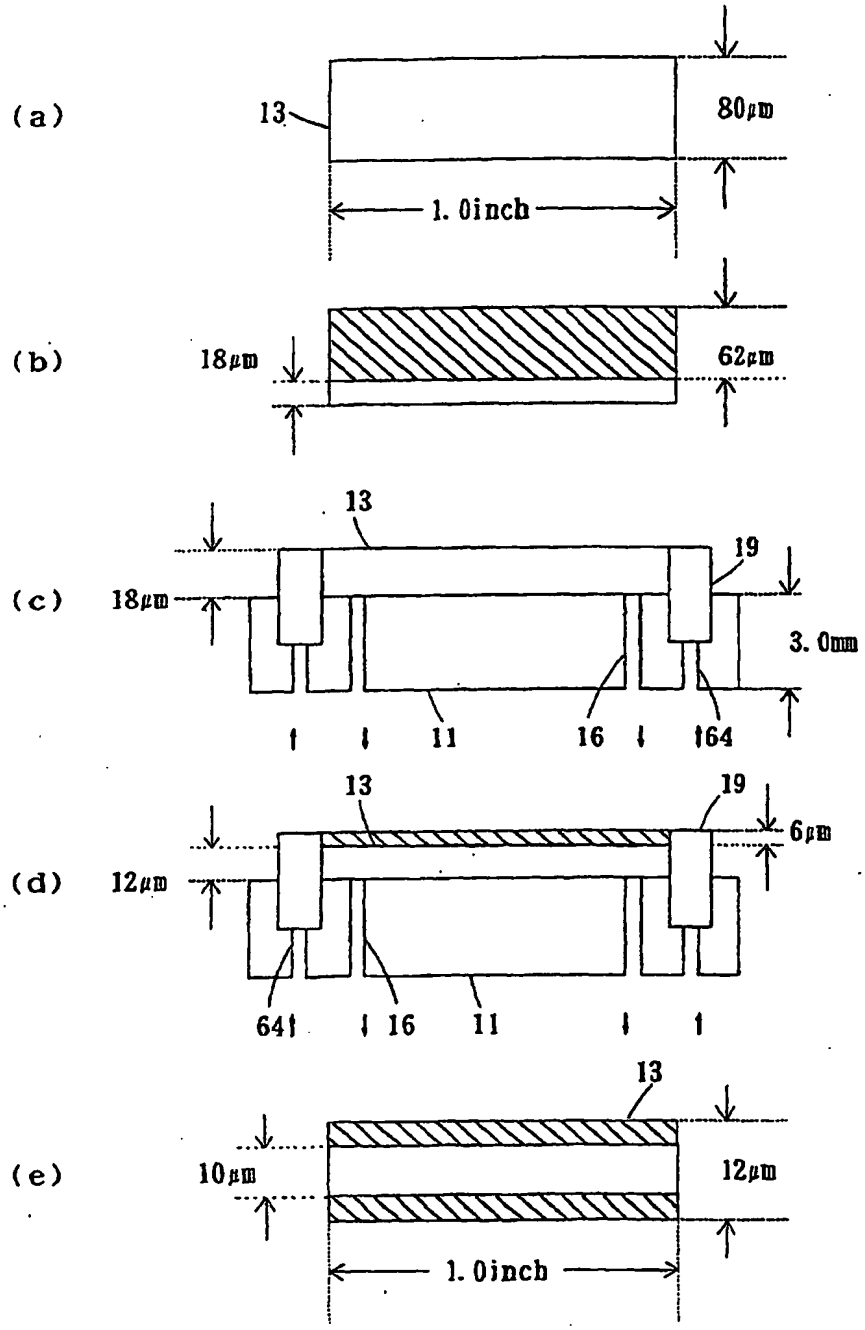
(a)
13
80μm
1.0inch
(b)
18μm
62μm
(c)
13
19
18μm
3.0mm
11
16
64
(d)
13
19
6μm
12μm
64
16
11
(e)
13
10μm
12μm
1.0inch

Fig.46

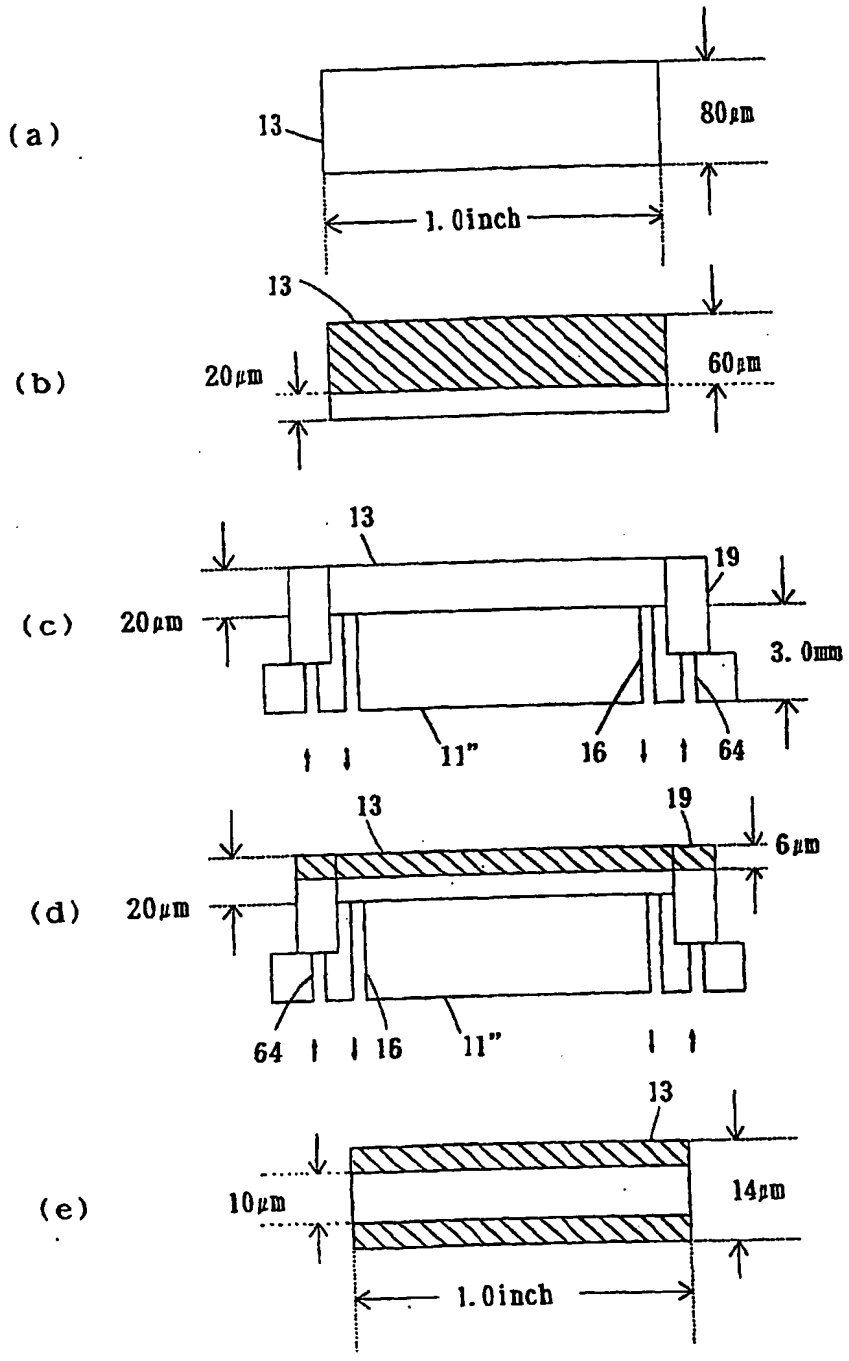
(a)
13
80μm
1.0inch
(b)
13
20μm
60μm
(c)
13
19
20μm
3.0mm
11"
16
64
(d)
13
19
6μm
20μm
64
16
11"
(e)
13
10μm
14μm
1.0inch

Fig.47

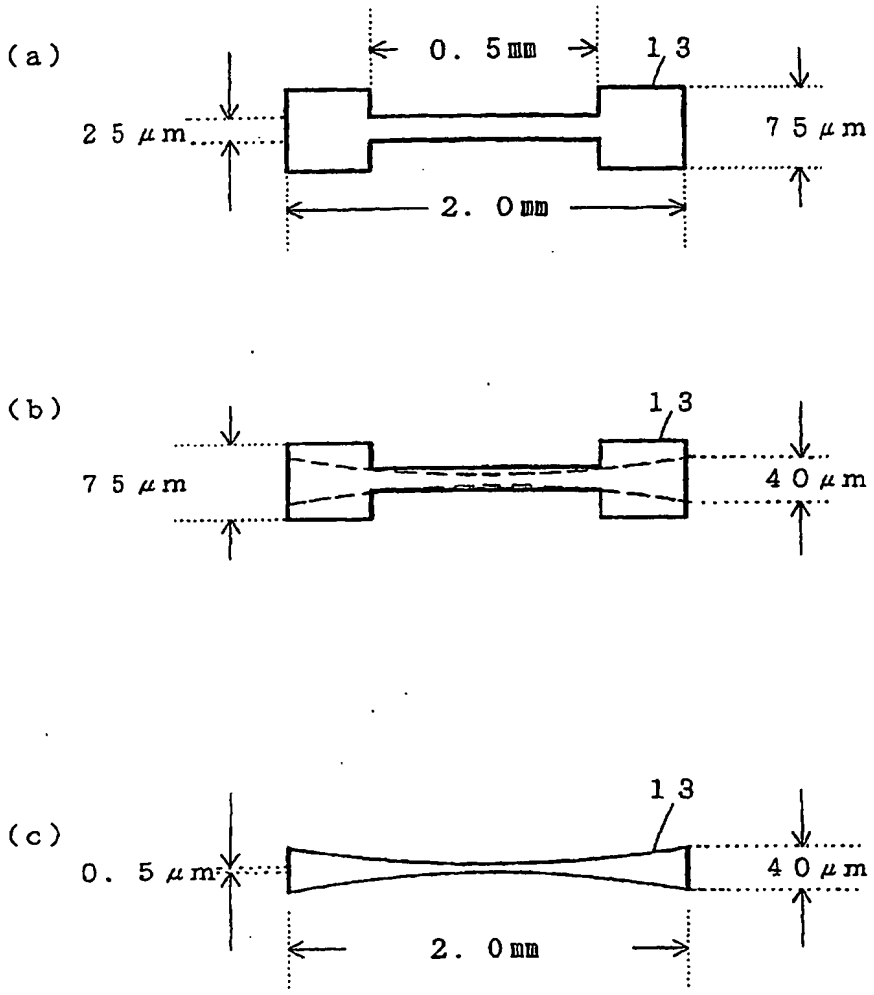

Fig. 48

(a)

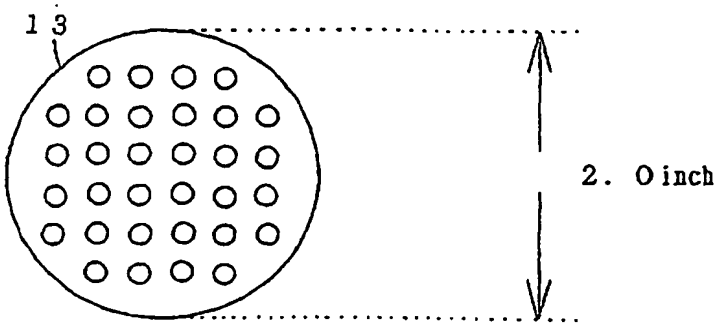

(b)

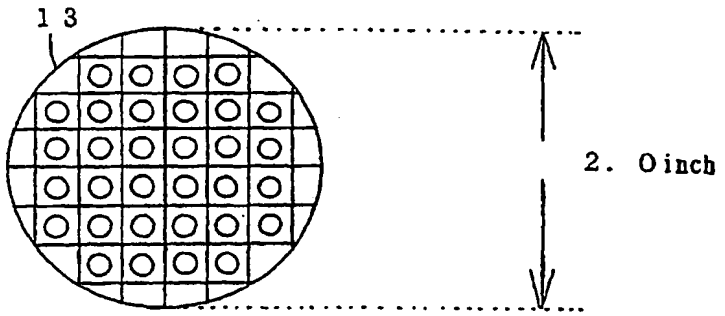

(c)

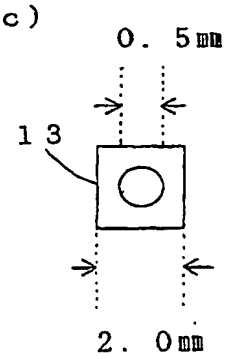

(d)

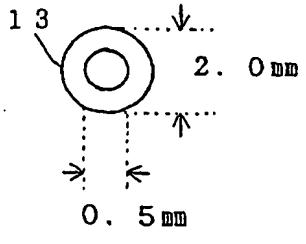

Fig.49

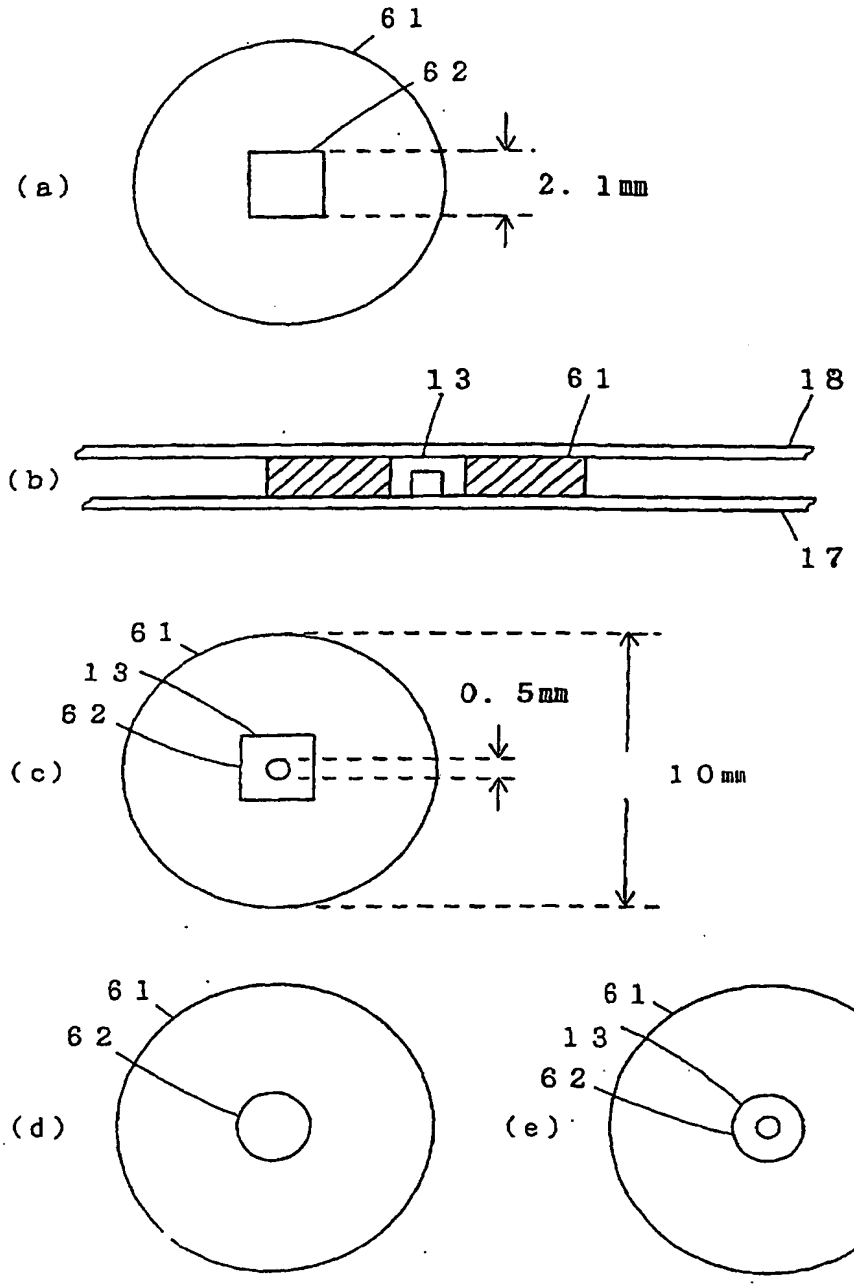

Fig.50

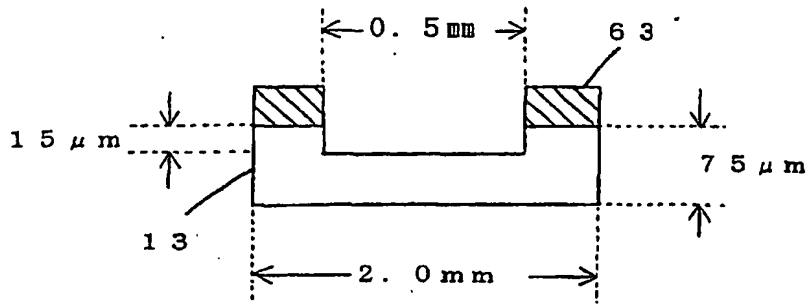

Fig.5l

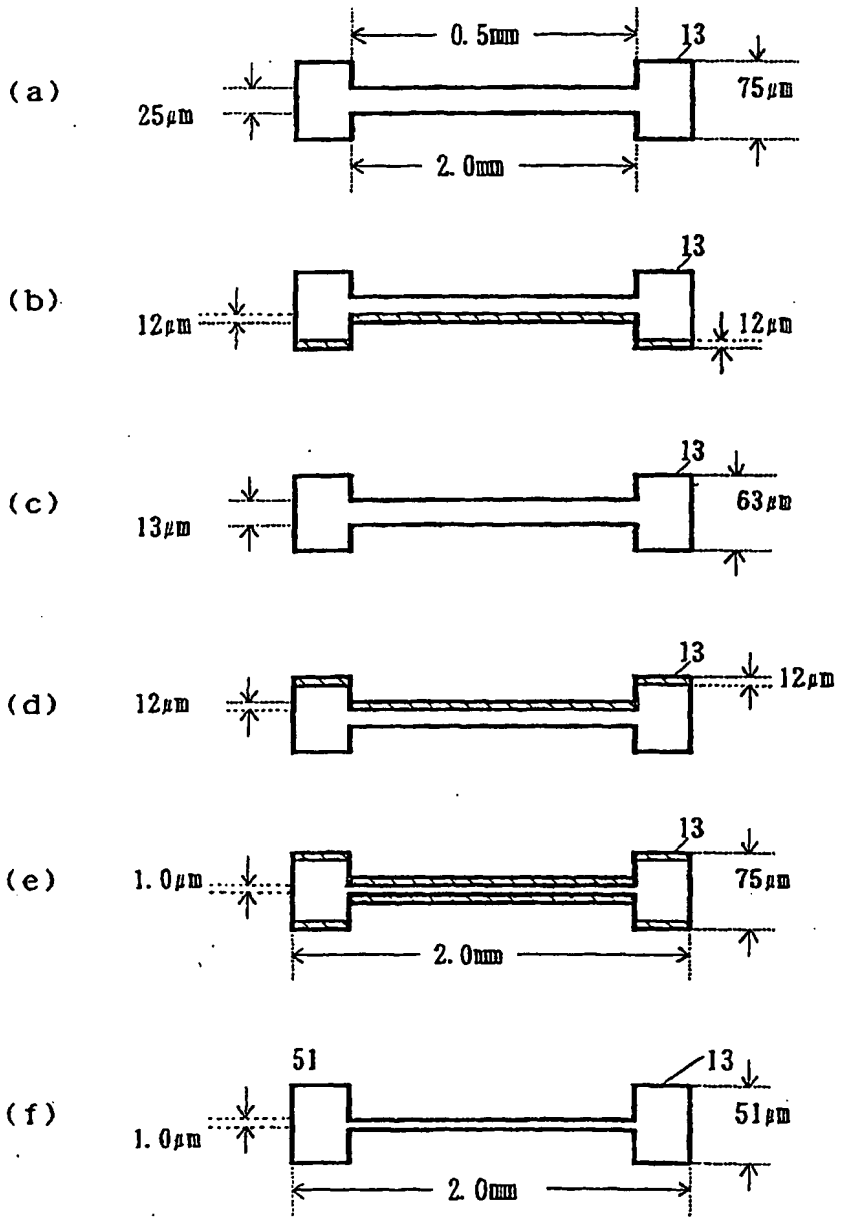
(a)
0.5mm
13
75μm
25μm
2.0mm
(b)
13
12μm
12μm
(c)
13
63μm
13μm
(d)
13
12μm
12μm
(e)
13
1.0μm
75μm
2.0mm
(f)
51
13
1.0μm
51μm
2.0mm

Fig.52

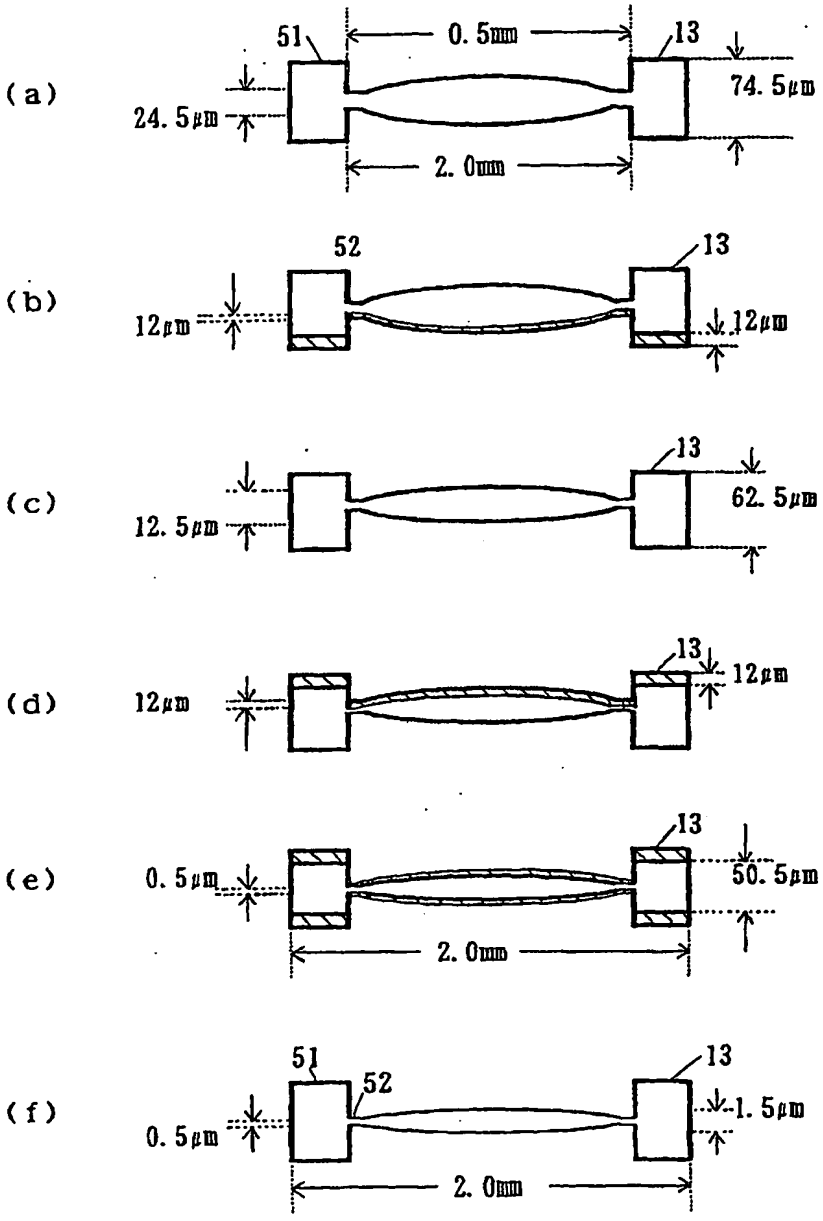
(a)
51
0.5mm
13
74.5μm
24.5μm
2.0mm
(b)
52
13
12μm
12μm
(c)
13
62.5μm
12.5μm
(d)
13
12μm
12μm
(e)
13
0.5μm
50.5μm
2.0mm
(f)
51
52
13
1.5μm
0.5μm
2.0mm

Fig.53

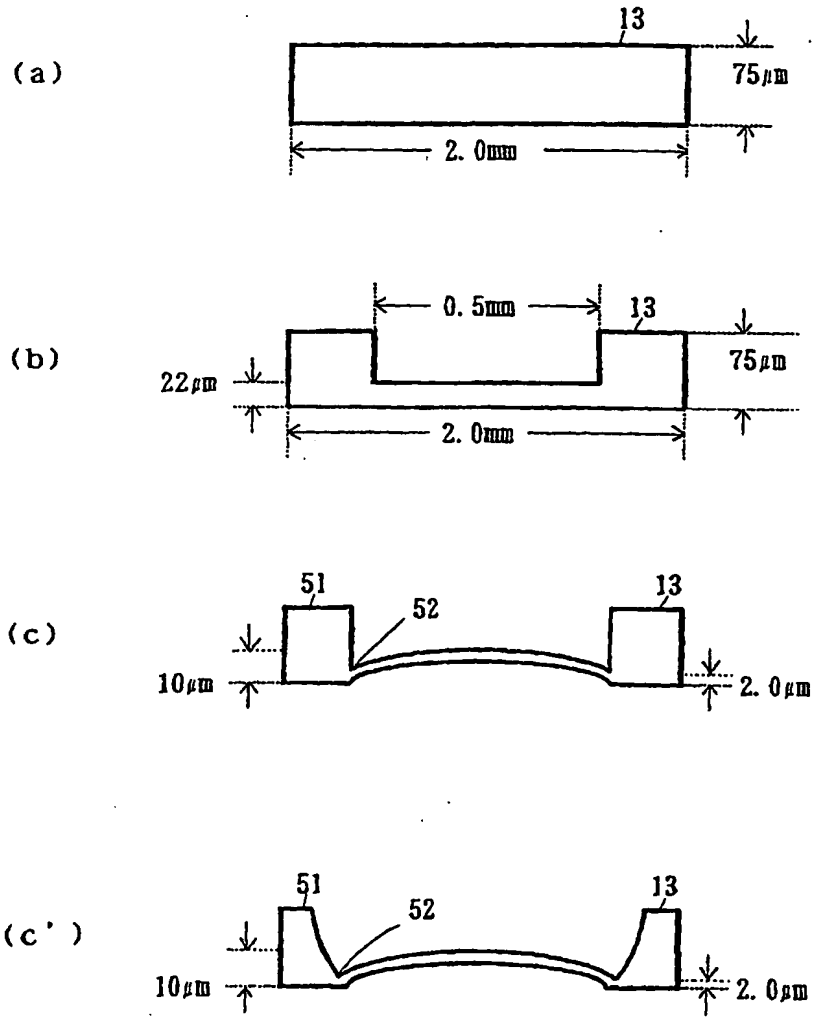
(a)
13
75μm
2.0mm
(b)
0.5mm
13
22μm
75μm
2.0mm
(c)
51
52
13
10μm
2.0μm
(c')
51
52
13
10μm
2.0μm

Fig.54

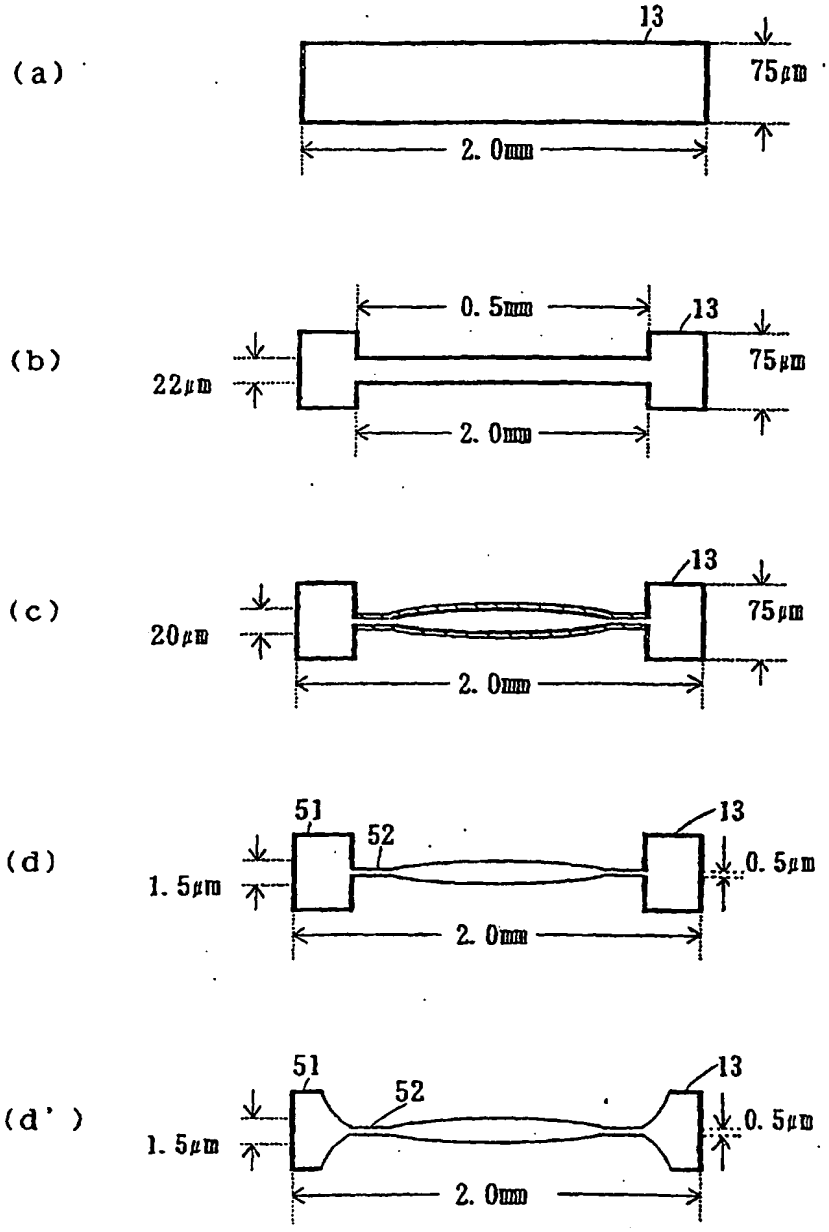
(a)
13
75μm
2.0mm
(b)
0.5mm
13
22μm
75μm
2.0mm
(c)
13
20μm
75μm
2.0mm
(d)
51
52
13
1.5μm
0.5μm
2.0mm
(d')
51
52
13
1.5μm
0.5μm
2.0mm

Fig.55

(a)

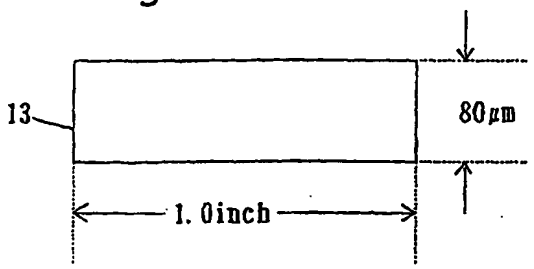

(b)

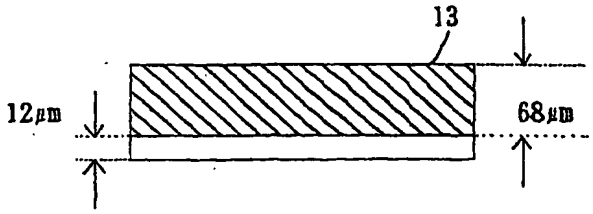

(c)

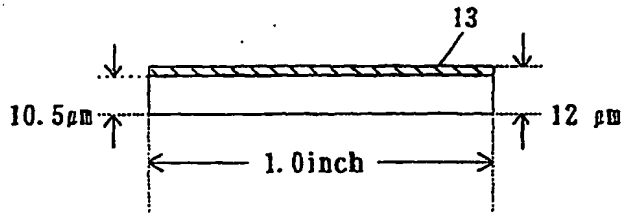

Fig.56

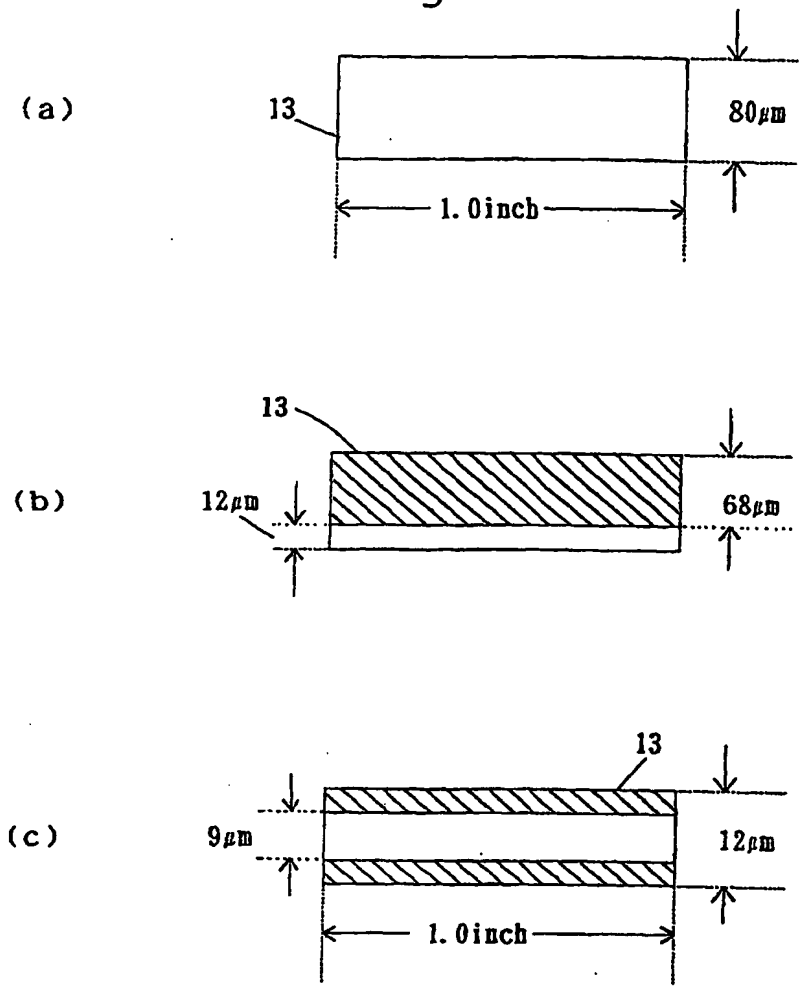

Fig.57

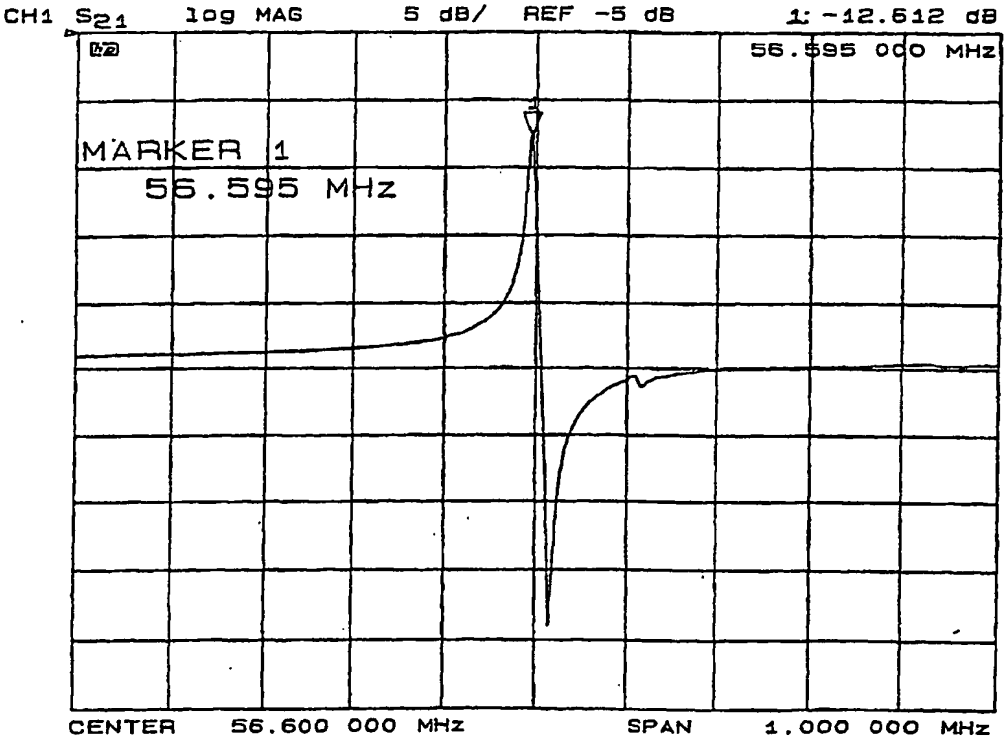
CH1 S21 log MAG 5 dB/ REF -5 dB 1: -12.612 dB
56.595 000 MHz
MARKER 1
56.595 MHz
CENTER 56.600 000 MHz
SPAN 1.000 000 MHz

Fig. 58

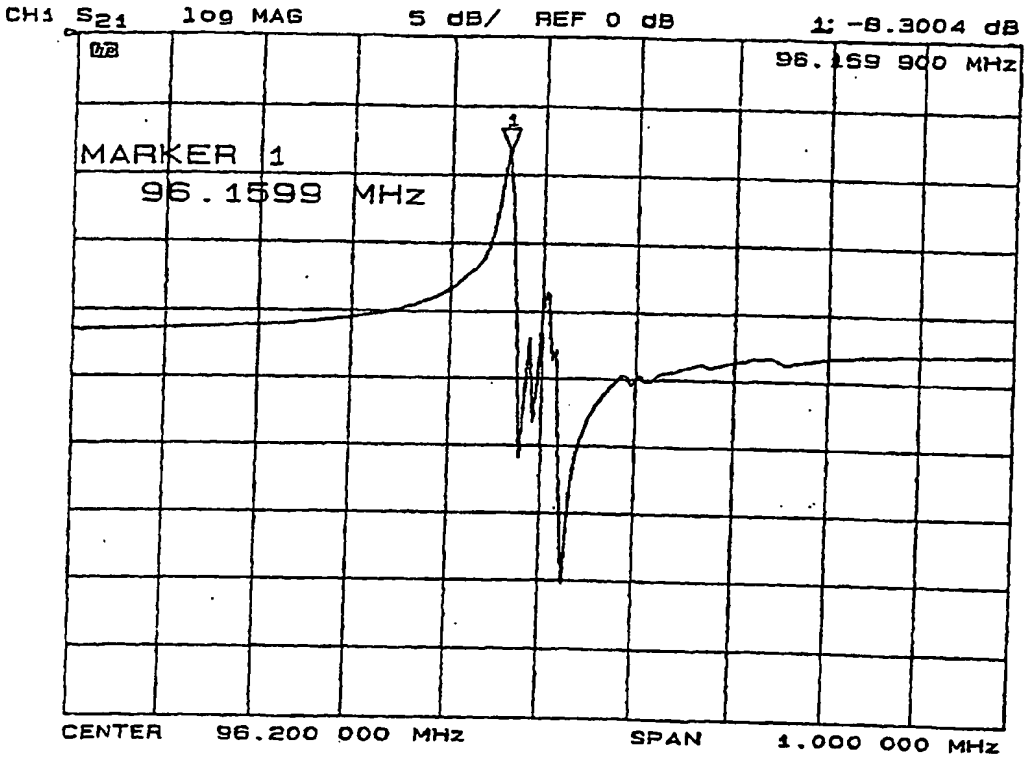
CH1 S21 log MAG 5 dB/ REF 0 dB
1: -8.3004 dB
96.159 900 MHz
MARKER 1
96.1599 MHz
CENTER 96.200 000 MHz
SPAN 1.000 000 MHz

Fig.59

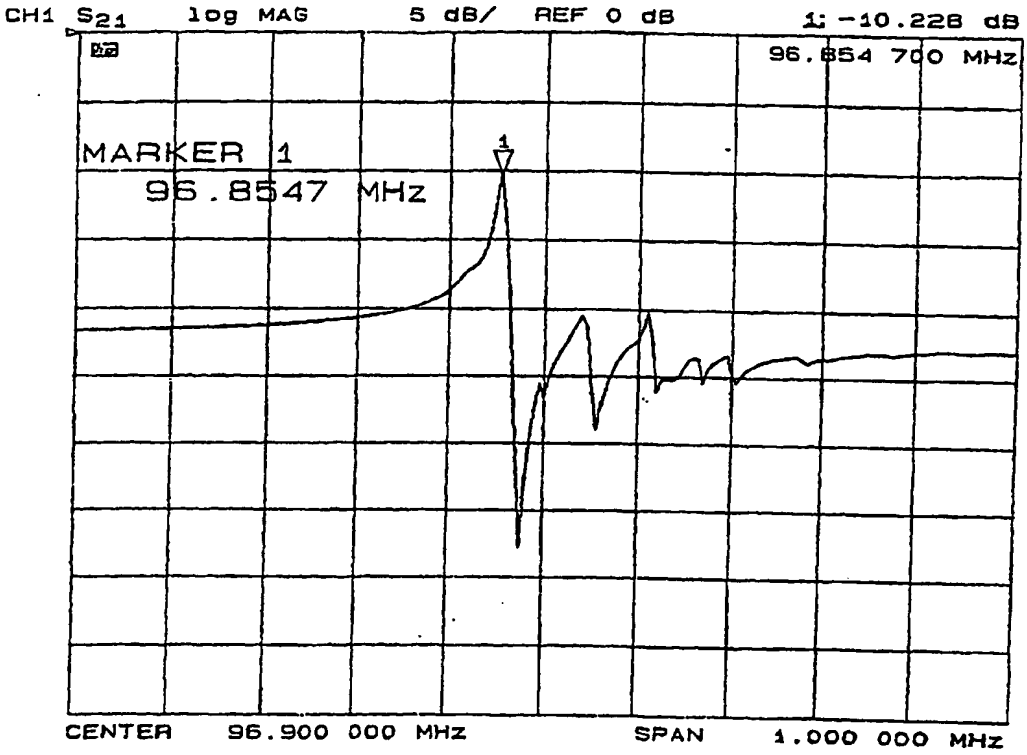
CH1 S21 log MAG 5 dB/ REF 0 dB
1: -10.228 dB
96.854 700 MHz
MARKER 1
96.8547 MHz
CENTER 96.900 000 MHz
SPAN 1.000 000 MHz

Fig.60

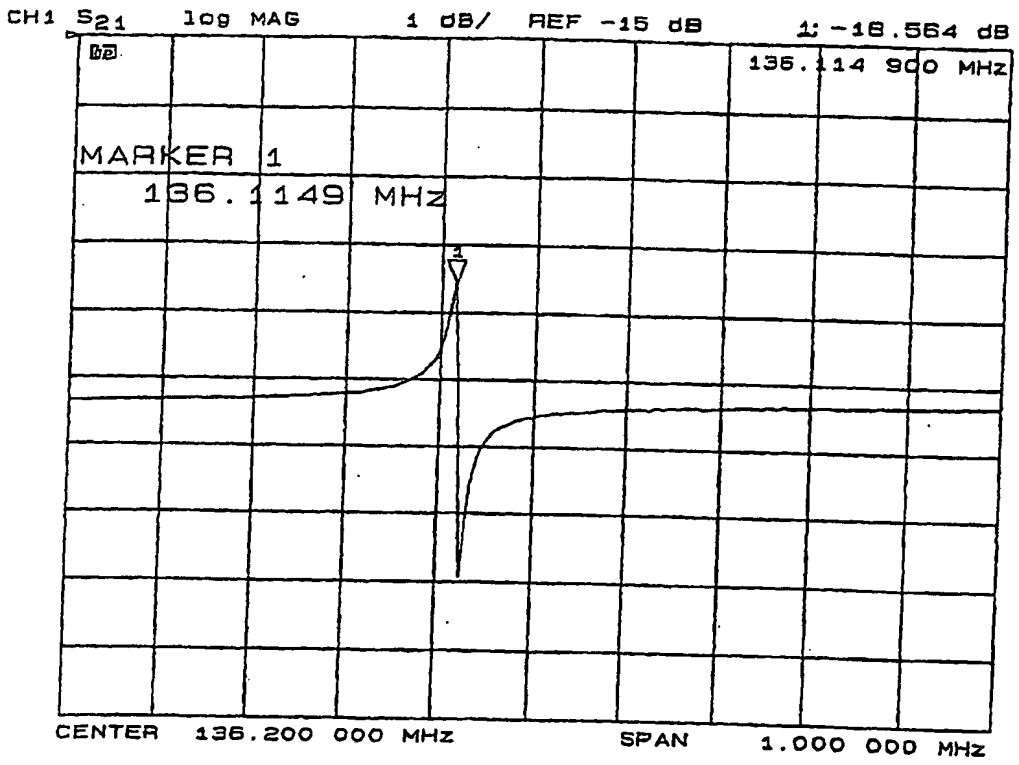
CH1 S21 log MAG 1 dB/ REF -15 dB 1: -18.564 dB
136.114 900 MHz
MARKER 1
136.1149 MHz
1
CENTER 136.200 000 MHz
SPAN 1.000 000 MHz

Fig. 61

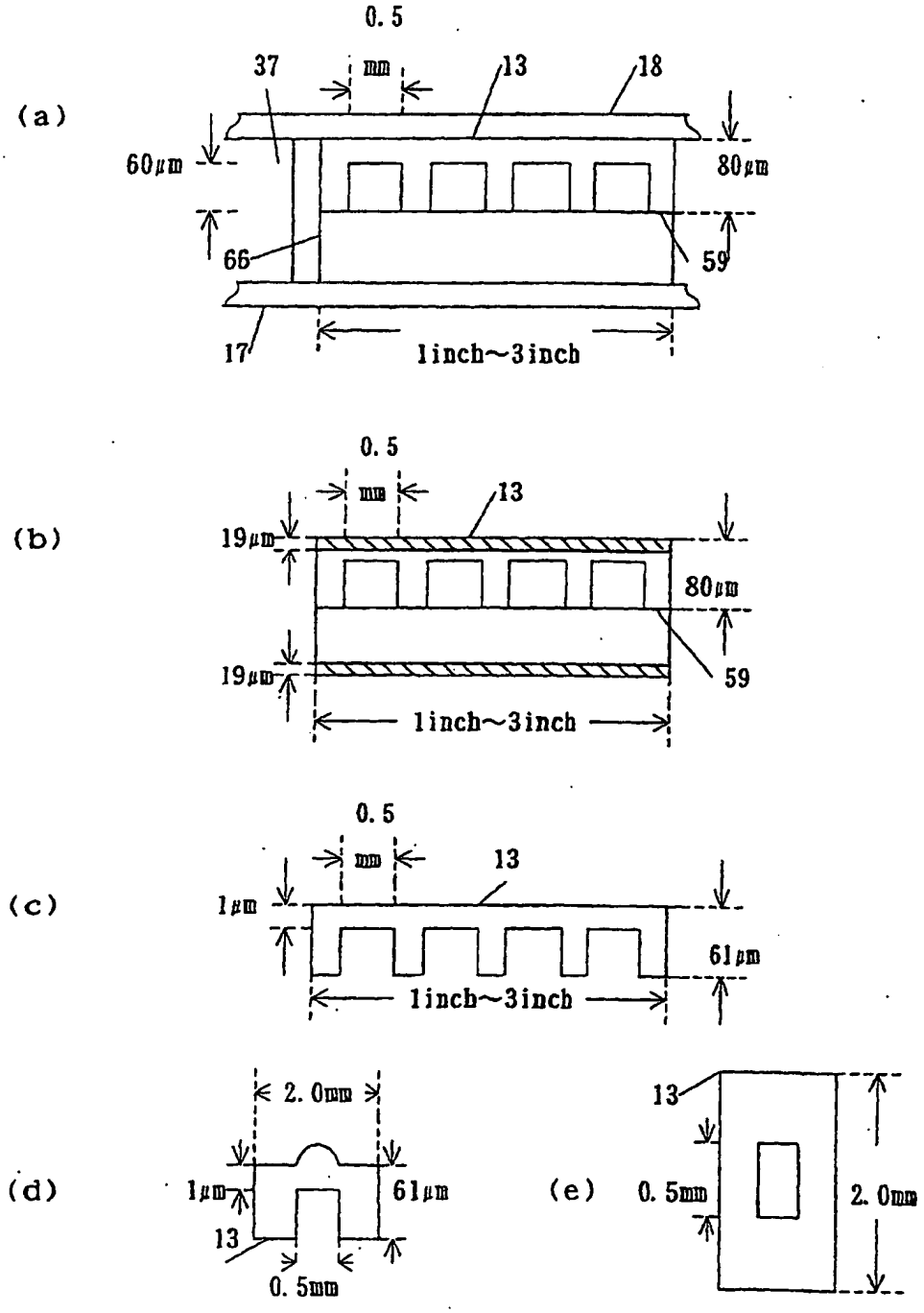
(a)
0.5
mm
37
13
18
60μm
80μm
66
59
17
1inch~3inch
(b)
0.5
mm
13
19μm
80μm
19μm
59
1inch~3inch
(c)
0.5
mm
13
1μm
61μm
1inch~3inch
(d)
2.0mm
1μm
61μm
13
0.5mm
(e)
13
0.5mm
2.0mm

Fig. 62

(a)

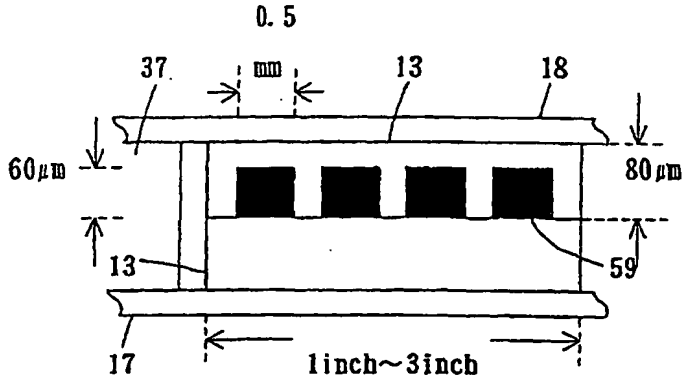
0.5
mm
37
13
18
60μm
80μm
13
59
17
1inch~3inch

(b)

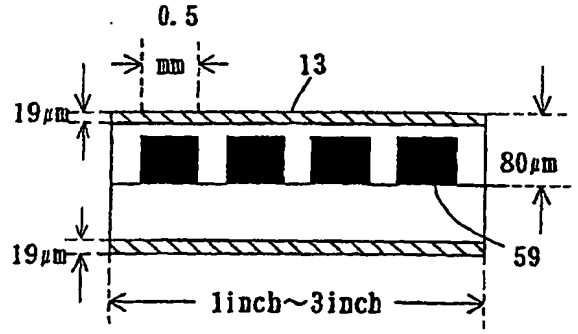
0.5
mm
13
19μm
80μm
19μm
59
1inch~3inch

(c)

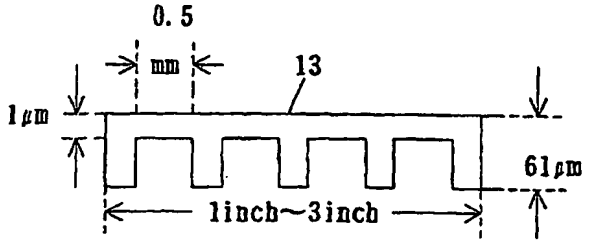
0.5
mm
13
1μm
61μm
1inch~3inch

Fig.63

(a)

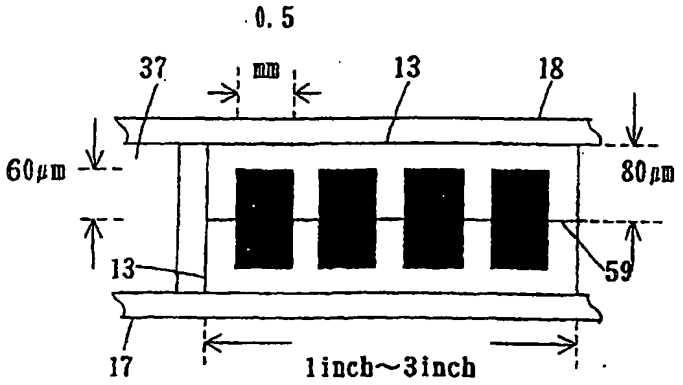
0.5
mm
37
13
18
60μm
80μm
13
59
17
1inch~3inch

(b)

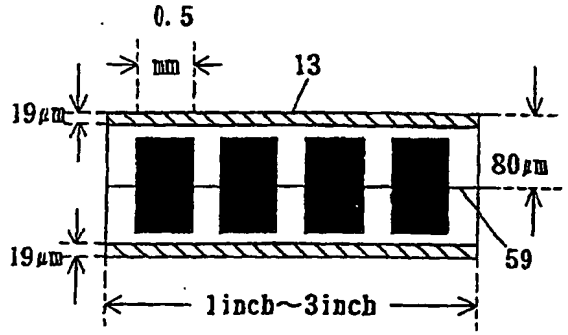
0.5
mm
13
19μm
80μm
19μm
59
1inch~3inch

(c)

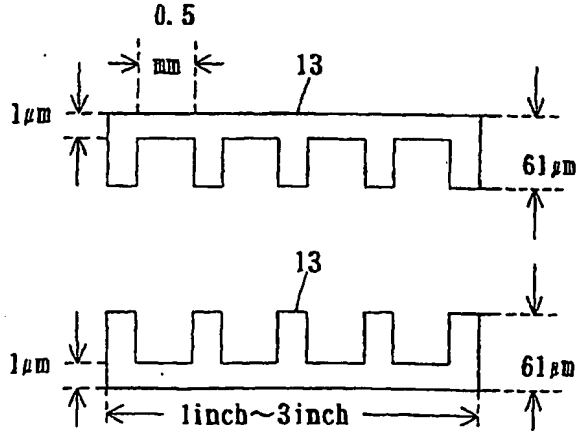
0.5
mm
13
1μm
61μm
13
1μm
61μm
1inch~3inch

Fig. 64

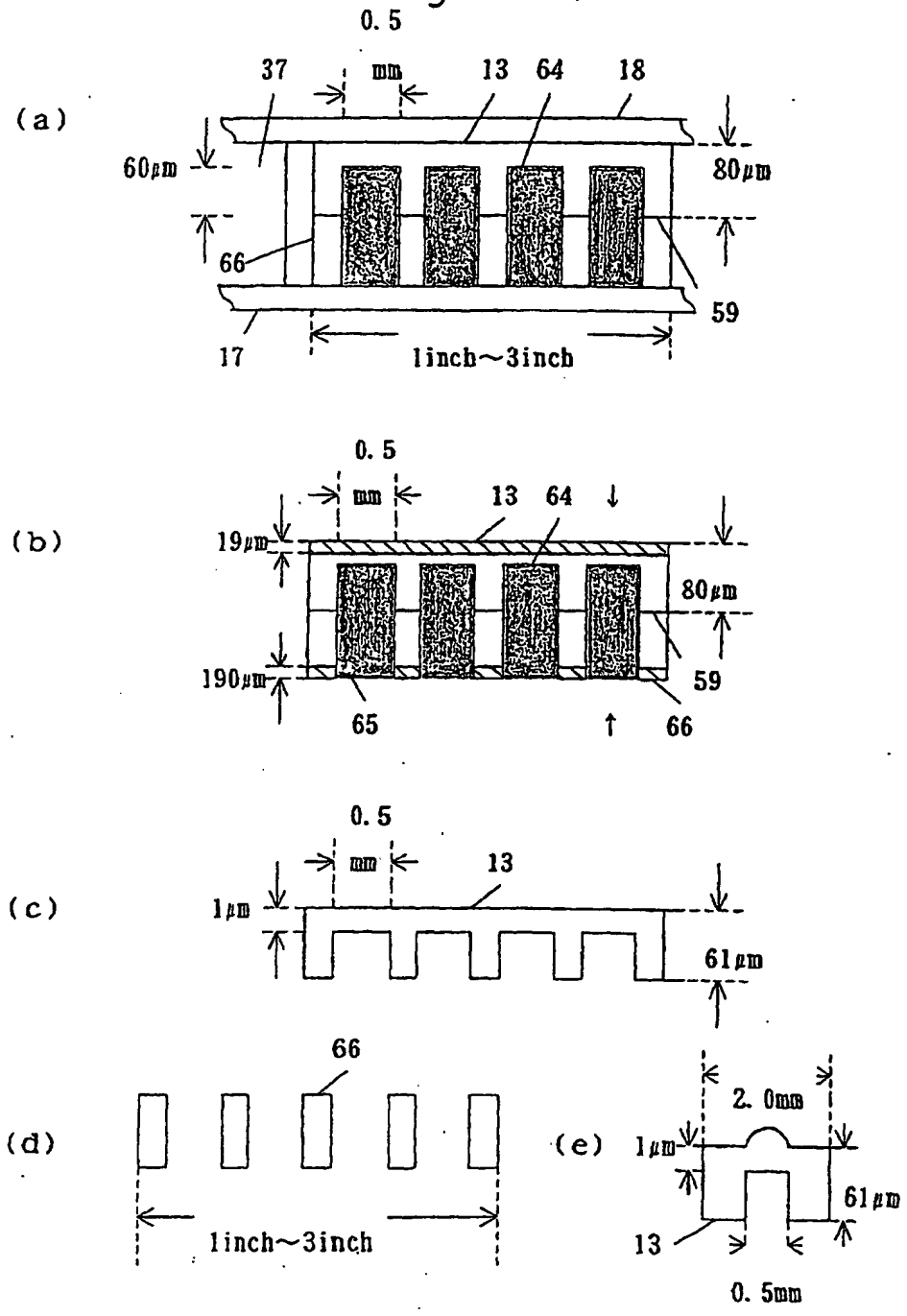
(a)
0.5
mm
37
13
64
18
60μm
80μm
66
59
17
1inch~3inch
(b)
0.5
mm
13
64
19μm
80μm
190μm
59
65
66
(c)
0.5
mm
13
1μm
61μm
(d)
66
1inch~3inch
(e)
2.0mm
1μm
61μm
13
0.5mm

Fig.65

(a)

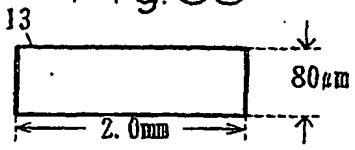
13
80μm
2.0mm

(b)

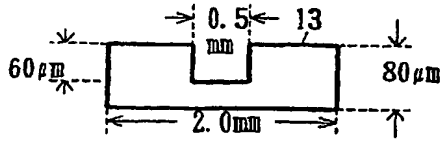
0.5
mm
13
60μm
80μm
2.0mm

(c)

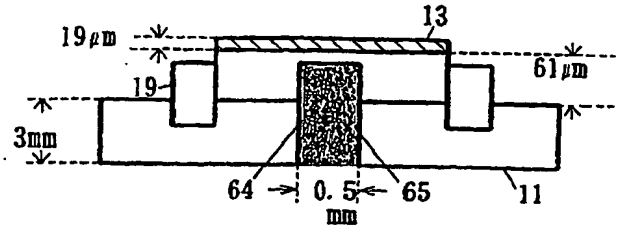
19μm
13
61μm
19
3mm
64
0.5
mm
65
11

(d)

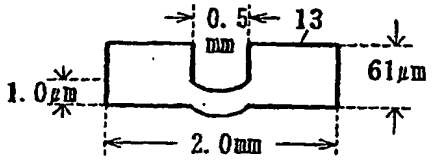
0.5
mm
13
1.0μm
61μm
2.0mm

(e)

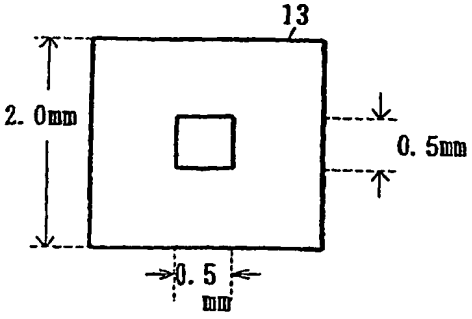
13
2.0mm
0.5mm
0.5
mm

Fig.66

(a)

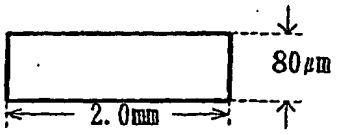
80μm
2.0mm

(b)

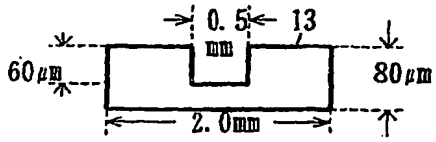
0.5
mm
13
60μm
80μm
2.0mm

(c)

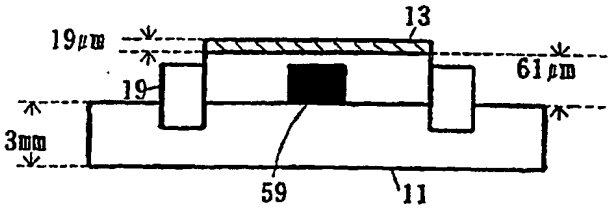
19μm
13
61μm
19
3mm
59
11

(d)

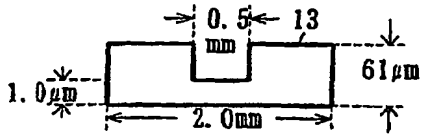
0.5
mm
13
61μm
1.0μm
2.0mm

(e)

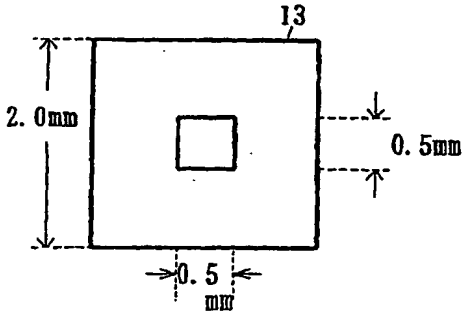
13
2.0mm
0.5mm
0.5
mm

Fig.67

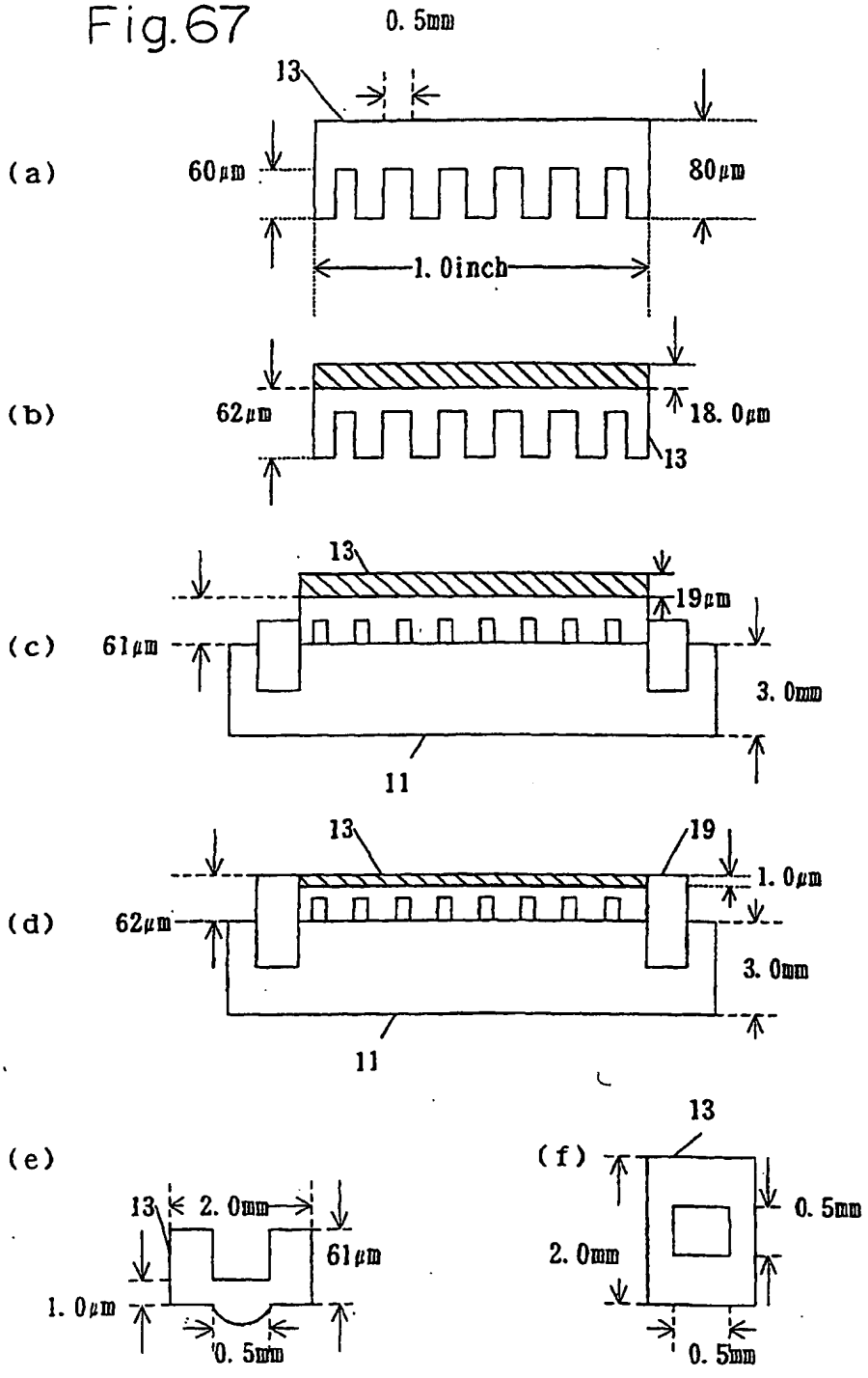
0.5mm
13
(a)
60μm
80μm
1.0inch
(b)
62μm
18.0μm
13
(c)
13
19μm
61μm
3.0mm
11
(d)
13
19
1.0μm
62μm
3.0mm
11
(e)
13
2.0mm
61μm
1.0μm
0.5mm
(f)
13
0.5mm
2.0mm
0.5mm

Fig.68

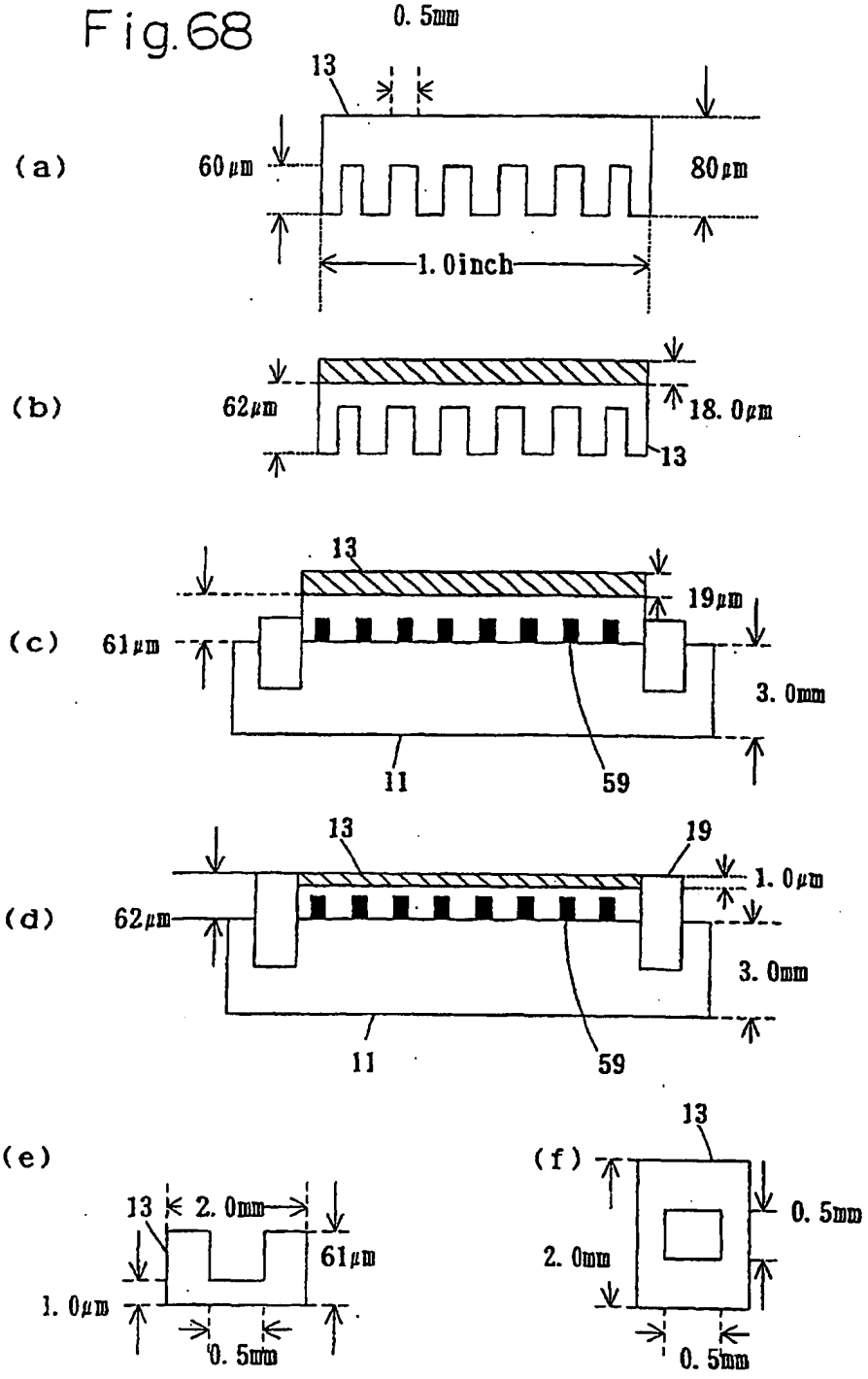
0.5mm
13
(a)
60μm
80μm
1.0inch
(b)
62μm
18.0μm
13
(c)
13
19μm
61μm
3.0mm
11
59
(d)
13
19
1.0μm
62μm
3.0mm
11
59
(e)
13
2.0mm
61μm
1.0μm
0.5mm
(f)
13
0.5mm
2.0mm
0.5mm

Fig.69

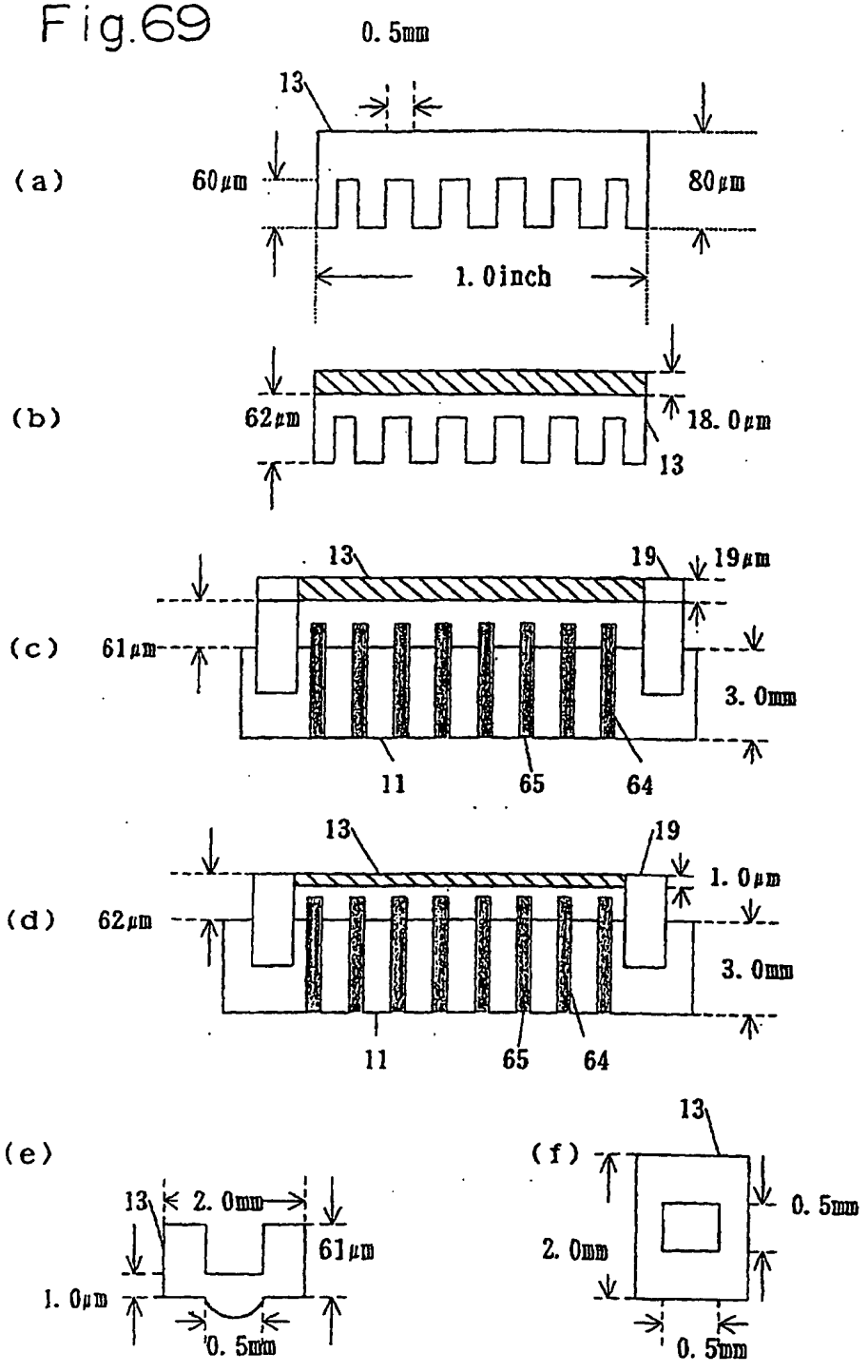
0.5mm
13
(a)
60μm
80μm
1.0inch
(b)
62μm
18.0μm
13
(c)
13
19
19μm
61μm
3.0mm
11
65
64
(d)
13
19
1.0μm
62μm
3.0mm
11
65
64
(e)
13
2.0mm
61μm
1.0μm
0.5mm
(f)
13
0.5mm
2.0mm
0.5mm

Fig. 70

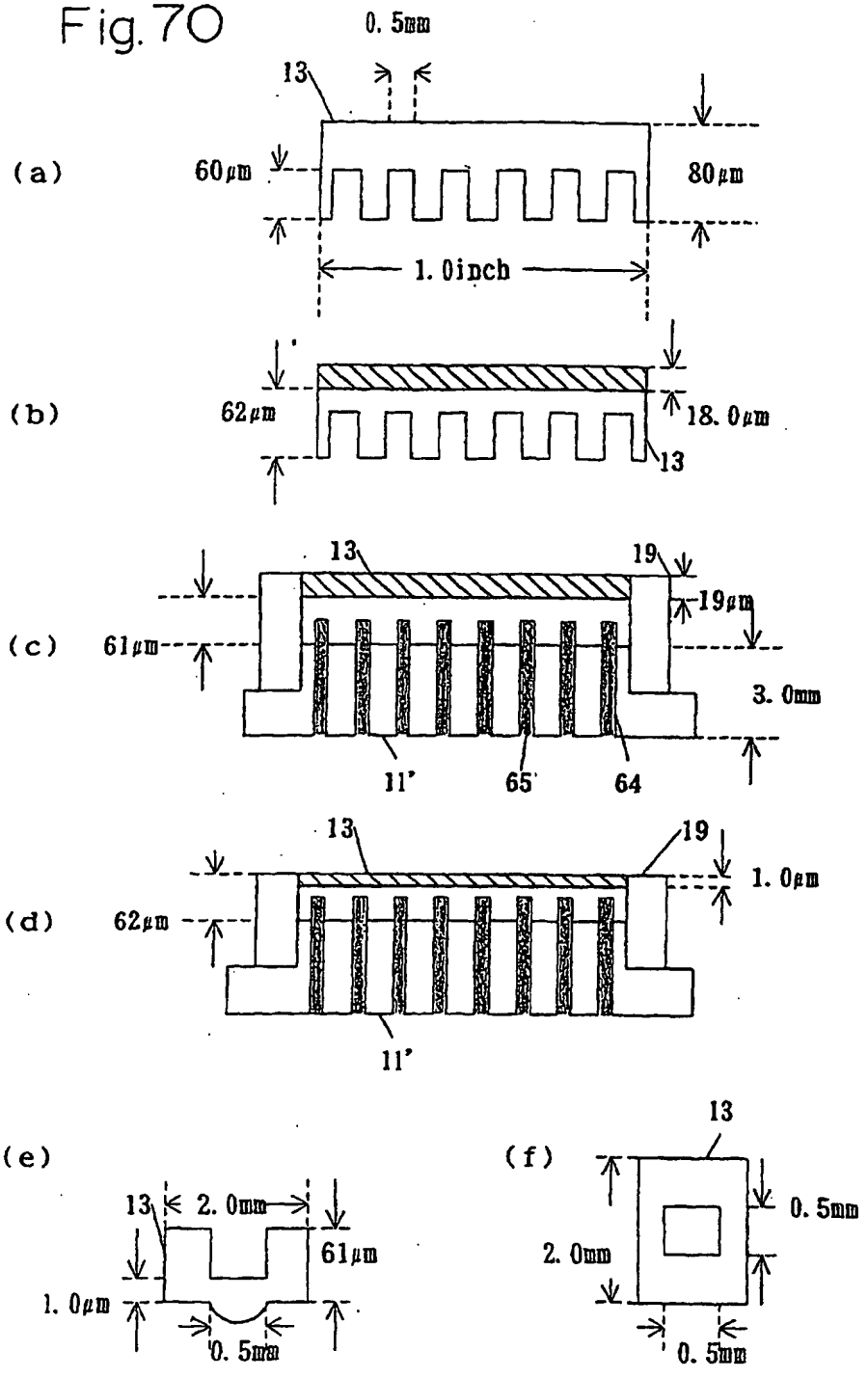
0.5mm
13
(a)
60μm
80μm
1.0inch
(b)
62μm
18.0μm
13
13
19
19μm
(c)
61μm
3.0mm
11'
65
64
13
19
1.0μm
(d)
62μm
11'
13
(e)
2.0mm
61μm
1.0μm
0.5mm
13
(f)
0.5mm
2.0mm
0.5mm

Fig. 71

(a)

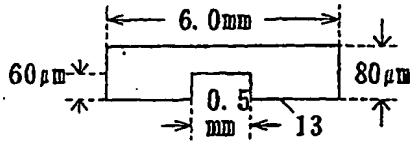
6.0mm
60μm
80μm
0.5
mm
13

(b)

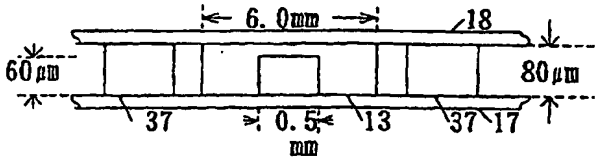
6.0mm
18
60μm
80μm
37
0.5
mm
13
37
17

(c)

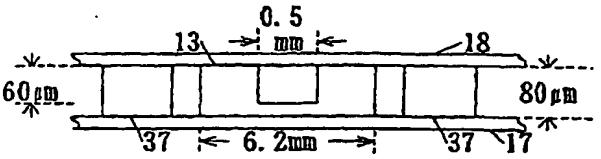
0.5
13
mm
18
60μm
80μm
37
6.2mm
37
17

(d)

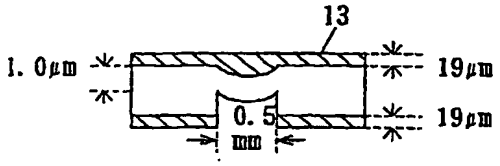
13
1.0μm
19μm
0.5
mm
19μm

(e)

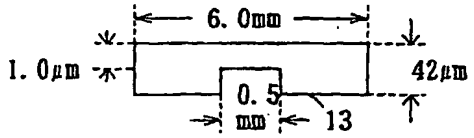
6.0mm
1.0μm
42μm
0.5
mm
13

Fig.72

(a)

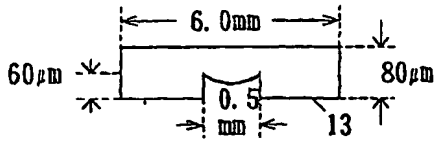

(b)

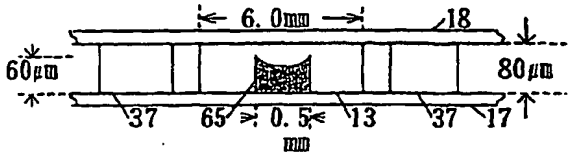

(c)

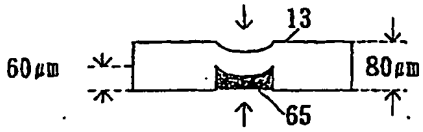

(d)

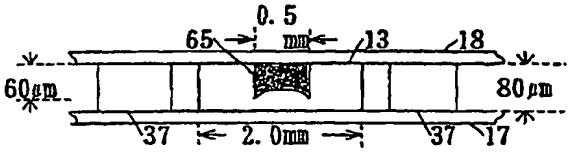

(e)

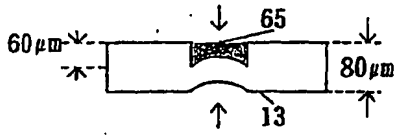

(f)

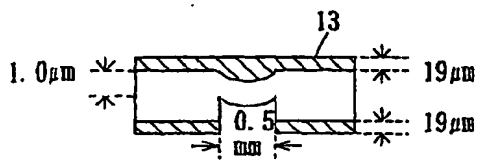

(g)

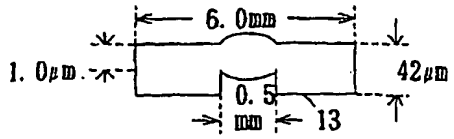

Fig. 73

(a)

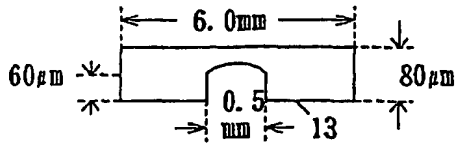
6.0mm
60μm
80μm
0.5 mm
13

(b)

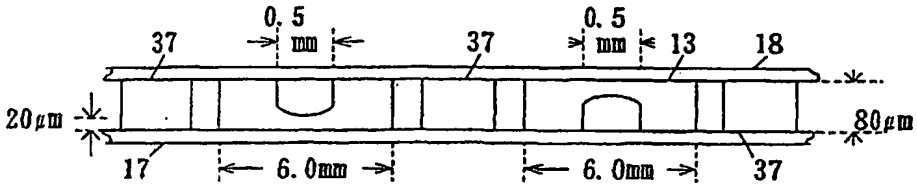
0.5 mm
37
37
0.5 mm
13
18
20μm
80μm
17
6.0mm
6.0mm
37

(c)

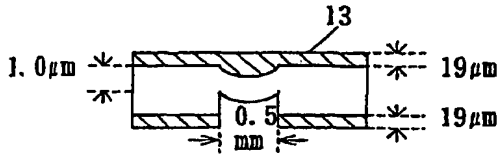
13
1.0μm
19μm
0.5 mm
19μm

(d)

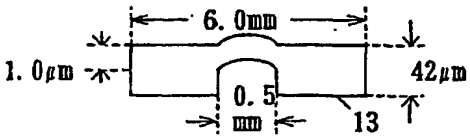
6.0mm
1.0μm
42μm
0.5 mm
13

Fig.74

(a)

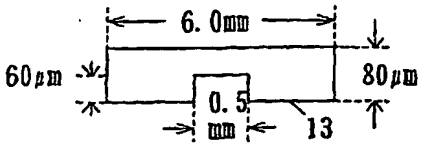
6.0mm
60μm
80μm
0.5 mm
13

(b)

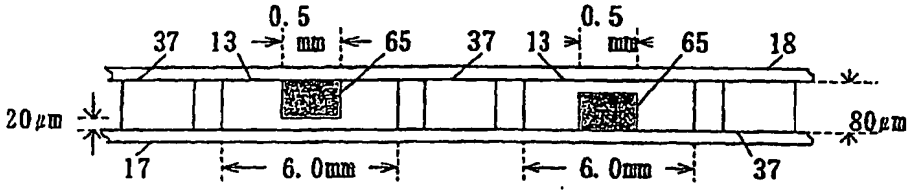
0.5 mm
37
13
65
37
13
0.5 mm
65
18
20μm
80μm
17
6.0mm
6.0mm
37

(c)

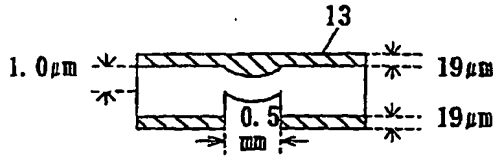
13
1.0μm
19μm
0.5 mm
19μm

(d)

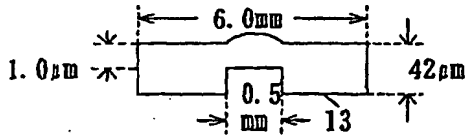
6.0mm
1.0μm
42μm
0.5 mm
13

Fig. 75

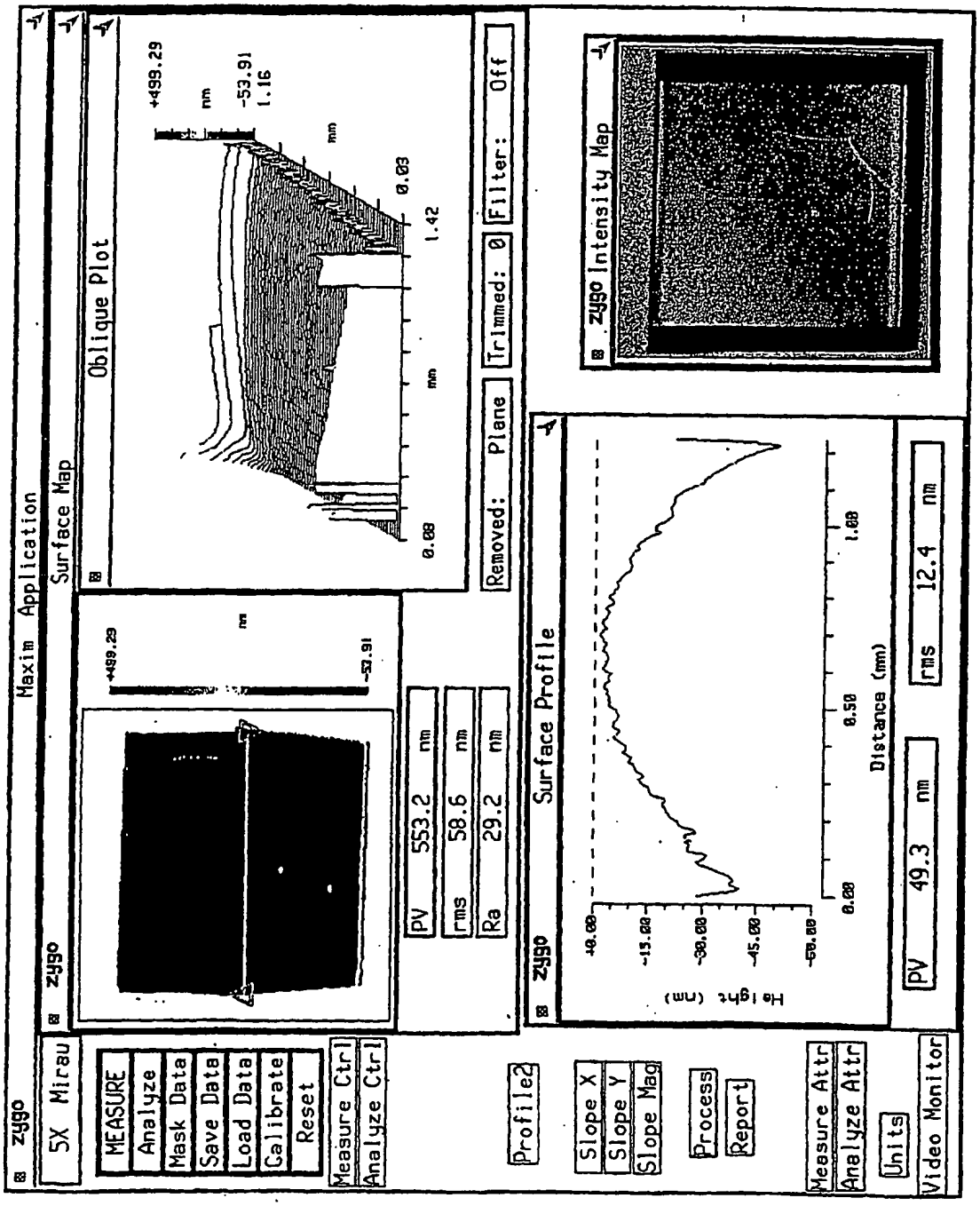
zygo
Maxim Application
5X Mirau
zygo
Surface Map
Oblique Plot
+499.29
nm
-53.91
1.16
0.00
mm
1.42
0.03
MEASURE
Analyze
Mask Data
Save Data
Load Data
Calibrate
Reset
Measure Ctrl
Analyze Ctrl
+499.29
nm
-53.91
PV 553.2 nm
rms 58.6 nm
Ra 29.2 nm
Removed: Plane
Trimmed: 0
Filter: Off
zygo Intensity Map
zygo
Surface Profile
Height (nm)
+0.00
-15.00
-30.00
-45.00
-60.00
0.00
0.50
1.00
Distance (mm)
PV 49.3 nm
rms 12.4 nm
Profile2
Slope X
Slope Y
Slope Mag
Process
Report
Measure Attr
Analyze Attr
Units
Video Monitor

Fig.76

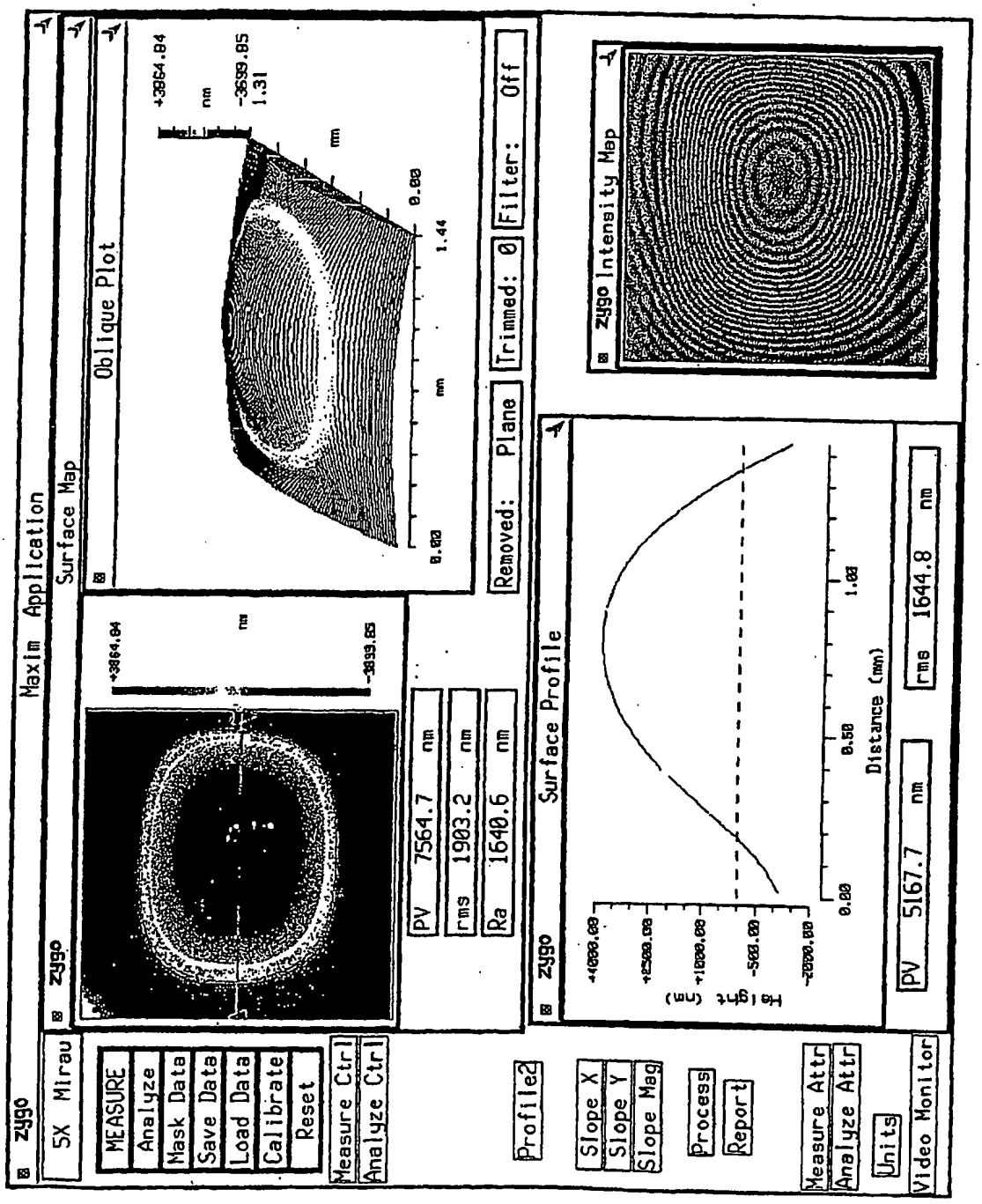
Maxim Application
zygo
SX Mirau
MEASURE
Analyze
Mask Data
Save Data
Load Data
Calibrate
Reset
Measure Ctrl
Analyze Ctrl
Surface Map
Oblique Plot
+3864.84
nm
-3939.85
1.31
mm
0.000
1.44
PV 7564.7 nm
rms 1903.2 nm
Ra 1640.6 nm
Removed: Plane
Trimmed: 0
Filter: Off
Profile2
Slope X
Slope Y
Slope Mag
Process
Report
Measure Attr
Analyze Attr
Units
Video Monitor
Surface Profile
Height (nm)
Distance (mm)
0.00
0.50
1.00
PV 5167.7 nm
rms 1644.8 nm
Zygo Intensity Map

Fig.77

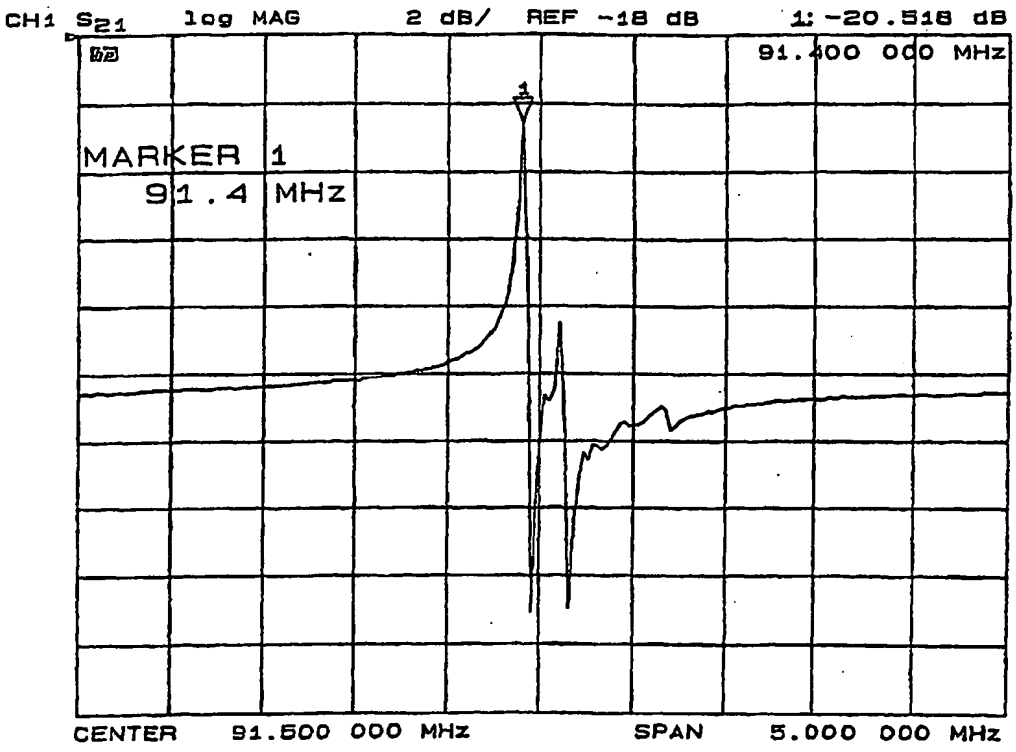
CH1 S21 log MAG 2 dB/ REF -18 dB 1: -20.516 dB
91.400 000 MHz
MARKER 1
91.4 MHz
CENTER 91.500 000 MHz
SPAN 5.000 000 MHz

Fig. 78

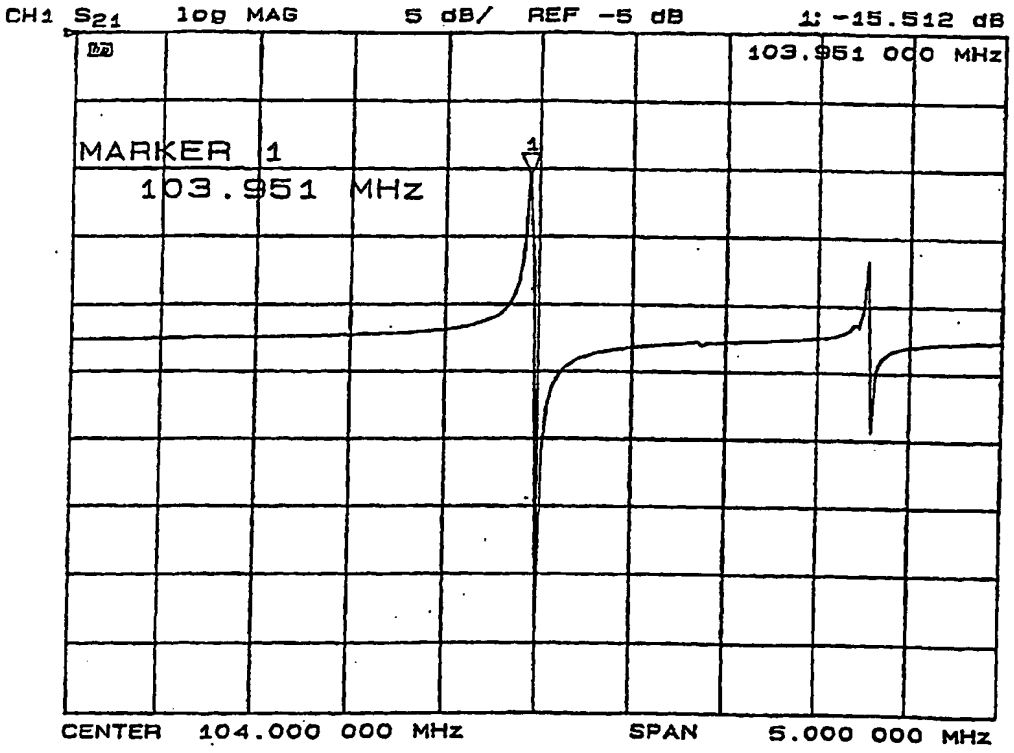
CH1 S21 log MAG 5 dB/ REF -5 dB 1: -15.512 dB
103.951 000 MHz
MARKER 1
103.951 MHz
1
CENTER 104.000 000 MHz
SPAN 5.000 000 MHz

Fig.79

(a)

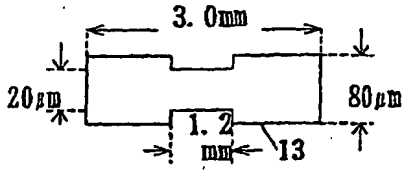
3.0mm
20μm
80μm
1.2 mm
13

(b)

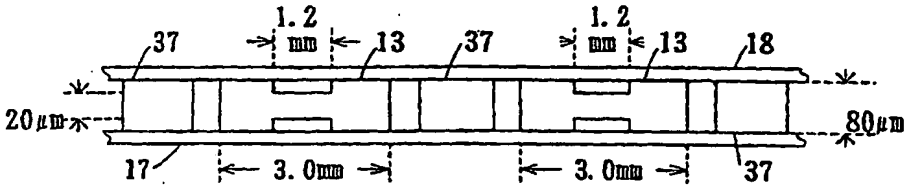
37
1.2 mm
13
37
1.2 mm
13
18
20μm
80μm
17
3.0mm
3.0mm
37

(c)

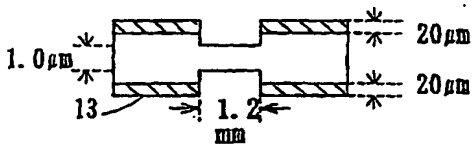
1.0μm
20μm
20μm
13
1.2 mm

(d)

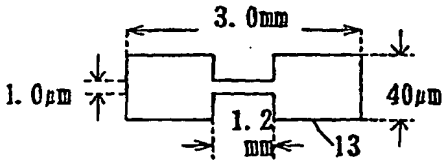
3.0mm
1.0μm
40μm
1.2 mm
13

Fig.80

(a)

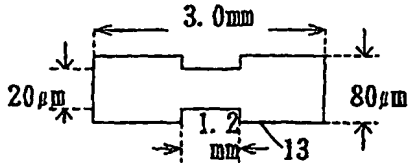
3.0mm
20μm
80μm
1.2 mm
13

(b)

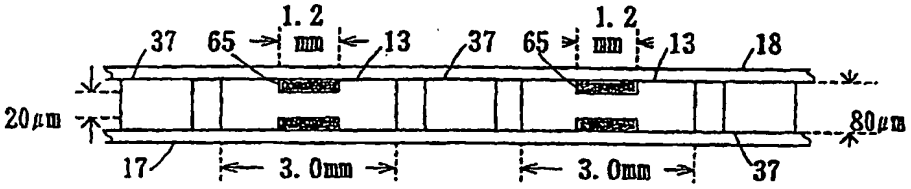
37
65
1.2 mm
13
37
65
1.2 mm
13
18
20μm
80μm
17
3.0mm
3.0mm
37

(c)

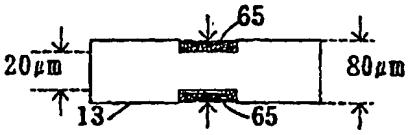
65
20μm
80μm
13
65

(d)

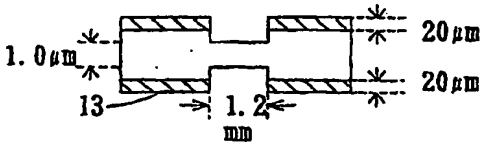
1.0μm
20μm
20μm
13
1.2 mm

(e)

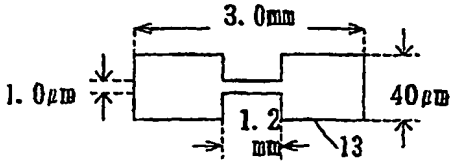
3.0mm
1.0μm
40μm
1.2 mm
13

Fig. 81

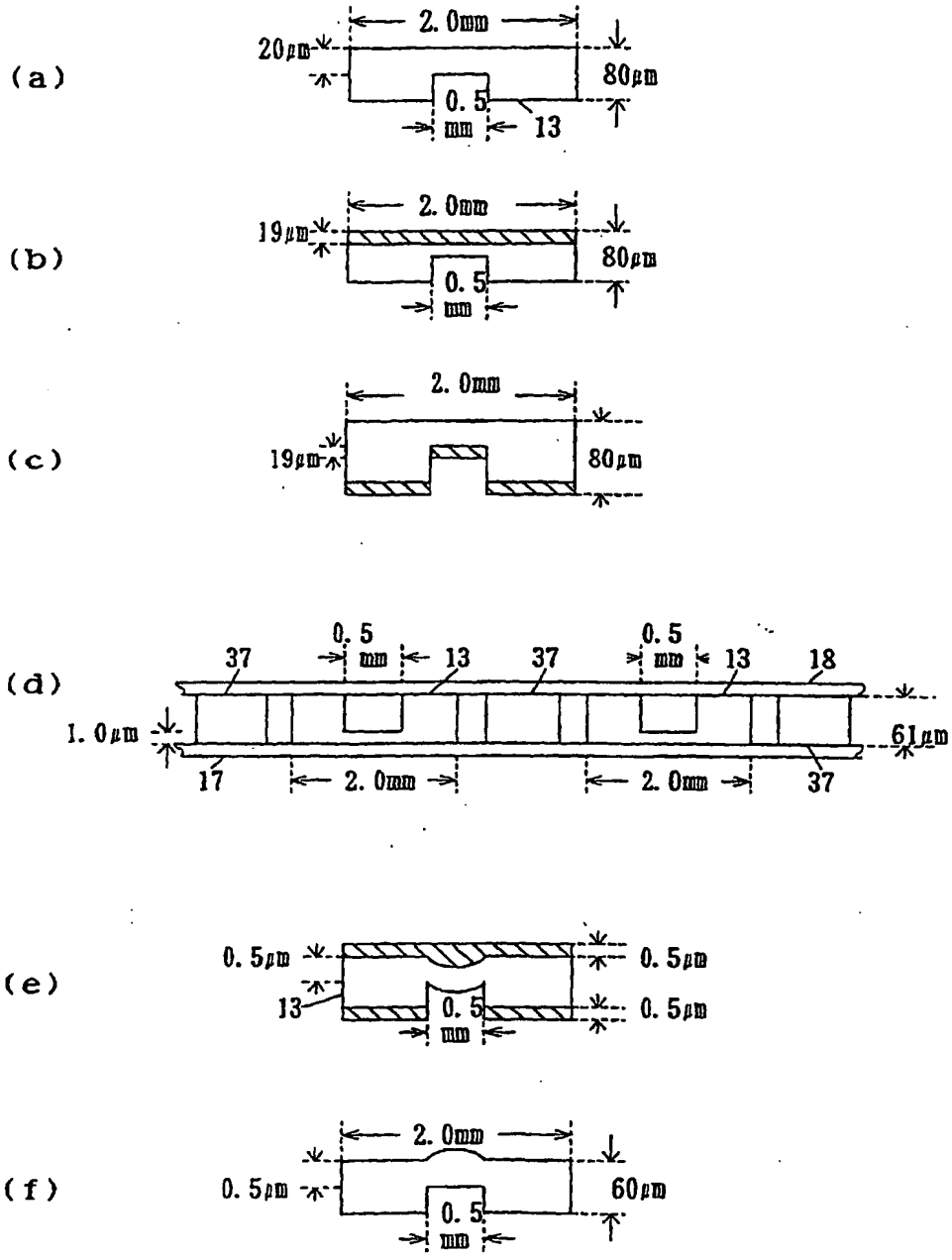
(a)
2.0mm
20μm
80μm
0.5 mm
13
(b)
2.0mm
19μm
80μm
0.5 mm
(c)
2.0mm
19μm
80μm
(d)
0.5 mm
37
13
37
0.5 mm
13
18
1.0μm
61μm
17
2.0mm
2.0mm
37
(e)
0.5μm
0.5μm
13
0.5 mm
0.5μm
(f)
2.0mm
0.5μm
60μm
0.5 mm

Fig. 82

(a)

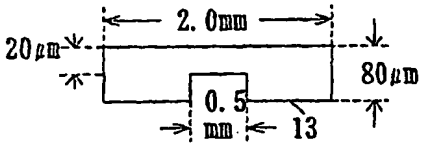

(b)

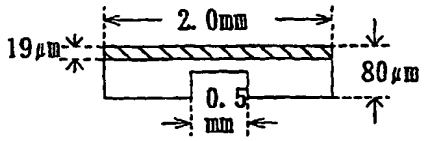

(c)

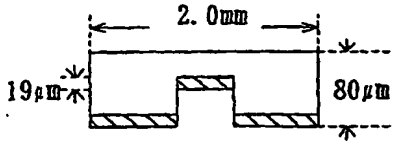

(d)

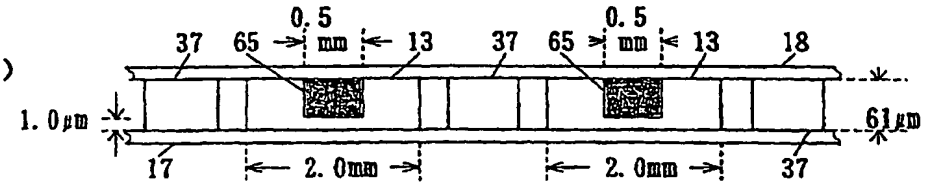

(e)

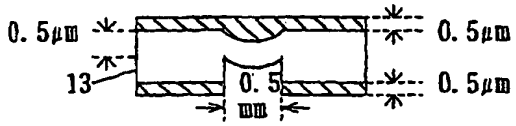

(f)

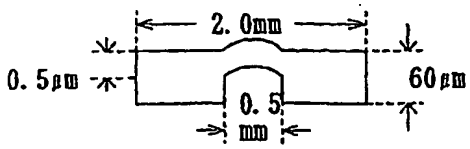

Fig.83

(a)

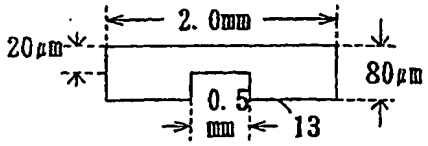

(b)

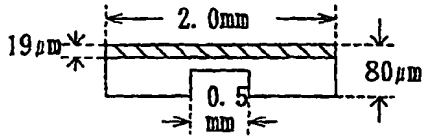

(c)

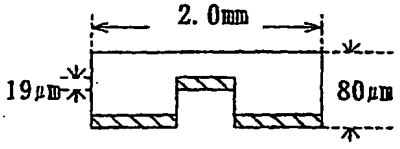

(d)

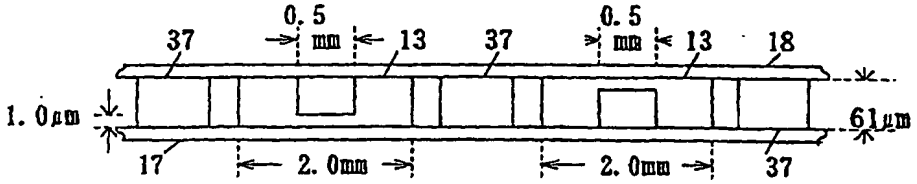

(e)

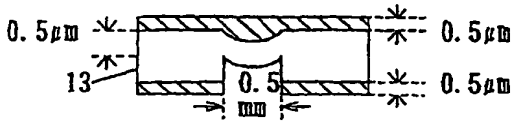

(f)

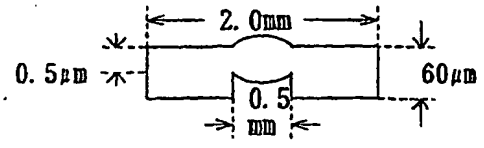

Fig. 84

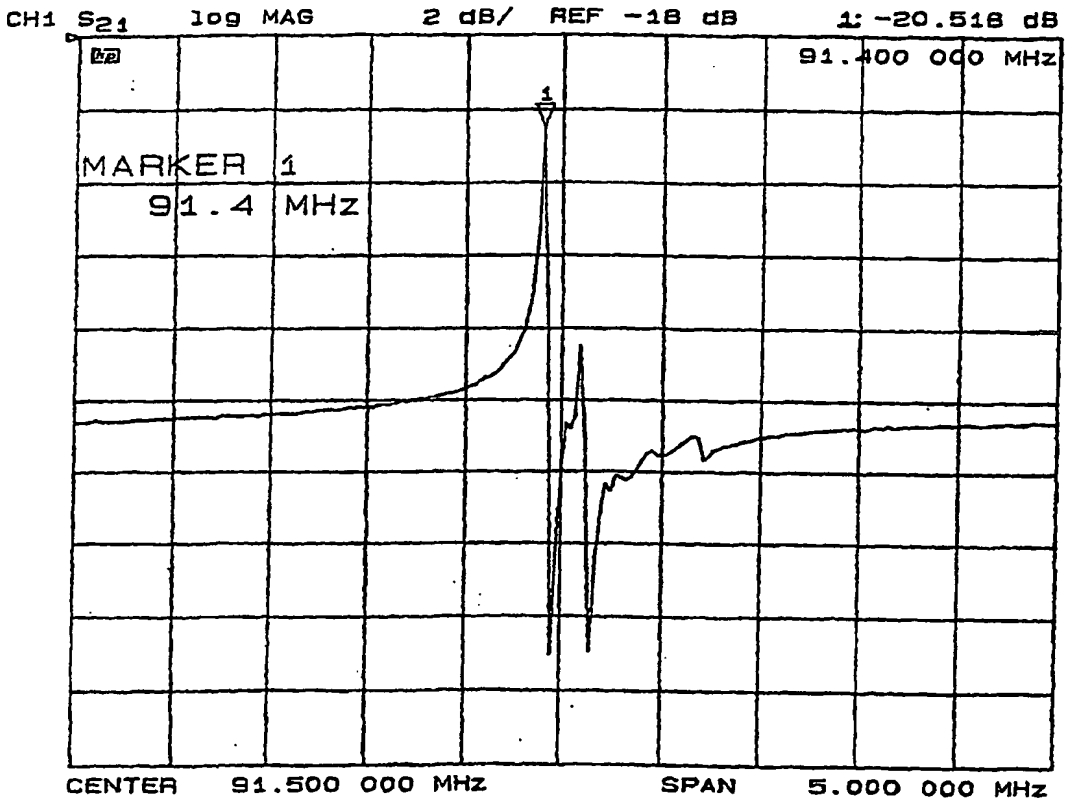
CH1 S21 log MAG 2 dB/ REF -18 dB 1: -20.518 dB
91.400 000 MHz
MARKER 1
91.4 MHz
CENTER 91.500 000 MHz
SPAN 5.000 000 MHz

Fig.85

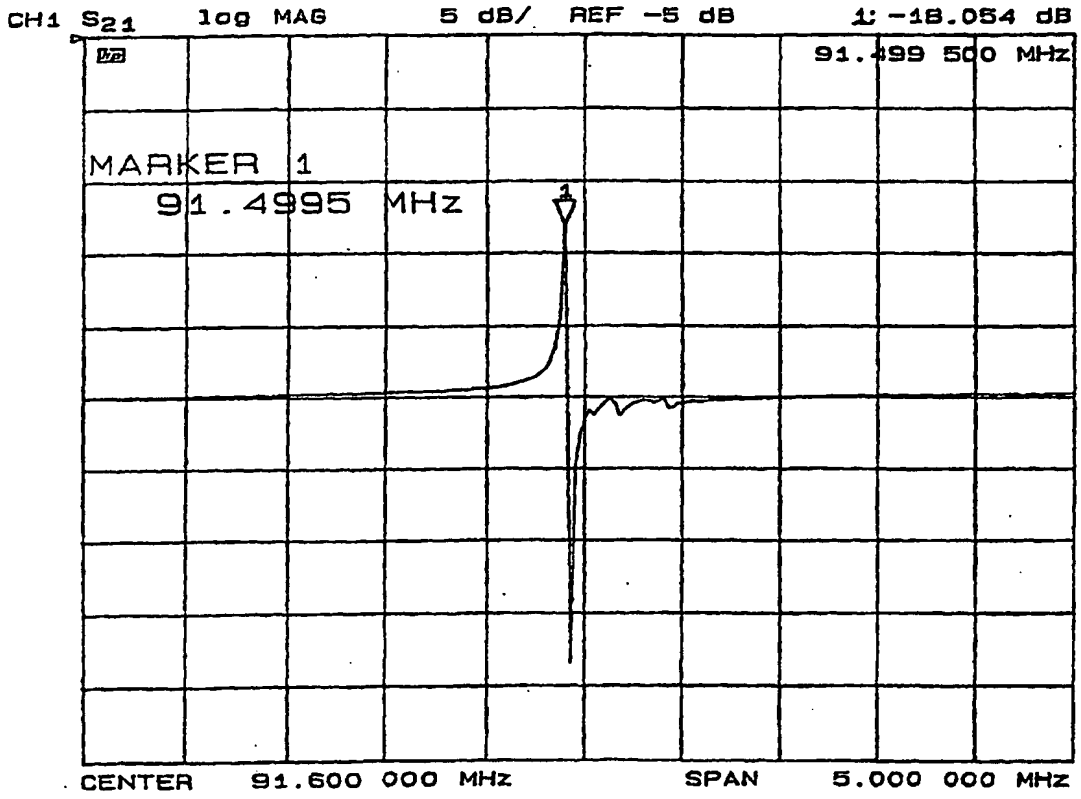
CH1 S21 log MAG 5 dB/ REF -5 dB 1: -18.054 dB
91.499 500 MHz
MARKER 1
91.4995 MHz
CENTER 91.600 000 MHz
SPAN 5.000 000 MHz

Fig. 86

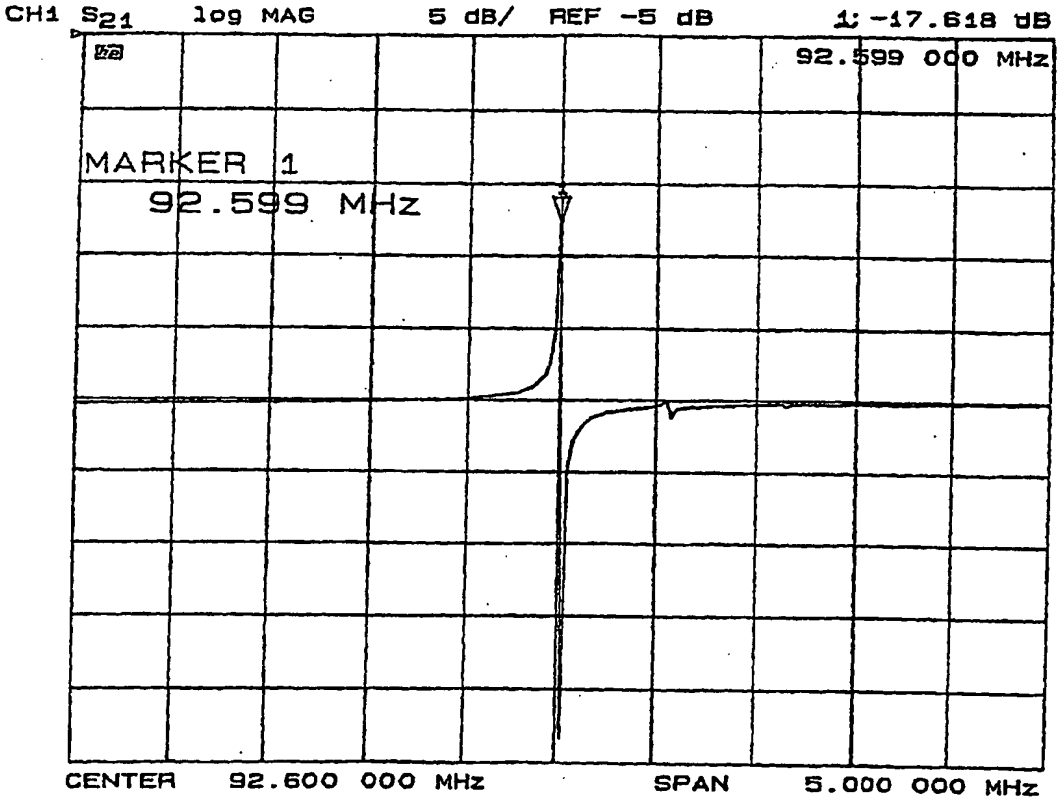
CH1 S21 log MAG 5 dB/ REF -5 dB 1: -17.618 dB
92.599 000 MHz
MARKER 1
92.599 MHz
CENTER 92.600 000 MHz
SPAN 5.000 000 MHz

Fig.87

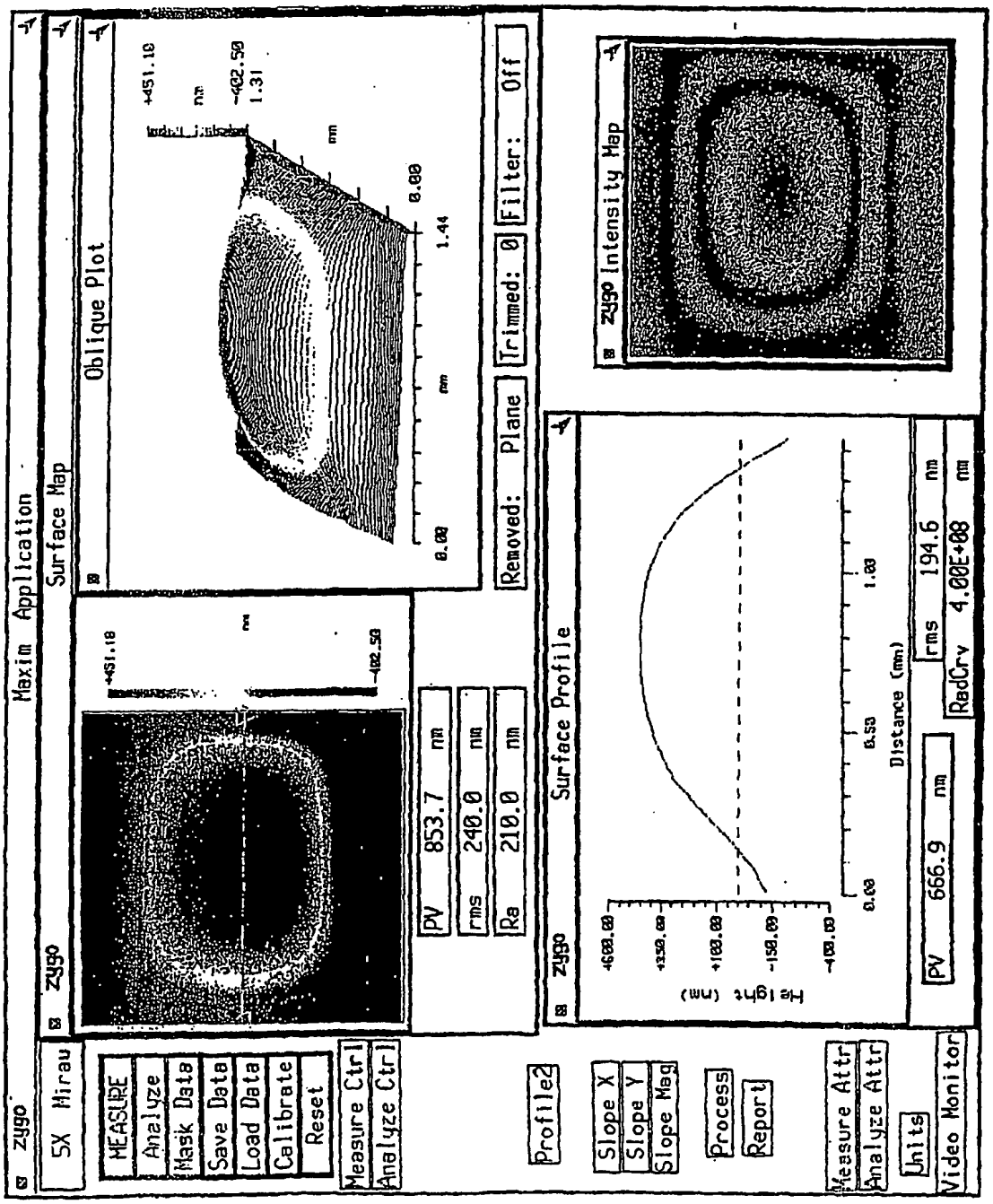
Maxim Application
zygo
SX Mirau
MEASURE
Analyze
Mask Data
Save Data
Load Data
Calibrate
Reset
Measure Ctrl
Analyze Ctrl
Surface Map
zygo
+451.18
-402.59
PV 853.7 nm
rms 240.0 nm
Ra 210.0 nm
Oblique Plot
+451.18
-402.59
1.31
0.00
1.44
0.00
Removed: Plane
Trimmed: 0
Filter: Off
zygo Intensity Map
Profile2
Slope X
Slope Y
Slope Mag
Process
Report
Measure Attr
Analyze Attr
Units
Video Monitor
zygo
Surface Profile
Height (nm)
+300.00
+150.00
+100.00
-150.00
-300.00
0.00
0.50
1.00
Distance (mm)
PV 666.9 nm
rms 194.6 nm
RadCrv 4.00E+00 nm

Fig.88

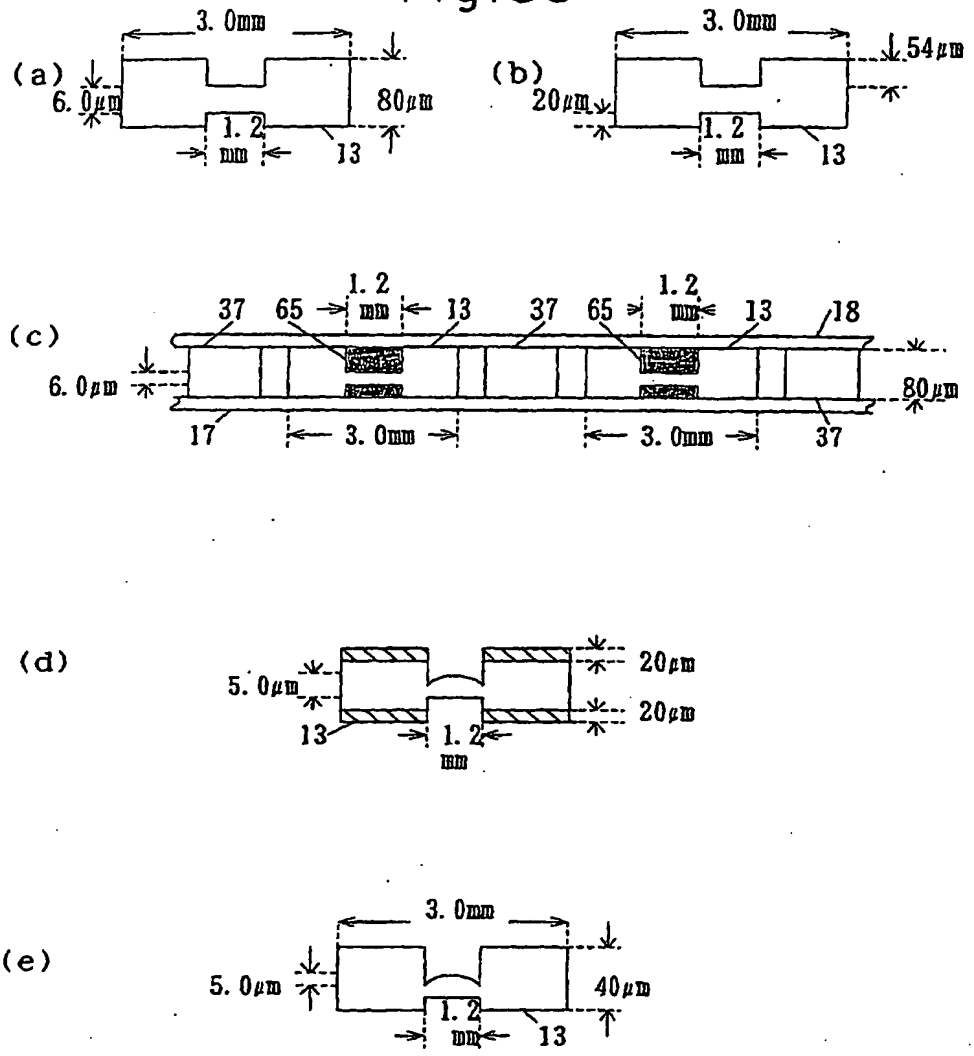
(a)
3.0mm
6.0μm
80μm
1.2 mm
13
(b)
3.0mm
54μm
20μm
1.2 mm
13
(c)
1.2 mm
37
65
13
37
65
1.2 mm
13
18
6.0μm
80μm
17
3.0mm
3.0mm
37
(d)
5.0μm
20μm
20μm
13
1.2 mm
(e)
3.0mm
5.0μm
40μm
1.2 mm
13

Fig. 89

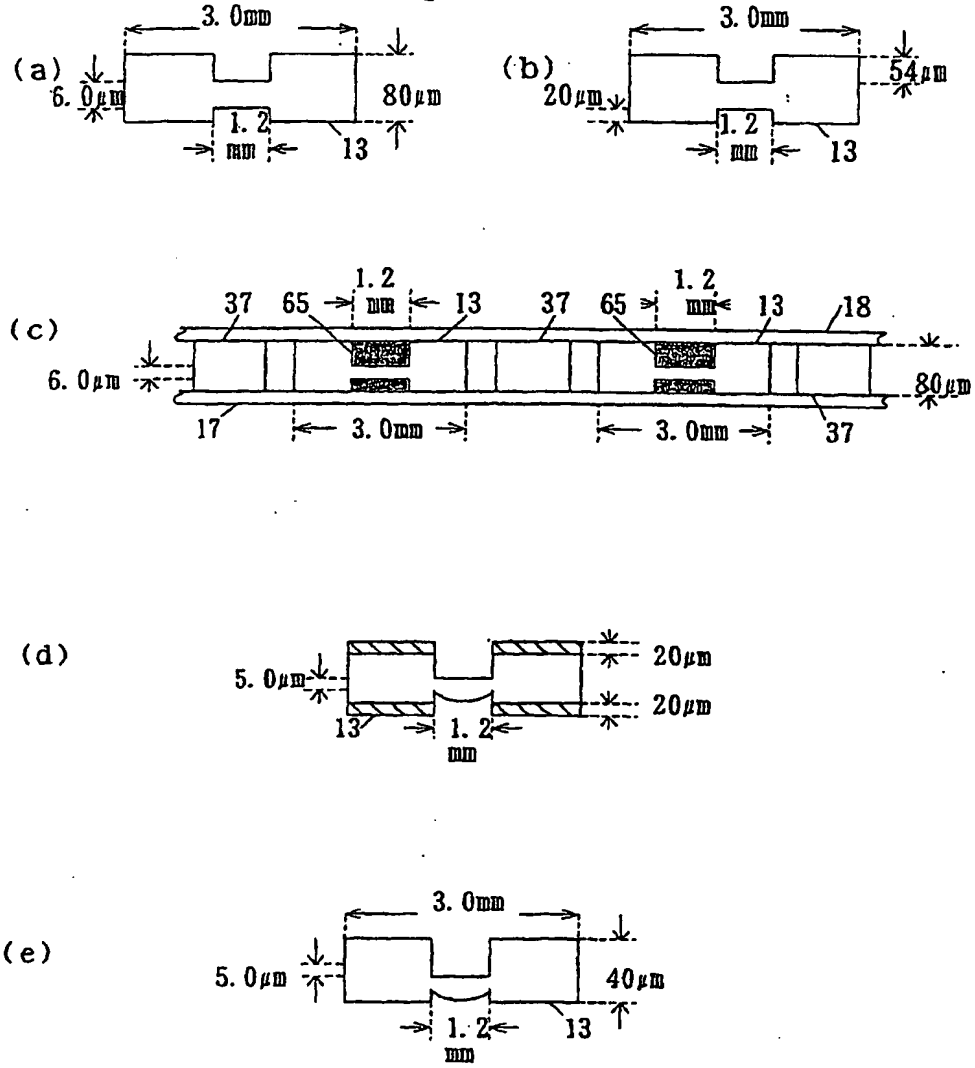
(a)
3.0mm
6.0μm
80μm
1.2 mm
13
(b)
3.0mm
20μm
54μm
1.2 mm
13
(c)
37
65
1.2 mm
13
37
65
1.2 mm
13
18
6.0μm
80μm
17
3.0mm
3.0mm
37
(d)
5.0μm
20μm
20μm
13
1.2 mm
(e)
3.0mm
5.0μm
40μm
1.2 mm
13

Fig.90

(a)

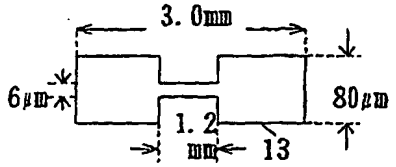
3.0mm
6μm
80μm
1.2 mm
13

(b)

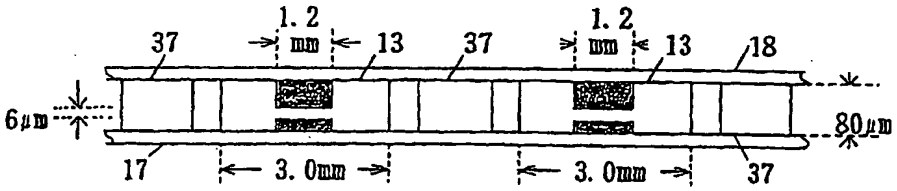
37
1.2 mm
13
37
1.2 mm
13
18
6μm
80μm
17
3.0mm
3.0mm
37

(c)

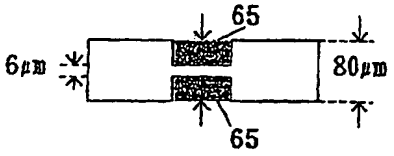
65
6μm
80μm
65

(d)

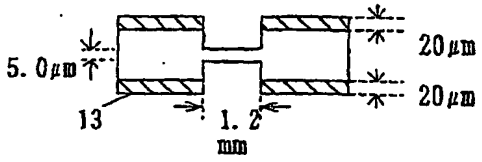
5.0μm
20μm
20μm
13
1.2 mm

(e)

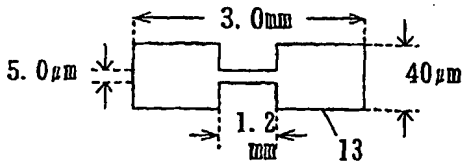
3.0mm
5.0μm
40μm
1.2 mm
13

Fig. 91

(a)

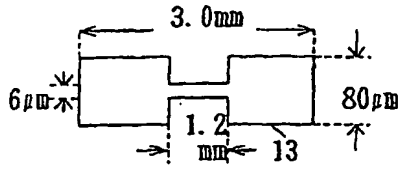
3.0mm
6μm
80μm
1.2 mm
13

(b)

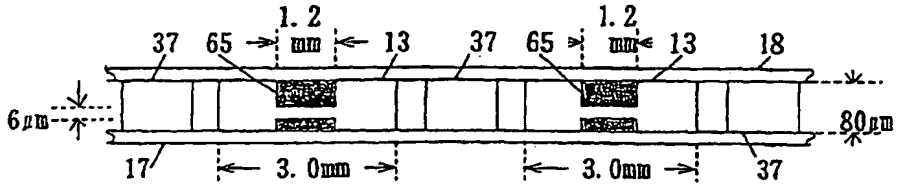
1.2 mm
37
65
13
37
65
1.2 mm
13
18
6μm
80μm
17
3.0mm
3.0mm
37

(c)

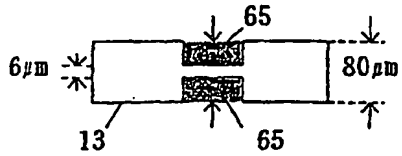
65
6μm
80μm
13
65

(d)

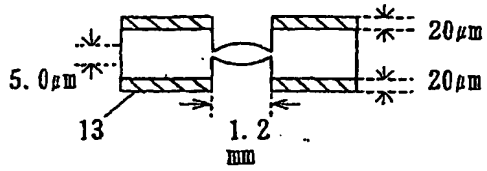
20μm
5.0μm
20μm
13
1.2 mm

(e)

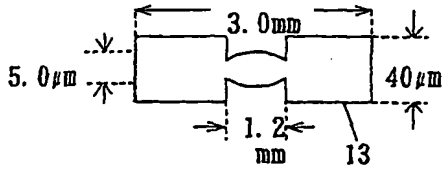
3.0mm
5.0μm
40μm
1.2 mm
13

Fig.92

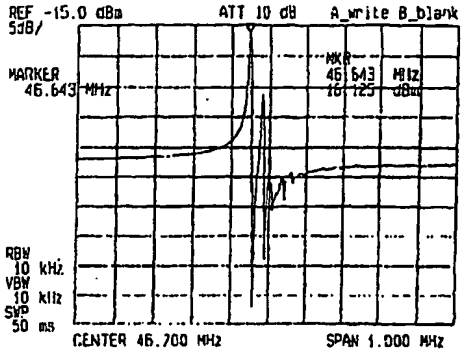

(a) RIE

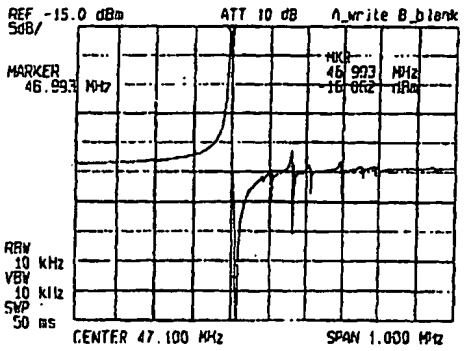

(b) Mechanical polishing after RIE

Fig. 1 Reactance-frequency characteristics
RIE : RF power 240 w, Press. 6.7 Pa,
Gas C_2F_6, 20 sccm

Fig.93

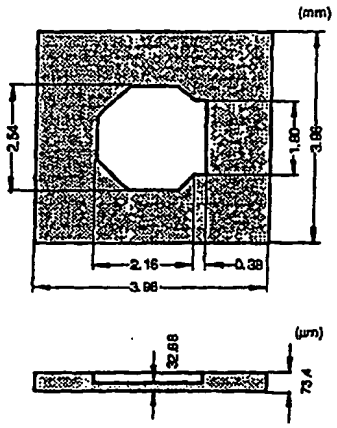

(a) Initial shape of machining material

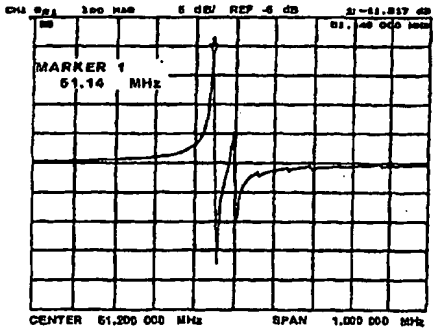

(b) Reactance-frequency characteristics

Fig. 2 Machining material used

Fig. 94

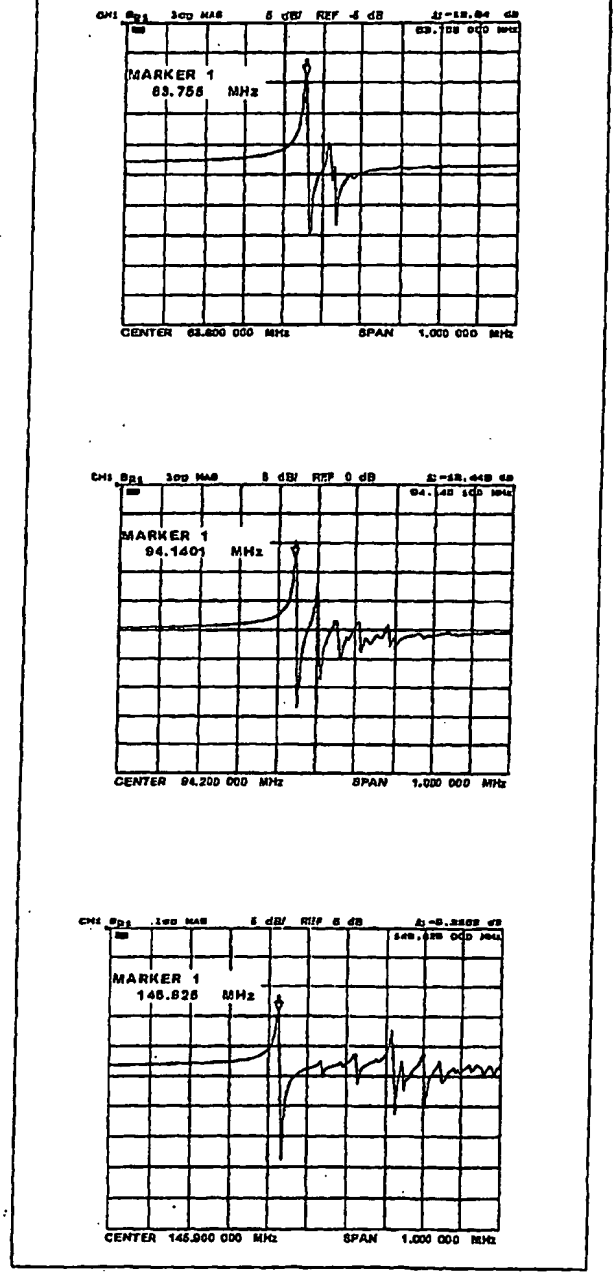

Fig. 3 Reactance-frequency characteristics of machining blanks after RIE

Fig. 95

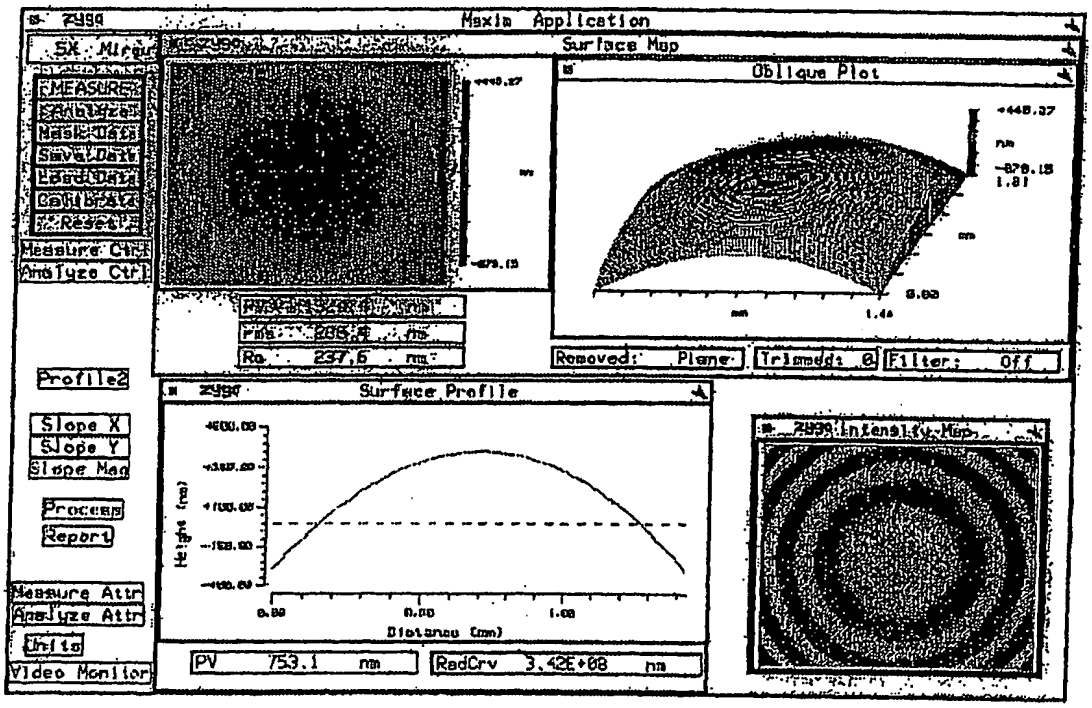

Fig. 4 Measured shape of the flat side oscillating part of the single inverted mesa type quartz blank by using an interference microscope

Fig. 96

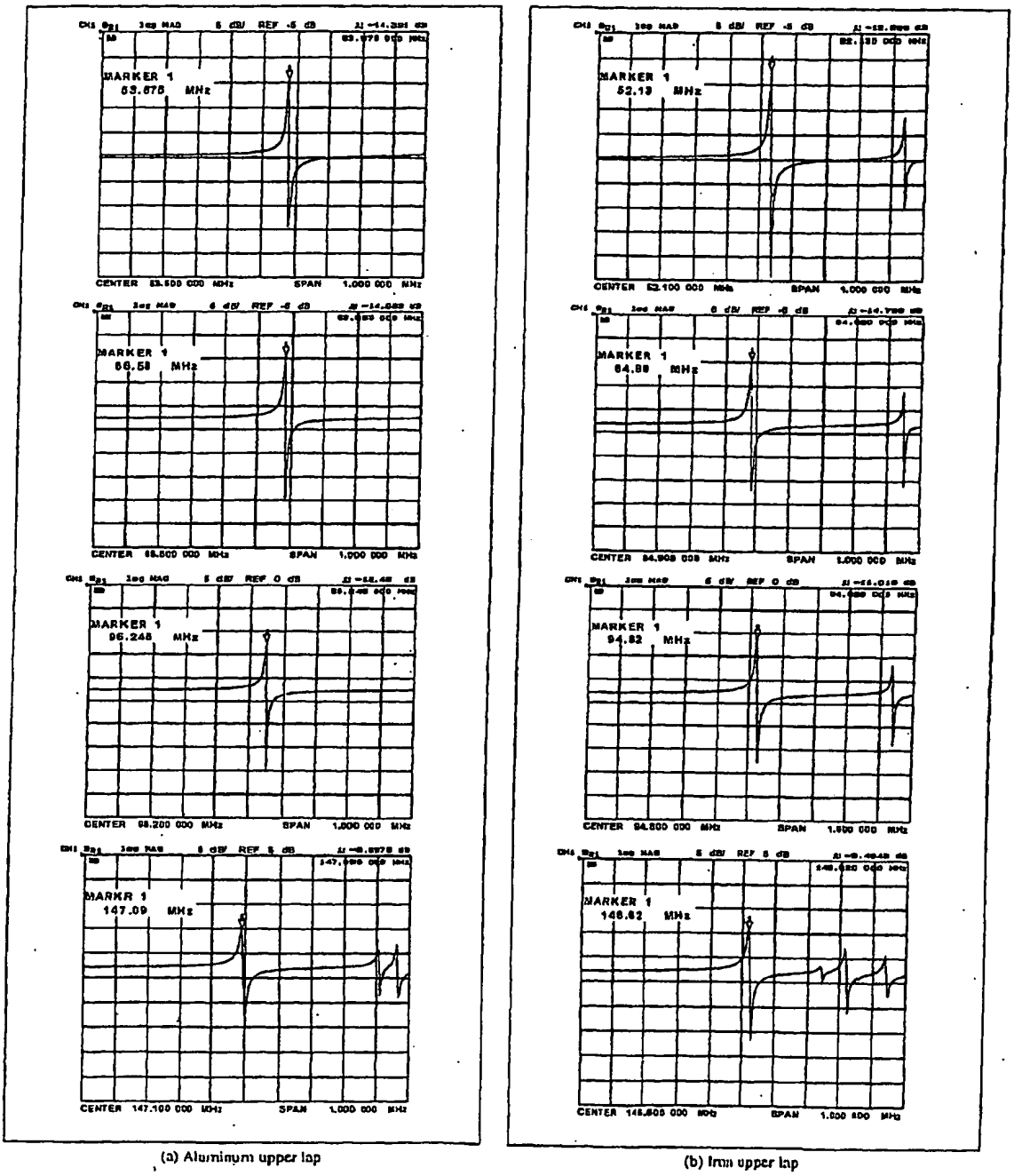

(a) Aluminum upper lap

(b) Iron upper lap

Fig. 5 Reactance-frequency characteristics of blanks polished

Fig.97

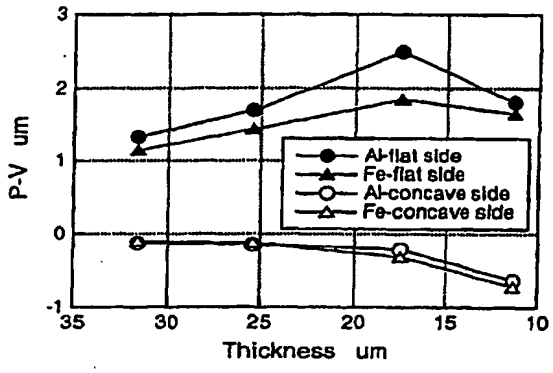

Fig. 6 Peak to valley of the central oscillating part

Fig.98

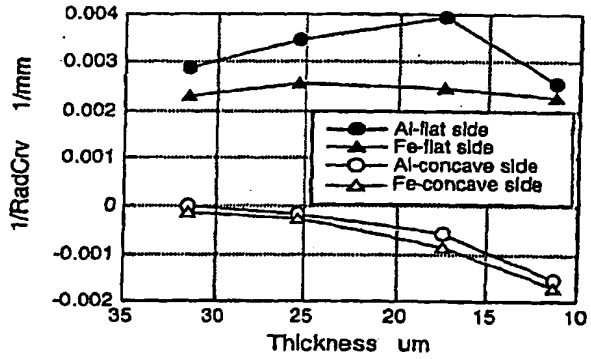

Fig. 7 Curvature radius of the central oscillating part

Fig.99

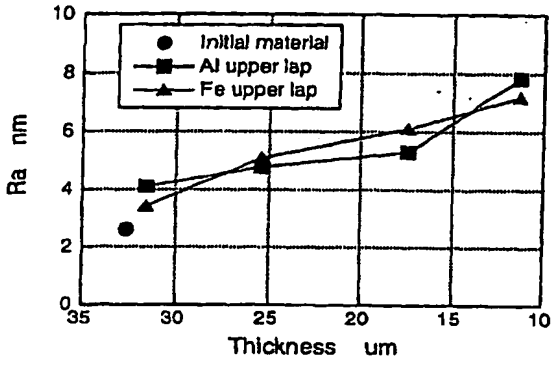

Fig. 8 Surface roughness at the central concave

Fig.100

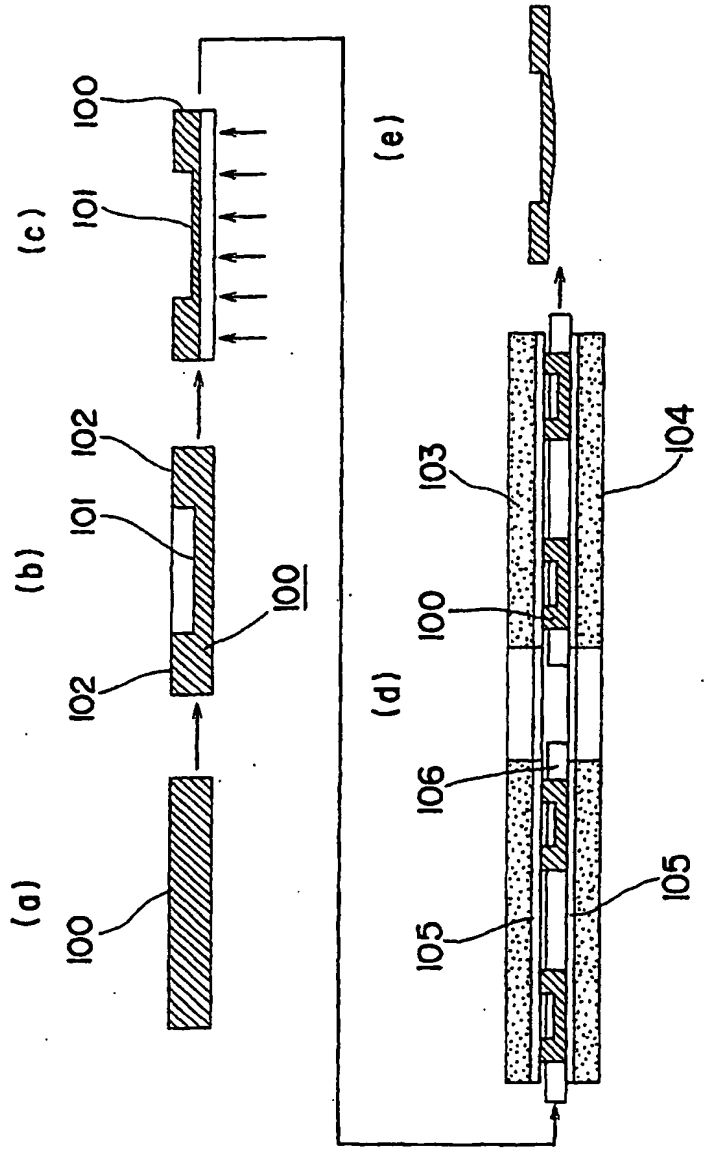

Fig.101

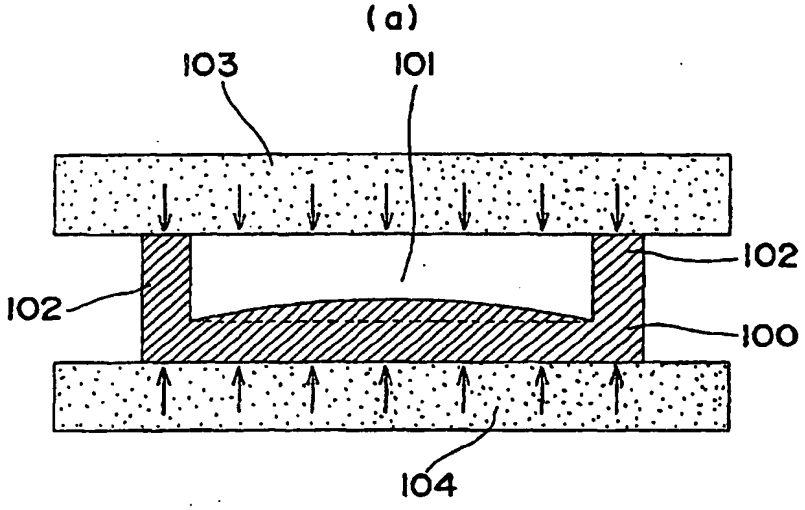

INTERNATIONAL SEARCH REPORT

International application No.
PCT/JP00/01691

A. CLASSIFICATION OF SUBJECT MATTER
Int.Cl[7] H01L41/08, H01L41/22, H03H9/19

According to International Patent Classification (IPC) or to both national classification and IPC

B. FIELDS SEARCHED

Minimum documentation searched (classification system followed by classification symbols)
Int.Cl[7] H01L41/08, H01L41/22, H03H9/19

Documentation searched other than minimum documentation to the extent that such documents are included in the fields searched
Jitsuyo Shinan Koho 1922-1996 Toroku Jitsuyo Shinan Koho 1994-2000
Kokai Jitsuyo Shinan Koho 1971-2000 Jitsuyo Shinan Toroku Koho 1996-2000

Electronic data base consulted during the international search (name of data base and, where practicable, search terms used)

C. DOCUMENTS CONSIDERED TO BE RELEVANT

Category*	Citation of document, with indication, where appropriate, of the relevant passages	Relevant to claim No.
X	EP, 713255, A (NGK INSULATORS,LTD.), 22 May, 1996 (22.05.96), Full text; Figs. 1 to 9 & JP, 8-148697, A & DE, 69501629, C	1-6,34
X	JP, 8-51241, A (NGK INSULATORS, LTD.), 20 February, 1996 (20.02.96), Full text; Figs. 1 to 7 (Family: none)	1-6,34
Y	JP, 53-71595, A (Fujikoshi Kikai Kogyo K.K., Nakazawa Mitsuo),	1-7
X	26 June, 1978 (26.06.78), Full text; Figs. 1 to 8 (Family: none)	34,35
Y	JP, 52-137290, A (Seiko Instr. & Electronics Ltd.), 16 November, 1977 (16.11.77),	1-7
X	Full text; Figs. 1 to 4 (Family: none)	34,35
Y	JP, 7-50438, A (Matsushita Electric Ind. Co., Ltd.), 21 February, 1995 (21.02.95), Full text; Figs. 1 to 8 (Family: none)	8-15, 17-23,25-29

☒ Further documents are listed in the continuation of Box C. ☐ See patent family annex.

* Special categories of cited documents:
"A" document defining the general state of the art which is not considered to be of particular relevance
"E" earlier document but published on or after the international filing date
"L" document which may throw doubts on priority claim(s) or which is cited to establish the publication date of another citation or other special reason (as specified)
"O" document referring to an oral disclosure, use, exhibition or other means
"P" document published prior to the international filing date but later than the priority date claimed
"T" later document published after the international filing date or priority date and not in conflict with the application but cited to understand the principle or theory underlying the invention
"X" document of particular relevance; the claimed invention cannot be considered novel or cannot be considered to involve an inventive step when the document is taken alone
"Y" document of particular relevance; the claimed invention cannot be considered to involve an inventive step when the document is combined with one or more other such documents, such combination being obvious to a person skilled in the art
"&" document member of the same patent family

Date of the actual completion of the international search	Date of mailing of the international search report
04 July, 2000 (04.07.00)	11 July, 2000 (11.07.00)
Name and mailing address of the ISA/ Japanese Patent Office	Authorized officer
Facsimile No.	Telephone No.

Form PCT/ISA/210 (second sheet) (July 1992)

INTERNATIONAL SEARCH REPORT

International application No.
PCT/JP00/01691

C (Continuation). DOCUMENTS CONSIDERED TO BE RELEVANT

Category*	Citation of document, with indication, where appropriate, of the relevant passages	Relevant to claim No.
X	JP, 1-288102, A (Seiko Electronic Components Ltd.), 20 November, 1989 (20.11.89),	8,16
Y	Full text; Figs. 1 to 2 (Family: none)	9-15, 17-23,25-29
Y	JP, 48-34494, A (Nippon Telegr. & Teleph. Corp. <NTT>), 18 May, 1973 (18.05.73),	24
X	Full text; Figs. 1 to 2 (Family: none)	34,35

Form PCT/ISA/210 (continuation of second sheet) (July 1992)

4p－K－15　積層導波路ホログラムメモリ（V）— 積層媒体からの再生実験 —

MWH Memory (V) – reproduction from multilayered waveguide medium –

NTT SP 研，*NTT PH 研　黒川義昭，田辺隆也，山本学，*八木生剛，*今井欽之，*舘彰之
NTT SP Labs, *NTT PH Labs　Y. Kurokawa, T. Tanabe, M. Yamamoto, *S. Yagi, *T. Imai and *A. Tate
E-mail: kurokawa.yoshiaki@lab.ntt.co.jp

我々は，次世代大容量メモリとして，積層導波路構造を有する媒体を用いたホログラム ROM（MWH ROM）の研究開発を進めている[1]．本報告では，積層媒体評価用装置を試作し，実際に導波路を10層積層した媒体[2]から再生を行なった結果について報告する．

再生する層の選択は，図1に示したように媒体を積層方向に移動することにより行なった．MWH はディテクタ上に直接再生光の焦点を結ぶように媒体設計を行なうことが可能であるため，試験機のディテクタ（今回は CCD を用いた）にはレンズを設けていない．図2に CCD 上に直接得られた再生像を示すが，再生層間のクロストークのない明瞭な画像が得られている．

図1 再生装置

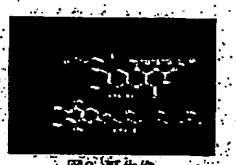
図2 再生像

MWH ROM の再生では，再生しようとする導波層に入射光をいかに結合させるかが重要である．今回，再生光を MWH に入射する端面と逆の端面（出射端と呼ぶ）における光強度を用いた入射光の位置決めについて検討した．図3には，入射光を図2の像が得られた位置，およびその位置から2μm 積層方向に移動した状態で得られた出射端面の光強度分布を示す．入射光が特定の層と結合している場合には，その層からの光強度が強く観察されるのに対し，入射光がずれた場合には強度が弱くなると共に他の層からの光も観察されるようになることがわかる．このことを利用し，入射光を目的とする導波層のみに結合することができる．

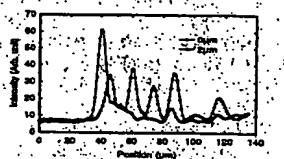

図3 出射端強度分布

[参考文献] 1)八木 他，1999 年秋応物学会予稿 p.994　2) 石原 他，本大会発表予定

※ 本研究は(財)光技術産業振興協会が受託した NEDO の次世代光メモリプロジェクトの一環として行なわれています．

3a－Q－1　垂直応力印加による水晶のツイン制御

Twin control in a crystalline quartz by application of normal stress

分子科学研究所，ｽﾀﾝﾌｫｰﾄﾞ大学*，早稲田大学**
栗村直，庄司一郎，平林拓範，ﾏｰﾃｨﾝﾌｪｲﾔｰ*，上江洲由晃**，中島啓幾**
Institute for Molecular Science, Stanford Univ.*, Waseda Univ.**
Sunao KURIMURA, Ichiro SHOJI, Takunori TAIRA, Martin FEJER, Yoshiaki UESU**, and Hirochika NAKAJIMA***

水晶結晶（α-SiO_2）は広く光学材料として利用されており，光学的透明領域が広い，レーザー損傷に強い，化学的に安定である，などの特長を有する．レーザー共振器内では波長板（λ/4）として利用されており，低損失で高いパワーまで対応できる熱的にも安定した材料である．我々はこれを紫外・可視域の擬似位相整合（QPM）波長変換材料として提案し，ツイン制御を行なってきている．従来は水晶上に形成した金属薄膜による面内熱応力を用いてドメインとツインを制御し，周期ツインを実現してきた[1]．しかしこの方法では熱応力が表面付近に局在するためツインの形成領域が表面数μmに限られ，λ/4波長変換は困難である．そこで今回垂直応力を利用する新たな手法を採用して深いツインを得たので報告する．

水晶では応力印加によるd_{ij}の弾性ｽﾃｨﾌﾈｽ（ﾊｲﾄﾞｽﾃｨﾌﾈｽ項）を利用することで，ツインを発生させることができる．ここでは図1に示す独自に開発した装置を用いて応力を印加した．この装置ではピストンロッドの間に基板を挟入し，油圧を利用して応力を印加する．ツイン間のｴﾈﾙｷﾞｰ差ΔGは，(1/2)[d][S][σ]（σ: 応力，S: 弾性ｺﾝﾌﾟﾗｲｱﾝｽ）となり，結晶切断面に垂直な圧縮性応力の場合，極座標を用いて$\Delta G = 2\sigma_3^2 S_{14} \sin^3\theta \cos\theta \cos 3\phi$となる（$\sigma_3$:応力の大きさ）[1]．厚さ330μmの基板はΔGを最大にする$\theta = 60°$，で用い，400℃にて応力1x10⁸ (MPa)を印加した．水晶は発酸ｴｯﾁﾝｸﾞにより1mm角を残して2.5μm段差を生じさせ，応力を1mm角領域に集中させた．発生したツイン（図2）はほぼ1mm角の領域を埋め，裏面に到達していることがわかる．裏面の形状からもわかるようにツインの成長方向は結晶の異方性を反映しており，今後基板方位を選ぶことでQPMに適した構造をめざしていく．水晶のﾊﾟﾀｰﾆﾝｸﾞにご協力いただいた日本ｶﾞｲｼ株式会社の近藤厚男氏，今枝英能留氏に感謝いたします．本研究は科研費萌芽研究12875013を受けています．

1）栗村他，応用物理69，548(2000)

図1　応力印加装置

図2　ツイン写真

3a－Q－2　クランク状光接続を用いた3次元光コネクタの開発

3D-Optical connector by crank type optical connection.

超先端電子技術開発機構，沖電気工業（株）*　○岡部豊，牛窪孝*
ASET, Oki Electric Industry Ltd., *　Y. Okabe, and T. Ushikubo*
okabe@psi-aset-unet.ocn.ne.jp

1．はじめに　光部品が搭載された光プリント板では，搭載されている光ＭＣＭ間，あるいはマザーボードとサブボード間の高密度な光接続が必要となる．特に，同一平面内にはない３次元的な光接続については，光プリント板上の光配線では接続できない．本発表では，高密度な光接続を実現するため，図１に示すような３次元的に光接続する光クランク接続コネクタを提案し，報告を行う．

2．結果および考察　クランク接続コネクタの構成部品としては，平面マイクロレンズ（ＰＭＬ）とアルミによる反射鏡を利用した．実際にクランク接続コネクタを作製して，ファイバを用いた光学測定の結果，本コネクタの挿入ロスとしては，約３．５ｄＢの値を得た．これは，ＰＭＬのファイバへの結合効率で２．５ｄＢ，反射部分で０．５ｄＢであった．図２には，コネクタを作製した時のコネクタ設置部のトレランス測定を行った．この結果１ｄＢ減少するには約２０μｍ，３ｄＢ減少する点は約２５μｍであることがわかった．現在使用されているＳ-ＭＦコネクタのトレランスに比べ，１ｄＢ減少では５倍程度のトレランスの緩さがあり，本コネクタ使用時には大きな利点となることが想定される．以上より，クランク接続コネクタは３次元光コネクタとして，有効な方式であることが証明された．

本研究は，ＮＥＤＯから委託され実施したものである．

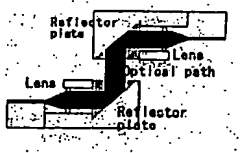

図1.クランク接続コネクタ概念図

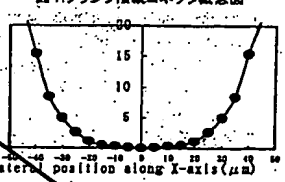

図2．クランクコネクタ接合部分のトレランス

紫外波長変換をめざした擬似位相整合水晶

栗村　直 ・ Martin M. Fejer ・ 平等　拓範
上江洲　由晃 ・ 中島　啓幾

応用物理　第69巻　第5号　(2000年)　抜刷

最近の展望

紫外波長変換をめざした擬似位相整合水晶

栗村　直* ・ Martin M. Fejer** ・ 平等　拓範*
上江洲　由晃*** ・ 中島　啓幾**

強誘電体の周期分極反転は擬似位相整合(QPM)を実現し非線形光学に革命をもたらした．本稿では，自発分極をもたない非線形光学材料に反転構造を導入する手法として，応力によるツイン制御を提案し，これを水晶に適用する．紫外透明材料である水晶において，期待される波長変換特性やツイン制御の熱力学についても紹介する．

Keywords : quasi phase matching, quartz, twin, domain, wavelength conversion, ultraviolet, second harmonic generation, stress, QPM, PPLN

1. まえがき

擬似位相整合 (Quasi Phase Matching : QPM) 波長変換デバイスは，変換効率が高い，設計自由度が大きい，複合機能化・集積化が可能である，などの利点をもつことから近年注目されている[1]．空間領域，周波数領域，時間領域で位相整合特性をデザインできるため，従来結晶にQPM構造を導入することは新規結晶を開発したと同等もしくはそれ以上のインパクトを与える．例えば，変換光の空間的強度分布を加工する[2]，波長変換の周波数帯域を広げる[3]，波長変換と同時にパルス圧縮[4]・整形[5]を行うなど，他の位相整合法では考えられない多彩な設計性を有する．

また，QPMでは新たな波長領域へ波長変換を行う場合に，未知の材料ではなく，光学定数，化学特性，熱特性，レーザー損傷特性，加工性，量産性などの知られた既存の材料を使用することができる．すなわち，既知の材料においても非線形光学定数の変調周期を変えるだけであらゆる波長に対応でき，変調技術のみを確立すれば既存材料の透明領域すべてが利用可能である．このためQPMにおいては非線形光学定数の変調構造をいかに導入するか，変調可能な材料をいかに探索するかが重要な課題となる[6]．従来QPM材料は主に強誘電体材料に限られてきたが，これは強誘電体が自発分極をもち，電界による分極反転が可能であることに起因する．すなわち，電極をパターニングして電界を印加することで，周期的に非線形光学定数を変調することができるからである．例えば$LiNbO_3$ (LN) 系材料では，光損傷に強い$MgO : LiNbO_3$での分極反転[7]が複屈折整合で不可能な青色発生を可能にし，安定な小型青色光源を実現させた[8~10]．変調可能な材料を広げていくことが新たな用途の開拓につながっているよい例といえる[11,12]．一方，代表的なQPM材料であるLN，$LiTaO_3$ (LT)，$KTiOPO_4$ (KTP)などは強誘電体に属し，いずれも分極反転が可能であるが，300 nm近辺に吸収端をもつため紫外への波長変換は困難である．紫外領域で透明な非線形光学材料としてはBaB_2O_4 (BBO)，$CsLiB_6O_{10}$ (CLBO)や水晶が知られているが，自発分極をもたないため，魅力的な特性をもちつつQPMが実現できない．つまり，これらの材料に新たな変調方法を提案できれば，QPM技術ひいては波長変換技術において大きなブレークスルーをもたらす可能性がある．本稿では，強誘電体以外の材料において変調構造を導入する手法として，応力によるツイン制御を提案し，水晶で観察された周期ツインを報告する．またQPM水晶で予想される紫外波長変換特性やツイン制御の熱力学についても解説する．

2. ドメイン(分域)制御材料の探索指針

QPM材料を探索する場合の重要な検討項目は変調構造の導入が可能かどうか，である．現在，自発分極をもたない系にも結晶成長や基板の拡散接合での変調が試みられているが，成長・接合界面の散乱，入射面内もしくは光伝搬方向の不均一などが解決されておらず，実用技術の一歩手前でとどまっている．またガラスや有機材料では，高電界印加による電荷移動/双極子配向による変調構造の導入が報告されているが，緩和による経時変化が存在し，実用化の動きは見られていない．そこでここでは新たな試みとして，原理的に界面散乱がなく，強誘電ドメインと類似の熱

*分子科学研究所　〒444-8585　岡崎市明大寺町西郷中38．E-mail : kurimura@ims.ac.jp.
**スタンフォード大学ギンツトン研究所　〒94305-4085　米国カリフォルニア州スタンフォード．
***早稲田大学理工学部　〒169-0072　東京都新宿区大久保3-4-1．

分類番号　6.2, 1.6

Twin-controlled crystal quartz for quasi-phase-matched wavelength conversion in ultraviolet region.

Sunao KURIMURA*, Martin M. Fejer**, Takunori TAIRA*, Yoshiaki UESU*** and Hirochika NAKAJIMA***
*Institute for Molecular Science (38 Nishigo-naka, Myodaiji, Okazaki 444-8585)
**Ginzton Laboratory, Stanford University (Stanford, California 94305-4085)
***Waseda University (3-4-1 Okubo, Shinjuku-ku, Tokyo 169-0072)

力学が利用できるツイン（双晶）の利用を提案する．ツインとは「同一種結晶における規則的対称的共生で，ある対称操作によって一方を他方に合致させることができる[13]」ものであり，強誘電ドメインは自発分極をもったツインと考えてよい．ツイン制御でQPMを行う際に材料探索のガイドラインは以下のようになる．

①当該結晶にエネルギー的に等価な複数の領域が共存するか（ツインが存在しうるか）
②ツイン間を結びつける対称操作は何か
③その対称操作で対象となる非線形光学定数 d_{ijk} が変調できるか
④外力によるツインの制御が可能か
⑤QPMの周期条件を満たすことが可能か

表1には，代表的な非線形光学材料とその対称性をまとめてあり[14~16]，これを例に探索のガイドラインを解説する．複数の状態間遷移を外力で行う場合，必要とされる外力の大きさ（臨界値）を温度で制御できることはドメインを制御するうえで重要であり，相転移の有無およびその転移点は制御性・安定性の一つの目安となる．一般に相転移をする結晶は高温相で高い対称性をもち，低温相では低い対称性をもつ．このとき発生するドメインに関しては，相転移に伴って失われた対称操作で結びつけられる．これを強誘電体材料を例にみると，

1）LNの場合：ドメイン間は $2//X$（X 軸まわりの2回回転軸）で結びつけられ，各座標軸は $X\rightarrow X$，$Y\rightarrow -Y$，$Z\rightarrow -Z$ の変換をするため $d_{333}\rightarrow -d_{333}$ と変調できる．Z 軸方向に自発分極をもち，電界により Z 軸の反転が可能であり，ドメイン間の制御ができる．

2）KTPの場合：ドメイン間は $m//Z$ 面（ミラー面が Z 面に平行）で結びつけられ，各座標軸は $X\rightarrow X$，$Y\rightarrow Y$，$Z\rightarrow -Z$ の変換をするため $d_{333}\rightarrow -d_{333}$ と変調できる．Z 軸方向に自発分極をもち，電界により Z 軸の反転が可能であり，ドメイン間の制御ができる．

以下では，同様の検討を水晶について行っていくことにする．

3. 水晶の物性と期待される波長変換特性

本研究では実用に耐えうるデバイスの観点から，非線形光学材料として水晶を選択した[17]．水晶は古くは宝石のアメジスト（紫水晶）として知られ，容易に研磨ができ十分な硬度（Mohs硬度7）をもつ．化学的安定性に優れ，低コストで調達でき，紫外150 nmまで透明領域をもつ．レーザー光に対する損傷しきい値が高い（400 GW/cm²@1064 nm, 31 ns pulse[15]）ことでも知られ，歴史的に最初の第2高調波発生（SHG）実験に利用されたが，複屈折が小さく位相整合がとれないため，波長変換材料としては用いられてこなかった．QPM構造が作製できれば有望な波長変換結晶となりうるが，自発分極をもたないため電界印加法は適用できない．そこで，われわれは水晶がもつツインを制御することで，QPM構造の導入を試みる．

表1　代表的な非線形光学結晶とその対称性．

LN($LiNbO_3$)	$3m(C_{3v})$	~1200	$\bar{3}m(D_{3d})$	$2//X$	$d_{22}=25$
LT($LiTaO_3$)	$3m(C_{3v})$	~610	$\bar{3}m(D_{3d})$	$2//X$	$d_{22}=14$
KTP($KTiOPO_4$)	$mm2(C_{2v})$	946	$mmm(D_{2h})$	$m//Z$ 面	$d_{32}=15$
KN($KNbO_3$)	$mm2(C_{2v})$	225	$mmm(D_{2h})$	$m//Z$ 面	$d_{32}=20$
BT($BaTiO_3$)	$4mm(C_{4v})$	120	$m\bar{3}m(O_h)$	$3//\langle 111\rangle$	$d_{31}=15$, $d_{15}=14$
BNN($Ba_2NaNb_5O_{15}$)	$mm2(C_{2v})$	260	$4mm(C_{4v})$	$m//(110)$	$d_{32}=17$, $d_{31}=12$
Quartz(α-SiO_2)	$32(D_3)$	573	$\bar{6}22(D_6)$	$2//Z$(ドフィーネ)	$d_{11}=0.30$
BBO(β-BaB_2O_4)	$3m(C_{3v})$	925	$\bar{3}m(D_{3d})$	$2//X$	$d_{22}=2.2$
LBO($Li_2B_4O_7$)	$4mm(C_{4v})$		—	unknown	$d_{33}=0.93$, $d_{31}=0.12$
LBO(LiB_3O_5)	$mm2(C_{2v})$		—	—	$d_{32}=0.85$
CLBO($CsLiB_6O_{10}$)	$\bar{4}2m(D_{2d})$		—	—	$d_{36}=0.86$
KDP(KH_2PO_4)	$\bar{4}2m(D_{2d})$		—	—	$d_{36}=0.39$

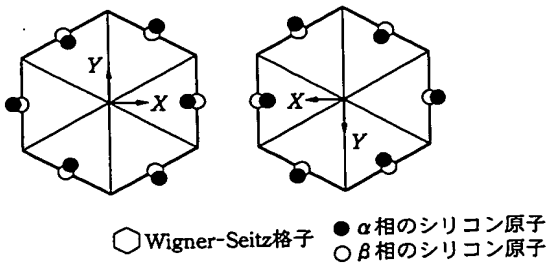

図1　ドフィーネツインにおけるシリコン原子の配置．

単結晶水晶 SiO_2 は室温で α 相（Trigonal）に属し，点群32の対称性をもつ．高温相は点群622の β 相（Hexagonal）であり，573°Cに α-β 転移点を有する．独立な非線形光学定数は d_{11} である（以下 d_{ijk} を d_{il} と縮約する）．水晶の結晶構造に関して，Z 軸からSi原子の配置を見たのが図1である[18]．六角形はWigner-Seitz格子を示し，高温相の β 相では各辺の中央にSi原子が位置している．室温相の α 相ではSi原子はシフトして対称性が低下している．Si原子の0.03 nmのシフト，酸素原子の0.06 nmのシフトでツイン間が入れ替わる．大きな原子のシフトを伴わないことも特徴の一つである．水晶のドフィーネツイン間は，表1にみるように Z 軸まわりの2回回転軸（$2//Z$）で結びつけられるため，$X\rightarrow -X$，$Y\rightarrow -Y$，$Z\rightarrow Z$ の変換をする．これよりツイン間で d_{11} の符号が変わり，ツインの周期配列でQPMが可能であることがわかる．また d_{11} に関して，屈折率分散[19]から1次のQPMSHGに対するツインの配列周期を計算すると図2のようになる．LNなどに比べて屈折率分散が緩やかであるため，要求される周期 Λ が大きいことがわかる．例えば1064 nmを532 nmに波長変換する場合，LNの周期7 μmに対して，水晶は49 μmでよく，532 nmから266 nmへの波長変換でも周期5.5 μmでQPM条件を満たす．

周知のように，近年波長変換においても共振器技術が導入され，小型で高効率な変換が可能になってきている．シングルパスでの波長変換には非線形光学定数の大きな材料が有利であるが，共振器内波長変換では実効的な光学長が長く取れるため光学的損失，許容幅が重要なパラメーターとなる．従来のBBO，CLBOでは波長・温度に対する許容幅が狭く[20]，これが変換効率を制限する要因の一つとなっていた．図3に屈折率分散およびその温度依存性[21]から計算した許容幅を示す．

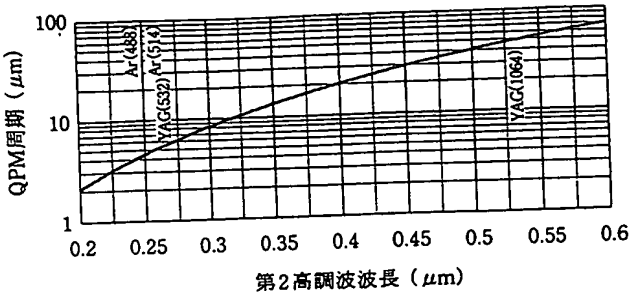

図2 QPM水晶の第2高調波発生におけるツイン周期の波長依存性.

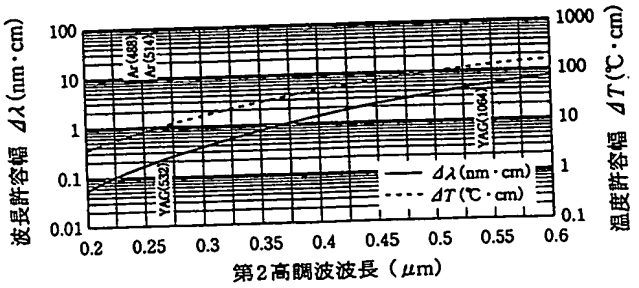

図3 QPM水晶の第2高調波発生における波長・温度許容幅の波長依存性.

QPM水晶では波長分散および屈折率の温度変化が小さいため，波長許容幅・温度許容幅（半値全幅）が広く，532 nmを266 nmに変換する場合，波長幅 $\Delta\lambda=0.22$ nm，温度幅 $\Delta T=10.7$℃と求められる．QPMでは周期パターンの設計により許容幅を広げることもできるため，システムに合わせた特性設計を行える点も強みといえる．266 nm発生の特性をまとめると表2のようになる．光損傷しきい値が高いこと，入射基本波の偏光が影響を受けないこととも相まって，可視光発生での高出力波長変換結晶としても検討に値する．

4. 応力印加による弾性エネルギーの取り扱い

ツイン制御の議論の準備として，結晶の熱力学的エネルギーを定義する．一般に固体内部でのGibbsの自由エネルギーを G とし，外場に対する2次の効果まで考慮すると，外力に対する G の変化分 dG は

$$dG=sdT-e_{ij}(d\sigma_{ij})-P_i(dE_j) \qquad (1)$$

と書ける．ここで s はエントロピー，T は温度，e_{ij} はひずみテンソルの ij 成分，σ_{ij} は応力テンソルの ij 成分，P_i は誘電分極の i 成分，E_i は電界の i 成分である．自発ひずみ $e^{(s)}_{ij}$ と弾性コンプライアンス S_{ijkl}，圧電テンソル d_{ijk}，誘電自発分極 $P^{(s)}{}_i$ を用いて，各変数に対して積分した総エネルギー G で書くと

$$G=sT-e^{(s)}_{ij}\sigma_{ij}+(1/2)S_{ijkl}(\sigma_{ij}\sigma_{kl})+d_{kij}E_k\sigma_{ij}-P^{(s)}{}_iE_i \qquad (2)$$

となる．ここでは $ijkl$ の添え字は可変とした．今，異なる物質定数をもつ二つの状態を(+)(−)とすると，この二つの状態間のエネルギー差 ΔG は以下のようになる．

$$\Delta G=G^{(+)}-G^{(-)}=(\Delta e^{(s)}_{ij})\sigma_{ij}+(1/2)(\Delta S_{ijkl})(\sigma_{ij}\sigma_{kl})+(\Delta d_{kij})E_k\sigma_{ij}+(\Delta P^{(s)}{}_i)E_i \qquad (3)$$

ΔG は外力 σ，E に対する二つの状態間のエネルギー差である．この ΔG が負で二つの状態間遷移に十分な外場が印加されるとき，エネルギーの高い状態からエネルギーの低い状態へ遷移が起こる．

表2 代表的な紫外波長変換結晶の特性（532 nm → 266 nm）.

QPM-SiO_2	0.19	0.22	10.7	0
BaB_2O_4	1.54	0.07	6.0	4.9
$CsLiB_6O_{10}$	0.84	0.13	8.3	1.8

強誘電体で一般的に用いられる電界印加による分極反転の手法は，ドメイン間で自発分極 $P^{(s)}$ の符号が異なることを利用するものであり，電界によるドメイン間のエネルギー差 $(\Delta P^{(s)}{}_i)E_i$ を利用している．今，自発分極をもたない系 $(\Delta P^{(s)}=0)$ に ΔG を導入するためには，$e^{(s)}$ もしくは S_{ijkl}，d_{ijk} のいずれかが，状態間で符号を変えなければならず，かつ状態間遷移に十分な外力が要求される（相転移をもつ結晶の場合には，外力の臨界値に強い温度依存性が期待できる）．ここでは応力による制御を念頭において，$(1/2)(\Delta S_{ijkl})(\sigma_{ij}\sigma_{kl})=(1/2)[\sigma]^T[\Delta S][\sigma]$ の項（バイエラスティック項）に着目して議論を進める．

$[S]$ は6×6のテンソルであるが，点群32に対して独立な弾性定数は $S_{11}(S_{1111})$，$S_{12}(S_{1122})$，$S_{13}(S_{1133})$，$S_{14}(S_{1123})$，$S_{33}(S_{3333})$，$S_{44}(S_{2323})$ となる．今後は S_{ijkl} の添え字を縮約して S_{ij} と表す．ツイン間で弾性コンプライアンスを調べると，符号を変えるのは S_{14} のみである．結果，電界 $E=0$ としてバイエラスティック項によるエネルギー差を応力 σ の関数として求めると

$$\Delta G=(1/2)[\sigma]^T[S][\sigma]=2S_{14}(\sigma_1\sigma_4-\sigma_2\sigma_4+2\sigma_5\sigma_6) \qquad (4)$$

となる．$\Delta G(\theta,\phi)$ の結晶方位依存性を評価[22]するために極座標変換を行う．座標は慣例に従って定義し，ベクトル方向が結晶切断面の法線にあたる．

1）結晶切断面に垂直な圧縮性応力の場合

このとき極座標系の応力テンソル $[\sigma']=(-\sigma_0,\ 0,\ 0,\ 0,\ 0,\ 0)^T$ と書かれ

$$\Delta G=(1/2)[\sigma]^T[S][\sigma]=2S_{14}\sigma_0^2\sin^3\theta\cos\theta\cos 3\phi \qquad (5)$$

となる．適切な結晶方位 θ,ϕ を選ぶことで ΔG を生じさせることができ，十分な応力を加えることで極性の反転が可能になる．垂直応力での過去の報告によると，この取り扱いで $\Delta G<0$ のときに極性が反転することが実証されている[22]．

2）結晶切断面に平行応力の場合

面内応力が θ 軸に対してなす角を ξ とすると極座標系

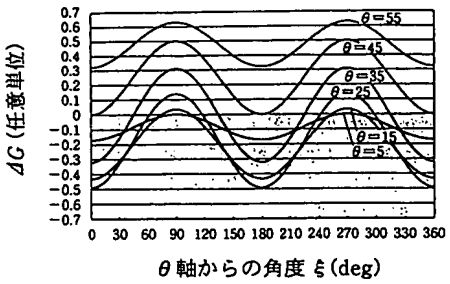

図4　水晶への面内応力印加によるバイエラスティックエネルギーの変化（θ は基板方位）.

の応力テンソル $[\sigma']=(0,\ 0,\ 0,\ 0,\ -\sigma_0\sin\xi,\ -\sigma_0\cos\xi)^T$ と書ける．上記と同様にこれを整理すると，

$$\begin{aligned}\Delta G&=(1/2)[\sigma]^T[S][\sigma]\\&=2S_{14}\sigma_0^2[2\sin^3\theta\cos\theta\cos\phi\{3-4\cos^2\phi\}\sin^2\xi\\&\quad+2\sin^2\theta(1-3\cos^2\theta)\sin\phi(4\cos^2\phi-1)\sin\xi\cos\xi\\&\quad+(1/2)\sin4\theta\cos\phi(4\cos^2\phi-3)\cos^2\xi]\end{aligned}\qquad(6)$$

となる．1）と同様に適切な結晶方位 θ，ϕ を選ぶことで $\Delta G<0$ の領域を選択でき，極性の反転が可能となる．面内応力の場合に ΔG を角度 ξ に対する関数として描くと図4のようになる．基板の方位 θ を5～55° までパラメーターとして計算した（$\phi=180°$ で固定）．適当な基板方位を選択することによって $\Delta G<0$ の領域が存在することがわかり，転移点直下で熱処理を行うことでツインを形成できる見通しが得られた．

5.　基板面内応力によるツイン形成

上記計算より，面内応力を用いてもツイン形成が可能であると推察され，熱応力によるツイン形成を試みた[23]．水晶基板上に金属薄膜を形成し，転移点直下で基板の熱膨張係数の差を利用して応力を印加する方法を用いた[24]．ここでは水晶（熱膨張係数 $\alpha=14\times10^{-6}$(1/K)，ヤング率 $E=9.56\times10^{10}$ (Pa)）に比べて熱膨張係数の差が大きく十分な弾性定数をもつ Cr（$\alpha=4.9\times10^{-6}$，$E=24.8\times10^{10}$）の蒸着膜を用いた．基板は4インチ径，厚さ 0.5 mm で $\theta=38°$，$\phi=180°$ のカット面をもつ市販の基板を用いた．応力のパターニングのために，Cr 蒸着膜を周期パターンに加工した．Cr の周期 Λ は 40～100 μm，膜幅の周期に対する比 R は 0.2～0.6 である．Cr 膜厚は 600 nm とし，Cr 膜の酸化防止のため Ar ガス中でランプアニーラー（Rapid Thermal Annealer）を用いて高速加熱した．また試料上の温度分布を均一化する目的で，試料の両面にシリコンウエハーを接触させた（図5）．これを5～12秒の短時間で転移点直下の 550°C付近まで温度上昇させ，熱応力を発生させた．

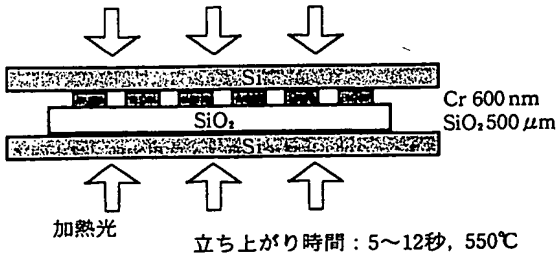

図5　ランプアニーラーを用いた高速加熱によるツイン形成法.

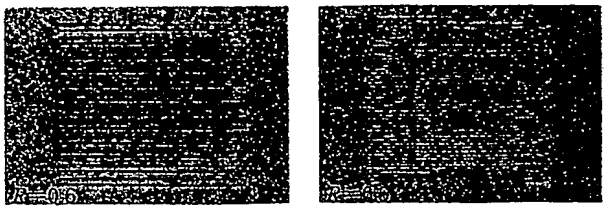

図6　面内熱応力による周期ツイン（周期 80 μm，R は Cr 膜の比）.

本手法を用いて，われわれの知る限り世界で初めて，周期ツインが形成された．Cr 薄膜の熱応力により得られた 80μm周期のツイン写真を図6に示す．ツインは応力の集中する Cr 膜の端から生じ広がる傾向があり，ツイン形成に十分な応力を得るためには $R=0.5$ 以上が必要であった．今回の手法で最短周期として 40 μm まで確認している．しかし形成されたツインの深さは数μm程度であり，バルク波長変換には不向きであった．そこでツインのアスペクト比を改善すべく，垂直応力によるツイン形成を検討した．

6.　垂直応力によるツイン形成

垂直応力によるツイン形成は，250°C以下では異方性の強い成長をすることが知られている[25]．しかし臨界応力の値が非常に高いこと，ツイン形成は屈折率変化を伴わないため観察が困難であること，などの理由で測定値にはばらつきがある．われわれは形成に必要な応力の温度依存性を求めるため，独自の応力印加装置[26]を用いて，基板に垂直な一軸性応力を印加した．ツイン観察は確実性を期すためエッチングを用いてツイン間の段差を観察する方法を採用した．図7は横軸に水晶の温度，縦軸に印加応力をとり，ツインの観察された点を○で示してある．われわれの測定データは，過去の報告（～10^7Pa @250°C）と比べて低い応力でツインが形成されているが，エッチングでは表面に局在するツインも観察できるため，QPM で対象とするような微小なツインも観察できるためと考えられる．今後はツインの高感度非破壊評価[27]も検討課題であろう．形成されたツインはエッチング写真に見るように裏面にまで到達しており，深さ方向のアスペクト比改善の可能性をもつ．今後の展開に期待したい．

7.　む　す　び

紫外発生用 QPM 波長変換材料として水晶を取り上げ，波長変換素子として良好な特性が期待できることを示した．非線形光学定数の変調方法として強誘電ドメインの制御に変わるツイン制御を提案し，その熱力学的な取り扱いを議論した．また実際に面内応力を利用してツインの制御を行い，周期ツインの形成に初めて成功した．強誘電体の電界印加分極反転法が QPM のブレークスルーとなった[28]

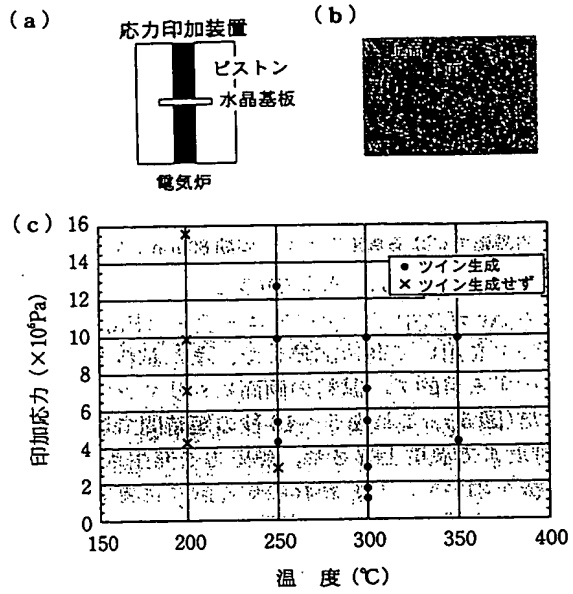

図7 一軸性垂直応力によるツイン生成実験．(a)応力印加装置，(b)エッチング後のツイン写真，(c)ツイン生成の温度依存性．

ように，今後，深さ方向にアスペクト比の高いツイン制御技術が確立されれば，広い透明領域を生かした広帯域なバルク波長変換への道が開けてくる．

謝 辞

本研究に関しご議論いただいた分子研の庄司一郎博士，スタンフォード大学の R. L. Byer 教授，R. Route 博士に感謝いたします．パターニングにご協力いただいた日本ガイシ(株)の近藤厚夫氏，今枝美能留氏，スタンフォード大学の J. Mansell 氏，R. Batchko 氏，応力印加にご協力いただいた US Geological Survey の Steve Kirby 博士に感謝いたします．なお本研究の一部は，電気通信普及財団の海外渡航助成および科学研究費基盤 B(2)・展開研究 10555016 の助成を受けています．

文 献

1) 栗村 直, 上江洲由晃：光学 26, 437 (1997).
2) G. Imeshev, *et al.*: Opt. Lett. 23, 673 (1998).
3) M. L. Bortz, *et al.*: Electron. Lett. 30, 34 (1994).
4) M. A. Arbore, *et al.*: Opt. Lett. 22, 1341 (1997).
5) G. Imeshev, *et al.*: Opt. Lett. 23, 864 (1998).
6) 栗村 直：固体物理 29, 75 (1994).
7) A. Kuroda, S. Kurimura and Y. Uesu: Appl. Phys. Lett. 69, 1565 (1996).
8) K. Mizuuchi, *et al.*: Electron. Lett. 33, 806 (1997).
9) A. Harada, *et al.*: Opt. Lett. 22, 805 (1997).
10) S. Sonoda, *et al.*: Appl. Phys. Lett. 21, 3048 (1997).
11) 栗村 直 (板生 清 他編)：光デバイス精密加工ハンドブック, p. 490 (オプトロニクス社, 1998).
12) J.-B. Hassaun: Laser Focus World 11, 16 (1997).
13) 結晶工学ハンドブック, p. 267 (共立出版).
14) 宮澤信太郎：光学結晶, p. 188 (培風館).
15) V. G. Dmitriev, *et al.*: *Handbook of Nonlinear Optical Crystals* (Springer, Berlin, 1995).
16) S. Furusawa, *et al.*: J. Phys. Soc. Jpn. 60, 2691 (1991).
17) S. Kurimura, *et al.*: 第 45 回応用物理学関係連合講演会講演予稿集, 28a-SG-18 (1998).
18) J. Van Landuyt, *et al.*: Phys. Rev. B 31, 2986 (1985).
19) S. H. Wemple, *et al.*: Phys. Rev. B 3, 1338 (1971).
20) Y. K. Yap, *et al.*: Opt. Lett. 21, 1348 (1996).
21) T. Toyota: J. Phys. C 17, L493 (1984).
22) M. V. Klassen-Neklyudova: *Mechanical Twinning of Crystals* (Consultant Bureau, New York, 1964).
23) S. Kurimura, R. Batchko, J. Mansell, R. Route, M. Fejer and R. Byer: Stanford University CNOM Annual Report, A 4 (1998).
24) T. Uno: Jpn. J. Appl. Phys. 36, 3000 (1997).
25) S. M. Shiau, *et al.*: Mater. Res. Bull. 19, 831 (1984).
26) S. H. Kirby, *et al.*: Bull. Mineral. 102, 124 (1979).
27) S. Kurimura and Y. Uesu: J. Appl. Phys. 81, 369 (1997).
28) 佐脇一平, 三浦道雄, 栗村 直：第 53 回応用物理学会学術講演会講演予稿集, 18a-X-2 (1992).

(2000 年 1 月 8 日 受理)

栗村 直（くりむら ただし）

1988 年早大・理工・物理卒．'90 年同大修士修了．'90 年～'93 年(株)富士通研究所．'93～'96 年早大大学院・理工博士課程．'96 年早大・理工・物理助手．'97～'99 年スタンフォード大学客員研究員．'99 年分子科学研究所助手，現在にいたる．擬似位相整合波長変換素子およびドメイン制御の研究に従事．'97 年早大博士（工学）．'96 年レーザー顕微鏡研究会優秀賞．

Martin M. Fejer

Prof. Fejer received his B. A. degree in Physics from Cornell University, and his Ph. D. in Applied Physics from Stanford University in 1986, where he is currently on the faculty of the Applied Physics department. He is a fellow of the Optical Society of America, and was the 1998 recipient of its R. W. Wood Prize. His current research focuses on nonlinear and guided-wave optics, engineered materials, and optical measurements.

平等 拓範（たいら たくのり）

1983 年福井大・工・電気卒．'85 年同修士修了．'85～'89 年三菱電機(株)LSI 研究所．'89～'98 年福井大学助手．'93～'94 年文部省派遣在外研究員（米国スタンフォード大学）．'98 年分子研助教授，現在にいたる．マイクロプロセッサー，メモリー，LD 励起固体レーザー，非線形波長変換法の研究に従事．'96 年東北大学博士(工学)．'99 年第 23 回(社)レーザー学会業績賞(論文賞)．'99年第 1 回(財)みやぎ科学技術振興基金研究奨励賞．

上江洲 由晃（うえず よしあき）

1966 年早大・理工・応用物理卒．'68 年同修士修了．'68～'69 年フランス国立科学研究機構 (CNRS) Bellevue 研究所．'71 年理学博士号（早大）取得．'71 年早大・理工・物理助手．'74 年早大・理工専任講師．'76 年早大・助教授．'81 年早大・教授，現在にいたる．非線形光学，有機超薄膜の J 会合体形成，強誘電・強弾性分域のパターン形成の研究に従事．

中島 啓幾（なかじま ひろちか）

1972 年早大・理工・応用物理・修士修了．'72～'96 年(株)富士通研究所．'96 年早大・教授，現在にいたる．磁気バブルメモリーの研究を経て，光通信用受動部品・光集積回路の研究に従事．工博．'93 年第 9 回桜井賞受賞．

Recent Developments

Quasi-Phase-Matching Quartz Aiming at Ultraviolet Wavelength Conversion

Sunao Kurimura, Martin M. Fejer, Takunori Taira, Yoshiaki Uesu, and Hirochika Nakajima

Periodic polarization reversal in ferroelectrics results in quasi-phase matching (QPM), which has brought about a revolution in nonlinear optics. In this paper, twin control through stress is proposed as a technique for introducing a reversal structure into nonlinear optical materials which do not undergo spontaneous polarization, and the method was applied to quartz. The expected wavelength-conversion characteristics and thermodynamics of twin control are described for quartz, which is transparent to ultraviolet light.

1. Foreword

Quasi-phase-matching (QPM) wavelength-conversion devices have attracted much attention in recent years for possessing several advantages such as high conversion efficiency, considerable degree of design freedom, and the capability of complex functions and integration[1]. Because phase-matching characteristics can be designed in the space, frequency, or time domains, the introduction of a QPM structure into conventional crystals has had an impact equal to or exceeding that of newly developed crystals. For example, the spatial intensity distribution of converted light may be altered,[2] or the frequency band of wavelength conversion may be broadened,[3] or in other ways phase-matching methods afford unexpectedly diverse design possibilities.

In QPM, when performing wavelength-conversion into a new wavelength area, a preexisting material with known optical constants, chemical properties, thermal properties, laser damage characteristics, machinability, mass-producibility and so on, can be used, instead of an unknown material. That is, simply by changing the modulation period of nonlinear optical constant, any wavelength can be accommodated even in a known material, and if modulation technology is established then all the transparent ranges of existing materials can be employed. For this reason, the manner in which a modulation structure of a nonlinear optical constant is introduced using QPM, and how to search for materials enabling such modulation, are important subjects for study[6]. Conventional QPM materials have for the most part been limited to ferroelectric materials; this is due to the fact that ferroelectrics have a spontaneous polarization, and that polarization reversal is possible by applying an electric field. That is, by patterning electrodes and applying an electric field, nonlinear optical constants can be periodically modulated. For example, in the case of $LiNbO_3$ (LN) material, polarization inversion[7] in $MgO:LiNbO_3$, which is resilient to optical damage, enables the generation

of blue light, which cannot be produced through birefringence matching, and a stable and compact blue-light light source has thus been realized.[8-10] This may be regarded as a good example of how efforts to broaden the range of materials in which modulation is possible lead to exploration of new applications.[11,12] On the other hand, the representative QPM materials LN, $LiTaO_3$ (LT), $KTiOPO_4$ (KTP), and so on are ferroelectrics, and polarization reversal is possible in all of them; but because they have an absorption edge near 300 nm, wavelength conversion into the ultraviolet is difficult. BaB_2O_4 (BBO), $CsLiB_6O_{10}$ (CLBO), and quartz are known as optically nonlinear materials which are transparent in the ultraviolet range, but because they do not have a spontaneous polarization, QPM cannot be induced, despite their attractive characteristics. That is, if a new modulation method could be proposed for these materials, there would be the possibility of a major breakthrough for QPM technology and also for wavelength conversion technology. In this paper, we propose twin control through stress as a method of introducing a modulation structure in materials other than ferroelectrics, and report on periodic twinning observed in quartz. In addition, the ultraviolet wavelength conversion characteristics expected in QPM quartz, and the thermodynamics of twin control, are explained.

2. Guidelines for Searching for Domain Control Materials

When searching for QPM materials, the most important matter for study is the possibility of introducing a modulation structure. At present, modulation is also attempted in crystal growth and in diffusion junctions with the substrate in systems not having spontaneous polarization, but problems such as dispersion at the growth or junction interface, and unevenness at the incident face or in the direction of light propagation, have not been resolved, and development has stopped some distance short of practical application. Among glass and organic materials, introduction of a modulation structure due to charge motion/twin orientation caused by strong electric fields has been reported, but there is aging due to relaxation, and no efforts toward practical application have been made. Here, then, as a new attempt, utilization of twins (twinning), which in principal have no interface dispersion and the thermodynamic behavior of which is similar to that of ferromagnetic domains, is proposed. Twinning is "the regular symmetric growth of the same type of crystal, in which a certain symmetric action causes one to coincide with the other"[13]; a ferroelectric domain may be regarded as a twin having spontaneous polarization. The following are guidelines for searching for materials when using QPM in twin control.

(1) Do multiple energetically equivalent regions coexist in the crystal? (Can twins exist?)
(2) What is the symmetric action binding twins?
(3) Can the nonlinear optical constants d_{ijk} which are the object of this symmetrical action be modulated?

(4) Is twin control possible through application of external forces?
(5) Can the QPM periodic conditions be satisfied?

Table 1 summarizes the representative nonlinear optical constants and their symmetry;[14-16] these are used as examples in explaining the search guidelines. When inducing multiple state transitions through application of external forces, the ability to control the magnitude of the forces required (critical values) through the temperature is important for controlling domains, and the presence of phase transitions, and their transition points, are criteria for judging controllability and stability. In general, in crystals which undergo phase transitions, high-temperature phases have a high degree of symmetry, and low-temperature phases have a low degree of symmetry; the domains which arise at these times are joined by symmetrical action which is lost upon phase transitions. The following are ferroelectric material examples.
1) LN: Domains are joined at 2//X (a twofold rotation axis about the X-axis), and the coordinate axes are transformed as X→X, Y→-Y, Z→-Z, so that the modulation d_{333}→-d_{333} is possible. There is spontaneous polarization in the Z-axis direction, and an electric field can be used to reverse the Z axis, so that domains can be controlled.
2) KTP: Domains are joined at the m//Z plane (with the mirror plane parallel to the Z plane), and the coordinate axes are transformed as X→X, Y→-Y, Z→-Z, so that the modulation d_{333}→-d_{333} is possible. There is spontaneous polarization in the Z-axis direction, and an electric field can be used to reverse the Z axis, so that domains can be controlled.

Below, similar studies are conducted for quartz.

3. Physical Properties of Quartz and Anticipated Wavelength-Conversion Characteristics

In this research, quartz was selected as the nonlinear optical material, in the interest of developing devices suited to practical application.[17] Quartz has long been known as the precious stone amethyst (a purple variety of quartz), can be ground easily, has a high hardness (7 on the Mohs scale) and excellent chemical stability, can be procured at low cost, is transparent up to 150 nm in the ultraviolet range, and has a high threshold for damage by laser light (400 GW/cm^2 at 1064 nm, 31 ns pulses[15]). Historically , quartz was used in the first experiments on second harmonic generation (SHG); but because of its small birefringence and absence of phase matching, it had not been used as a wavelength-conversion material. If a QPM structure could be created, it might become a promising wavelength-conversion crystal, but because it does not have spontaneous polarization, the electric field application method cannot be employed. We therefore attempted to introduce a QPM structure through control of twins in quartz crystals.

Single-crystal quartz, SiO_2, is in the α (trigonal) phase at room temperature, with point group 32 symmetry; the high-temperature phase is the β (hexagonal) phase of point group

622, and there is an α-β transition point at 573°C. The independent nonlinear optical constant is d_{11} (hereafter d_{ijk} is abbreviated to d_{i1}). Fig. 1 shows the arrangement of Si atoms in the quartz crystal structure seen along the Z axis.[18] The hexagons represent Wigner-Seitz cells. In the high-temperature β phase, Si atoms are positioned at the centers of each edge. In the room-temperature α phase, the Si atoms are shifted, and the symmetry is reduced. With an Si atom shift of 0.03 nm and an oxygen atom shift of 0.06 nm, a twin boundary is substituted. Another feature is the absence of a concomitant shift in large atoms. As indicated in Table, 1, Dauphiné twins in quartz are joined by a twofold rotation axis about the Z axis (2//Z), resulting in the transformation X→-X, Y→-Y, Z→Z. As a result the sign of d_{11} changes between the twins, and it is seem that QPM is possible for the twin periodic ordering. With respect to d_{11}, Fig. 2 shows the calculated ordering period of twins for first-order QPMSHG from the refractive index dispersion.[19] Compared with LN and other materials, the refractive index dispersion is gradual, and so the required period Λ is large. For example, when converting a 1064 nm wavelength to 532 nm, as opposed to an LN period of 7 μm, for quartz 49 μm is sufficient, and even in wavelength conversion from 532 nm to 266 nm, the QPM conditions are satisfied at a period of 5.5 μm.

As is well known, resonator technology has in recent years been deployed for wavelength conversion, and it has become possible to perform efficient conversion using small devices. Materials with large nonlinear optical constants are advantageous for single-pulse wavelength conversion, but because the effective optical length can be large in wavelength conversion within a resonator, optical losses and the tolerance range become important parameters. In conventional BBO and CLBO, the tolerance ranges for wavelength and temperature were narrow,[20] and this was one factor limiting conversion efficiency. Fig. 3 shows tolerance ranges calculated from the refractive index dispersion and temperature dependence of the dispersion.[21] In a QPM crystal, the wavelength dispersion and change with temperature in refractive index are small, so that the wavelength tolerance range and temperature tolerance range (half-maximum width) are broad, and when converting 532 nm into 266 nm, a wavelength range $\Delta\lambda = 0.22$ nm and temperature range $\Delta T = 10.7$°C are calculated. In QPM, the tolerance range can be broadened through design of the periodic pattern, and the ability to design characteristics according to the entire system is an added advantage. The characteristics for generation of 266 nm light are summarized in Table 2. Together with the high threshold for optical damage and the fact that the polarization of the incident fundamental wave is not affected, study as a high-output wavelength conversion crystal for generation of visible light is warranted.

4. Treatment of Elastic Energy due to Stress Application

As preparation for discussion of twin control, the thermodynamic energy of a crystal is defined. Taking the Gibbs free energy within a solid to be G and considering up to second-order effects of external fields, the change dG due to an external force can be written

$$dG=sdT-e_{ij}(d\sigma_{ij})-P_i(dE_j) \quad (1)$$

Here s is the entropy, T is temperature, e_{ij} are the ij components of the strain tensor, σ_{ij} are the ij components of the stress tensor, P_i are the i components of the dielectric polarization, and E_i are the i components of the electric field. Using the spontaneous strain $e^{(s)}_{ij}$ and elastic compliance S_{ijkl}, piezoelectric tensor d_{ijk}, and spontaneous dielectric polarization $P^{(s)}_i$, and taking G to be the total energy integrated over each variable, we have

$$G=sT-e^{(s)}_{ij}\sigma_{ij}+(1/2)S_{ijkl}(\sigma_{ij}\sigma_{kl}) +d_{kij}E_k\sigma_{ij}-P^{(s)}_iE_i \quad (2)$$

Here the subscripts ijkl are taken to be variable. If two states having different physical constants are represented by "+" and "-", then the energy difference between these two states ΔG is as follows.

$$\Delta G=G^{(+)}-G^{(-)}=(\Delta e^{(s)}_{ij})\sigma_{ij}+(1/2)(\Delta S_{ijkl}) (\sigma_{ij}\sigma_{kl})+(\Delta d_{kij})E_k\sigma_{ij}+(\Delta P^{(s)}_i)E_i \quad (3)$$

ΔG is the energy difference between two states for external forces σ and E. When this ΔG is negative and a sufficiently large external field is applied for transitions between the two states, a transition occurs from the higher-energy state to the lower-energy state.

The method of polarization reversal through electric field application which is generally used with ferroelectrics utilizes the different signs of the spontaneous polarization $P^{(s)}$ between domains, and makes use of the energy difference $(\Delta P^{(s)}_i)E_i$ between domains due to the electric field. In order to introduce a ΔG into a system not having spontaneous polarization ($(\Delta P^{(s)}=0$), it is necessary that either $e^{(s)}$ or S_{ijkl}, d_{ijk} change signs between states, and moreover a force sufficient for a transition between states is required (in the case of a crystal with phase transitions, a strong temperature dependence of the external force critical point can be expected). Below the discussion shall be developed keeping in mind control through stresses, and focusing on the term $(1/2)(\Delta S_{ijkl})(\sigma_{ij}\sigma_{kl}) = (1/2)[\sigma]^T[\Delta S][\sigma]$ (bielastic term).

[S] is a 6x6 tensor, but the independent elastic constants for point group 32 are S_{11} (S_{1111}), S_{12} (S_{1122}), S_{13} (S_{1133}), S_{14} (S_{1123}), S_{33} (S_{3333}), S_{44} (S_{2323}). Hereafter the subscripts of S_{ijkl} are abbreviated to S_{ij}. Upon investigating the elastic compliance between twins, the sign changes only for S_{14}. As a result, calculating the energy difference due to the bielastic term for electric field E=0 as a function of the stress σ gives

$$\Delta G=(1/2)[\sigma]^T[S][\sigma]$$
$$=2S_{14}(\sigma_1\sigma_4-\sigma_2\sigma_4+2\sigma_5\sigma_6= \quad (4)$$

A transformation into polar coordinates is performed in order to evaluate the crystal direction dependence of $\Delta G(\theta,\phi)$.[22] Coordinates are defined as is customary, with the vector direction being normal to a plane cutting the crystal.

1) Case of compressive elastic stress perpendicular to the plane cutting the crystal

At this time the stress tensor in polar coordinates is written $[\sigma'] = (-\sigma_0, 0, 0, 0, 0, 0)$,[T] and

$$\Delta G=(1/2)[\sigma]^T[S][\sigma]$$
$$=2S_{14}\sigma_0^2\sin^3\theta\cos\theta\cos3\phi \quad (5)$$

By choosing an appropriate crystal direction θ, ϕ, a ΔG can be induced, and by applying sufficient stress, polarization reversal is possible. According to past reports on normal stresses, it is confirmed that for this treatment the polarization is reversed when $\Delta G < 0$.[22]

2) Case of stress parallel to the plane cutting the crystal

If the angle made by the in-plane stress with the θ axis is ξ, then the stress tensor in polar coordinates can be written $[\sigma'] = (0, 0, 0, 0, -\sigma_0\sin\xi, -\sigma_0\cos\xi)^T$. Rearranging this similarly to the above, we have

$$\Delta G=(1/2)[\sigma]^T[S][\sigma]$$
$$=2S_{14}\sigma_0^2[2\sin^3\theta\cos\theta\cos\phi\{3-4\cos^2\phi\}\}\sin^2\xi$$
$$+2\sin^2\theta(1-3\cos^2\theta)\sin\phi(4\cos^2\phi-1)\sin\xi\cos\xi$$
$$+(1/2)\sin4\theta\cos\phi(4\cos^2\phi-3)\cos^2\xi] \quad (6)$$

Similarly to 1), by choosing an appropriate crystal direction θ and ϕ, a region in which $\Delta G < 0$ can be selected, and polarization reversal becomes possible. In the case of in-plane stress, describing ΔG as a function of the angle ξ results in Fig. 4. Calculations were performed taking the substrate direction θ as a parameter between 5 and 55° (with ϕ fixed at 180°). It is seen that by choosing an appropriate substrate direction, a region exists for which $\Delta G < 0$, and by performing heat treatment immediately below the transition point, the prospect of twin formation is obtained.

5. Twin Formation through Stress in the Plane of the Substrate

From the above calculations, it is inferred that in-plane stress can also be used for twin formation, and so an attempt was made to form twins through thermal stress[23]. A method was employed in which metal thin film was formed on a quartz substrate, and the difference in thermal expansion coefficients with the substrate was utilized up to immediately below the transition point to apply stress[24]. Here, for the evaporation-deposited film, Cr (thermal expansion coefficient $\alpha=4.9 \times 10^{-6}$, Young's modulus $E=24.8 \times 10^{10}$) with sufficient elasticity constant and a large difference in thermal expansion coefficient compared to quartz ($\alpha=14 \times 10^{-6}$(1/K), $E=9.56 \times 10^{10}$(Pa)) was employed. A commercially marketed

substrate having a cut plane of θ38°, φ180°, with a diameter of 4 inches and thickness of 0.5 mm, was employed. In order to perform stress patterning, the Cr evaporation-deposited film was machined into a periodic pattern. The Cr period Λ was from 40 to 100 μm, and the ratio R of the film width to the period was from 0.2 to 0.6. The Cr film thickness was 600 nm, and a ramp annealer (rapid thermal annealer) was used for rapid heating in the Ar gas employed to prevent oxidation of the Cr film. In order to render uniform the temperature distribution over the sample, silicon wafers were brought into contact with both faces of the sample (Fig. 5). The temperature was raised to the vicinity of 550°C, just below the transition point, in a short time of between 5 and 12 seconds, to generate thermal stress.

Using this technique, we succeeded in forming periodic twins, for the first time ever to our knowledge. Fig. 6 shows a photo of twins with a period of 80 μm, obtained through thermal stress due to the Cr thin film. The twins occur from the edges of the Cr film at which stress is concentrated and tend to spread outward; in order to obtain stress sufficient to form twins, R=0.5 or higher was necessary. The technique used was confirmed to result in a shortest period of 40 μm. However, the depth of the twins formed was several microns or so, unsuitable for bulk wavelength conversion. Hence twin formation through normal stresses was studied, in order to improve the twin aspect ratio.

6. Twin Formation through Normal Stresses

Twin formation through normal stresses is known to occur with strongly anisotropic growth below 250°C[25]. However, the extremely high critical stress value, and the fact that twin formation is not accompanied by a change in the refractive index, so that observation is difficult, and other reasons have resulted in scattering among measured values. In order to determine the temperature dependence of the stress necessary for formation, we have used our own stress application apparatus[26] to apply uniaxial stress normal to the substrate. In order to be able to expect reliable twin observation, a method was adopted in which etching was used to observe the steps between twins. Fig. 7 plots quartz temperature along the horizontal axis and the applied stress along the vertical axis; points at which twins were observed are indicated by circles. Our measurement data indicate that twins are formed at lower stresses than in past reports (approx. 10^7 Pa at 250°C), but because etching also enables observation of twins localized at the surface, it is thought that even minute twins relevant to QPM can also be observed. Hereafter, high-sensitivity non-destructive evaluation of twins[27] will also be a subject for study. The twins formed extend to the rear surface, as seen in the etching photos, and there is the possibility for improvement of the aspect ratio in the depth direction. Further developments are anticipated.

7. Conclusion

Quartz has been studied as a QPM wavelength-conversion material for generation of ultraviolet light, and it was shown that satisfactory characteristics as a wavelength-conversion element can be expected. Twin control in place of ferroelectric domain control was proposed as a method of modulation of nonlinear optical constants, and a thermodynamic approach was discussed. In-plane stresses were actually used to control twins, and periodic twins were formed successfully for the first time. Just as the method of polarization reversal in ferroelectrics through electric field application was a breakthrough for QPM,[28] hereafter, should technology for twin control with a high aspect ratio in the depth direction be established, the way should be prepared for bulk wavelength conversion over a broad range, taking advantage of the broad transparent wavelength region.

Acknowledgements

The authors wish to thank Dr. Ichiro Shoji of the Institute for Molecular Science, and Prof. R.L. Byer and Dr. R. Route of Stanford University for discussions related to this research. They are grateful to Mr. Atsuo Kondo and Mr. Minoru Imaeda of NGK Insulators Ltd. and to Mr. J. Mansell and Mr. R. Batchko of Stanford University for cooperation in the patterning, and to Dr. Steve Kirby of the US Geological Survey for cooperation in the stress application. A part of this research was conducted with the aid of foreign travel assistance from The Telecommunications Advancement Foundation and with a B(2) Grant-in-Aid for Scientific Research #10555016 from the Japan Society for the Promotion of Science.[i]

References

1) S. Kurimura and Y. Uesu: *Kougaku*, 26, 437 (1997).
2) G. Imeshev et al: Opt. Lett., 23, 673 (1998).
3) M.L. Bortz et al: Electron. Lett., 30, 34 (1994).
4) M.A. Arbore et al: Opt. Lett., 22, 1341 (1997).
5) G. Imeshev et al: Opt. Lett., 23, 864 (1998).
6) S. Kurimura: *Kotai Butsuri*, 29, 75 (1994).
7) A. Kuroda, S. Kurimura and Y. Uesu: Appl. Phys. Lett., 69, 1565 (1996).
8) K. Mizuuchi et al: Electron. Lett., 33, 806 (1997).
9) A. Harada et al: Opt. Lett., 22, 805 (1997).
10) S. Sonoda et al: Appl. Phys. Lett., 21, 3048 (1997).
11) S. Kurimura (K. Itao et al, ed.): *Hikari Debaisu Seimitsu Kakou Handobukku*, p. 490 (Optronics Co. Ltd.1998).
12) J.-B. Hassaun: Laser Focus World, 11, 16 (1997).
13) *Kesshou Kougaku Handobukku*, p. 267 (Kyoritsu).
14) S. Miyazawa: *Kougaku Kesshou*, p. 188 (Baifuukan).
15) V.G. Dmitriev et al: Handbook of Nonlinear Optical Crystals (Springer, Berlin, 1995).
16) S. Furusawa et al: J. Phys. Soc. Jpn., 60, 2691 (1991).
17) S. Kurimura et al: Preprints 45th Meeting Jpn. Soc. Appl. Phys. Rel. Socs., 28a-SG-18 (1998).

18) J. Van Landuyt et al: Phys. Rev. B 31, 2986 (1985).
19) S.H. Wemple et al: Phys. Rev. B 3, 1338 (1971).
20) Y.K. Yap et al: Opt. Lett., 21, 1348 (1996).
21) T. Toyota: J. Phys. C 17, L493 (1984).
22) M. V. Klassen-Neklyudova: Mechanical Twinning of Crystals (Consultant Bureau, New York, 1964).
23) S. Kurimura, R. Batchko, J. Mansell, R. Route, M. Fejer and R. Byer: Stanford University CNOM Annual Report, A4 (1998).
24) T. Uno: Jpn. J. Appl. Phys., 36, 3000 (1997).
25) S.M. Shiau et al: Mater. Res. Bull., 19, 831 (1984).
26) S.H. Kirby et al: Bull. Mineral., 102, 124 (1979).
27) S. Kurimura and Y. Uesu: J. Appl. Phys., 81, 369 (1997).
28) I. Sawaki, M. Miura and S. Kurimura: Preprints 53rd Conf. Jpn. Soc. Appl. Phys., 18a-X-2 (1992).

(Received January 8, 2000)

Fig. 1. Arrangement of silicon atoms in Dauphiné twins
Wigner-Seitz cells
α phase silicon atom
β phase silicon atom

Table 1. Representative nonlinear optical crystals and their symmetry properties
Crystal
Room-temperature symmetry
Transition point (°C)
High-temperature phase symmetry
Symmetry operations between domains
Nonlinear optical constants
m//Z plane
m//Z plane
2//Z (Dauphiné)

Fig. 2. Wavelength dependence of twin period in QPM quartz second harmonic generation
QPM period (μm)
Second harmonic wavelength (μm)

Fig. 3. Wavelength dependence of wavelength and temperature tolerance ranges in QPM quartz second harmonic generation
Wavelength tolerance range Δλ (nm-cm)
Temperature tolerance range ΔT (°C-cm)
Second harmonic wavelength (μm)

Table 2. Characteristics of representative ultraviolet wavelength-conversion crystals

Quartz
Effective nonlinear optical constants
Wavelength tolerance range

Temperature tolerance range
Walk-off angle

Fig. 4. Change in bielastic energy due to in-plane stress application to quartz (θ is the substrate direction)
ΔG (arbitrary units)
Angle ξ from θ axis (deg)

Fig. 5. Method of twin formation through rapid heating using ramp annealer
Heating light
Rise time: 5 to 12 sec, 550°C

Fig. 6. Periodic twins due to in-plane thermal stress (period 80 μm, R is the ratio to the Cr film)

Fig. 7. Twin generation experiments through uniaxial normal stress. (a) Stress application apparatus; (b) photo of twins after etching; (c) temperature dependence of twin generation
Stress application apparatus
Piston
Quartz substrate
Electric furnace
Applied stress ($x10^6$ Pa)
Temperature (°C)
Twins generated
Twins not generated

Top surface
Bottom surface

[i] Names, institutions, grant descriptions etc are best guesses or are inferred.

This Page is Inserted by IFW Indexing and Scanning Operations and is not part of the Official Record

BEST AVAILABLE IMAGES

Defective images within this document are accurate representations of the original documents submitted by the applicant.

Defects in the images include but are not limited to the items checked:

- ☐ BLACK BORDERS
- ☐ IMAGE CUT OFF AT TOP, BOTTOM OR SIDES
- ☑ FADED TEXT OR DRAWING
- ☑ BLURRED OR ILLEGIBLE TEXT OR DRAWING
- ☐ SKEWED/SLANTED IMAGES
- ☐ COLOR OR BLACK AND WHITE PHOTOGRAPHS
- ☐ GRAY SCALE DOCUMENTS
- ☐ LINES OR MARKS ON ORIGINAL DOCUMENT
- ☐ REFERENCE(S) OR EXHIBIT(S) SUBMITTED ARE POOR QUALITY
- ☐ OTHER: _____

IMAGES ARE BEST AVAILABLE COPY.
As rescanning these documents will not correct the image problems checked, please do not report these problems to the IFW Image Problem Mailbox.